Freie Universität Berlin

Synthesis and Characterization of Water-Soluble Dendronized Dye Systems as Fluorescent Labels for Bioimaging Applications

Inaugural-Dissertation

to obtain the academic degree

Doctor rerum naturalium (Dr. rer. nat.)

submitted to

the Department of Biology, Chemistry and Pharmacy

of Freie Universität Berlin

by

Katharina Huth

from Berlin, Germany

2018

The research presented in this thesis was accomplished from January 2014 to June 2018 under the supervision of Prof. Dr. Rainer Haag at the Institute of Chemistry and Biochemistry - Organic Chemistry of the Freie Universität Berlin.

1st Reviewer: Prof. Dr. Rainer Haag
Freie Universität Berlin

2nd Reviewer: PD Dr. habil. Kai Licha
Freie Universität Berlin

Date of Defense: August 17th, 2018

Statutory Declaration

Hereby I, Katharina Huth, born on January 22nd, 1987 in Berlin, declare that I have independently authored the submitted thesis with the topic "*Synthesis and Characterization of Water-Soluble Dendronized Dye Systems as Fluorescent Labels for Bioimaging Applications*". I have explicitly marked references that have been quoted either literally or by content from the used sources.

I also confirm that this work as well as parts of this work have not been previously published or accepted for the award of any other degree or diploma in any university or other tertiary institution in my name.

Berlin, June 25th 2018

Katharina Huth

Acknowledgements

My sincere thanks go to Prof. Dr. Rainer Haag for the opportunity to do my doctoral studies in his group, the freedom to pursue my research interests, and the scientific supervision during this time. I greatly thank PD Dr. habil. Kai Licha for his expert advice on chemical issues and for co-examining this thesis. Moreover, I thank Dr. Timm Heek for giving me insights into perylene chemistry and guiding my first steps in the Haag group. I would like to express my gratitude to Prof. Dr. Mohsen Adeli for always having an open ear for my research questions, giving me encouraging advice, and sharing his supportive ideas with me. I thank my collaboration partners for their helpful support and the stimulating discussions that have contributed to the outcome of the projects in this work. I would like to mention in particular Dr. Ying Li, Mareen Gläske, Dr. Antonio Setaro as well as Prof. Dr. Stephanie Reich and Prof. Dr. Kevin Pagel. Furthermore, I would like to single out my "biological collaborators" Dr. Jens Dernedde and Dr. Katharina Achazi; the projects of this thesis greatly benefited from their scientific expertise and biological experiments. Special thanks are also directed to Dr. Bala Naga Satyanarayana Thota (aka Balu) for his guidance and support as my subgroup leader.

I gratefully thank Prof. Dr. Steven C. Zimmerman and all members of the Z-group for the hospitality during my research exchange at the University of Illinois at Urbana-Champaign. The group seminars, subgroup meetings, and individual discussions have broadened my scientific horizons and given me new food for thought for my projects. Additionally, I would like to thank Prof. Zimmerman for supporting Ying and me in publishing the LDP project.

Special thanks to my colleagues I shared a laboratory and office with for the friendly working atmosphere and their general support in many ways. Special mention applies to Leonhard H. Urner (who is also an appreciated cooperation partner), Ehsan Mohammadifar, Magda Ferraro, Svenja Ehrmann, Alexander Oehrl, and Dr. Era Kapourani. Besides, I would also like to thank the people from our daily Weinhart/Haag lunch group for the interesting discussions and friendly get-together.

Additionally, I would like to express my thanks to the members of the Haag group for the pleasant work atmosphere and ubiquitous supportive attitude. Moreover, I acknowledge Katharina Goltsche for her assistance in dendron synthesis, Marleen Selent for performing HPLC purification, Cathleen Schlesener for conducting GPC measurements, as well as Elisa Quaas and Paul Hillmann for their assistance in the biological experiments.

I especially acknowledge Dr. Wiebke Fischer for her overall comprehensive support especially in the manuscript submission process as well as Jutta Hass and Eike Ziegler for the handling

of orders and financial matters. Furthermore, I thank Dr. Pamela Winchester for the careful proofreading and linguistic revision of my manuscripts and thesis.

In addition, I thank the service staff of the Core Facility BioSupraMol for conducting numerous analytical measurements within my doctoral studies.

I gratefully acknowledge the financial support for my doctoral work by Deutsche Forschungsgemeinschaft, in particular SFB 658, as well as the educational infrastructure provided by the Dahlem Research School.

My sincere appreciation goes to my fellow students and dear friends, Dr. Olaf Nachtigall and Dr. Melanie Göth, who were on hand with personal support and advice throughout my doctoral studies.

I am deeply indebted to Luigi Sbailò for motivating me and giving me personal support in these past years.

Last but not least, I owe a great debt of gratitude to my family, especially my beloved mother Angelika Huth, and close friends for their emotional and personal support during my entire studies.

Abstract

Perylene bisimides (PBIs) possess characteristics such as high chemical and photophysical stability, outstanding fluorescence properties, and availability of monofunctionalized derivatives. These features make them ideal candidates for an application as fluorescent label. However, their insolubility in water and the resulting aggregation tendency leading to fluorescence quenching have limited the full potential of these functional dyes. To overcome these limitations, several polyglycerol- (PG) dendronized monofunctionalized PBIs are presented as site-specific labels for cellular bioimaging. The general structure of the biolabels consists of a hydrophilic and sterically demanding PG dendron, the fluorescent PBI core, and a linker with a functional group. The PG dendron introduces water solubility and suppresses the aggregation tendency of the fluorophores. The monofunctional linker serves as a coupling-active unit for the site-specific conjugation of biomolecules or other components. To study the effect of steric shielding, the PBI labels were synthesized in different dendron generations ([G_{low}] *vs.* [G_{high}]). To additionally evaluate the impact of electrostatic shielding, the hydroxylated dendron headgroups of the labels were modified with ionically charged sulfate groups (OH *vs.* SO_4^-).

In the first project, a series of hydroxylated and sulfated [G1]- to [G3]-dendronized PBIs with a poly(ethylene glycol) (PEG) linker was synthesized, optically characterized, and studied as site-specific labels by conjugation to an antibody. The photophysical properties of the labels could be improved by increasing the steric bulk and amount of charge of the attached dendron, resulting in highly fluorescent PBIs with fluorescence quantum yields (FQYs) up to 100%. Receptor-binding, cytotoxicity, and cellular uptake studies confirmed the suitability of the PBIs as site-specific labels. In the second project, [G1]- to [G3]-dendronized PBIs were used for the synthesis of fluorescent polymer nanoparticles consisting of linear dendronized polyols (LDPs). The enhanced dendritic shielding effect of the various [G*n*]-PBIs was evidenced by an increase in FQY of their respective LDPs from 7.8 to 23%. The incorporation of two different fluorophores into one polymer backbone led to large Stokes shifts caused by the occurrence of Förster resonance energy transfer (FRET). The fluorophore-conjugated LDPs showed no cytotoxic side effects and were successfully employed in cellular bioimaging studies. In the third project, single-walled carbon nanotubes (SWNTs) were functionalized with linear polymers equipped with neutral or charged [G2]-dendronized PBIs, leading to fluorescent polymer-SWNT complexes. The polymer wrapping improved the cytocompatibility of the nanotubes and enabled the direct imaging of their cellular uptake via the PBI and SWNT emission using the 1st and 2nd optical windows. Charged complexes showed superior SWNT dispersibility, intracellular fluorescence intensity, and cellular uptake over their neutral counterparts. A final complementary study

affirmed the concept of dendritic site isolation of fluorophores using the example of a PG-dendronized near-infrared (NIR) cyanine derivative. The dye exhibited a pH-driven turn-on/turn-off fluorescence mechanism and showed good staining properties in the imaging of macrophages.

In summary, the introduction of (charged) sterically demanding PG dendrons and monofunctionalized linkers on core-unsubstituted PBIs led to water-soluble, highly fluorescent, and site-specific biolabels. These results demonstrate the versatile potential of dendronized PBIs as fluorescent labels and promise their diverse application in future bioimaging studies.

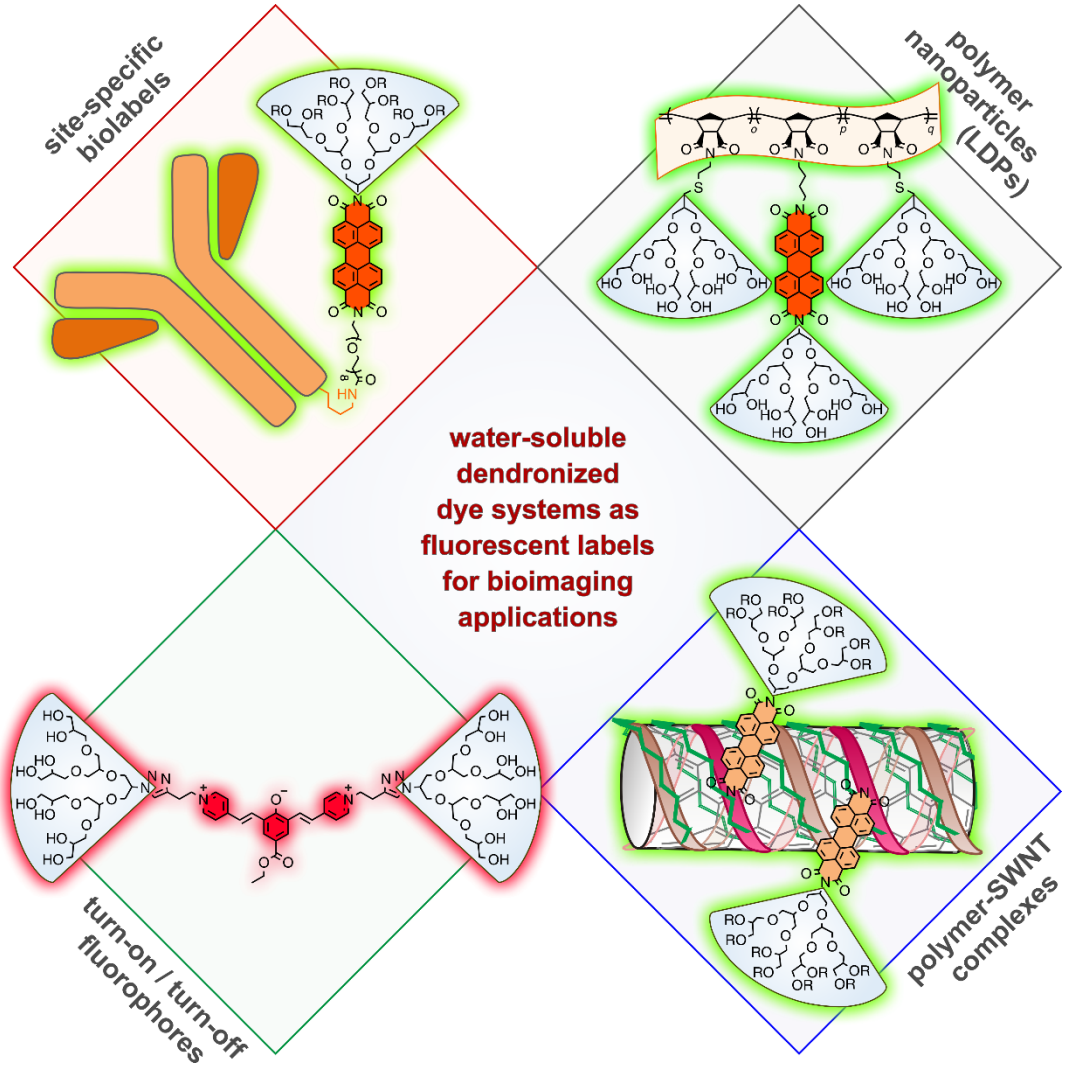

Overview of the four projects included in this thesis. The color highlighting of the structures corresponds to the wavelength of their emission maxima (R = OH or SO_4^-).

Kurzzusammenfassung

Perylenbisimide (PBIs) besitzen Merkmale wie hohe chemische und photophysikalische Stabilität, hervorragende Fluoreszenzeigenschaften und Verfügbarkeit von monofunktionalisierten Derivaten. Diese Eigenschaften machen sie zu idealen Kandidaten für eine Anwendung als Fluoreszenzlabel. Das volle Potential dieser funktionellen Farbstoffe wird jedoch durch ihre Wasserunlöslichkeit und die daraus resultierende fluoreszenzlöschende Aggregationsneigung beeinträchtigt. Um diese Limitation zu überwinden, werden verschiedene Polyglycerol- (PG) dendronisierte monofunktionalisierte PBIs als regiospezifische Labels für zelluläre Biobildgebung vorgestellt. Der allgemeine Aufbau der Biolabels besteht aus einem hydrophilen und sterisch anspruchsvollen PG Dendron, dem fluoreszenten PBI-Kern und einem Linker mit einer funktionellen Gruppe. Das PG Dendron erhöht die Wasserlöslichkeit und unterdrückt die Aggregationsneigung der Fluorophore. Der monofunktionelle Linker dient als kupplungsaktive Einheit für die regiospezifische Konjugation von Biomolekülen oder anderen Komponenten. Um den Effekt von sterischer Abschirmung zu untersuchen, wurden die PBI-Labels in verschiedenen Dendrongenerationen synthetisiert ([$G_{niedrig}$] *vs.* [G_{hoch}]). Um außerdem die Auswirkung von elektrostatischer Abschirmung zu beurteilen, wurden die hydroxylierten Dendrongruppen der Labels mit ionisch geladenen Sulfatgruppen modifiziert (OH *vs.* SO_4^-).

Im ersten Projekt wurde eine Reihe von hydroxylierten und sulfatierten [G1] - bis [G3]-dendronisierten PBIs mit einem Polyethylenglykol (PEG) Linker synthetisiert, optisch charakterisiert und als regiospezifische Labels durch Konjugation an einen Antikörper untersucht. Die photophysikalischen Eigenschaften der Labels konnten durch Erhöhung des sterischen Anspruchs und der Ladungsmenge des eingeführten Dendrons verbessert werden, was zu hoch fluoreszenten PBIs mit Fluoreszenzquantenausbeuten (FQAs) bis zu 100% führte. Rezeptorbindungs-, Zytotoxizitäts- und zelluläre Aufnahmestudien bestätigten die Eignung der PBIs als regiospezifische Labels. Im zweiten Projekt wurden [G1]- bis [G3]-dendronisierte PBIs für die Synthese von fluoreszenten Polymernanopartikeln bestehend aus linear dendronisierten Polyolen (LDPs) eingesetzt. Der verstärkte dendritische Abschirmungseffekt der verschiedenen [G*n*]-PBIs wurde durch den Anstieg der FQAs ihrer jeweiligen LDPs von 7,8 auf 23% ersichtlich. Die Einführung von zwei verschiedenen Fluorophoren in ein Polymerrückgrat führte zu großen Stokes-Verschiebungen, die durch das Auftreten von Förster-Resonanzenergietransfer (FRET) verursacht wurden. Die fluorophorkonjugierten LDPs zeigten keine zytotoxischen Nebenwirkungen und wurden erfolgreich in zellulären Biobildgebungsstudien eingesetzt. Im dritten Projekt wurden einwandige Kohlenstoffnanoröhren (EWNRs) mit linearen Polymeren funktionalisiert, die mit neutralen oder geladenen [G2]-dendronisierten PBIs ausgestattet waren, was zu

fluoreszenten Polymer-EWNR-Komplexen führte. Die Polymerumhüllung verbesserte die Zytokompatibilität der Nanoröhren und ermöglichte die direkte Abbildung ihrer zellulären Aufnahme über die PBI- und EWNR-Emission unter Verwendung des 1. und 2. optischen Fensters. Dabei zeigten geladene Komplexe eine überlegene Dispergierbarkeit von EWNR, intrazelluläre Fluoreszenzintensität und zelluläre Aufnahme gegenüber ihren neutralen Gegenstücken. Eine abschließende Nebenstudie bestätigte das Konzept der dendritischen Seitenisolierung von Fluorophoren am Beispiel eines PG-dendronisierten Nahinfrarot- (NIR) Cyaninderivates. Der Farbstoff wies einen pH-gesteuerten Anschalt-/Abschalt-Fluoreszenzmechanismus auf und zeigte gute Färbeeigenschaften bei der Bildgebung von Makrophagen.

Zusammenfassend führte die Einführung von (geladenen) sterisch anspruchsvollen PG Dendrons und monofunktionalisierten Linkern an kernunsubstituierten PBIs zu wasserlöslichen, hoch fluoreszenten und regiospezifischen Biolabels. Diese Ergebnisse zeigen das vielseitige Potential dendronisierter PBIs als Fluoreszenzlabels und versprechen deren vielfältige Anwendung in zukünftigen Biobildgebungsstudien.

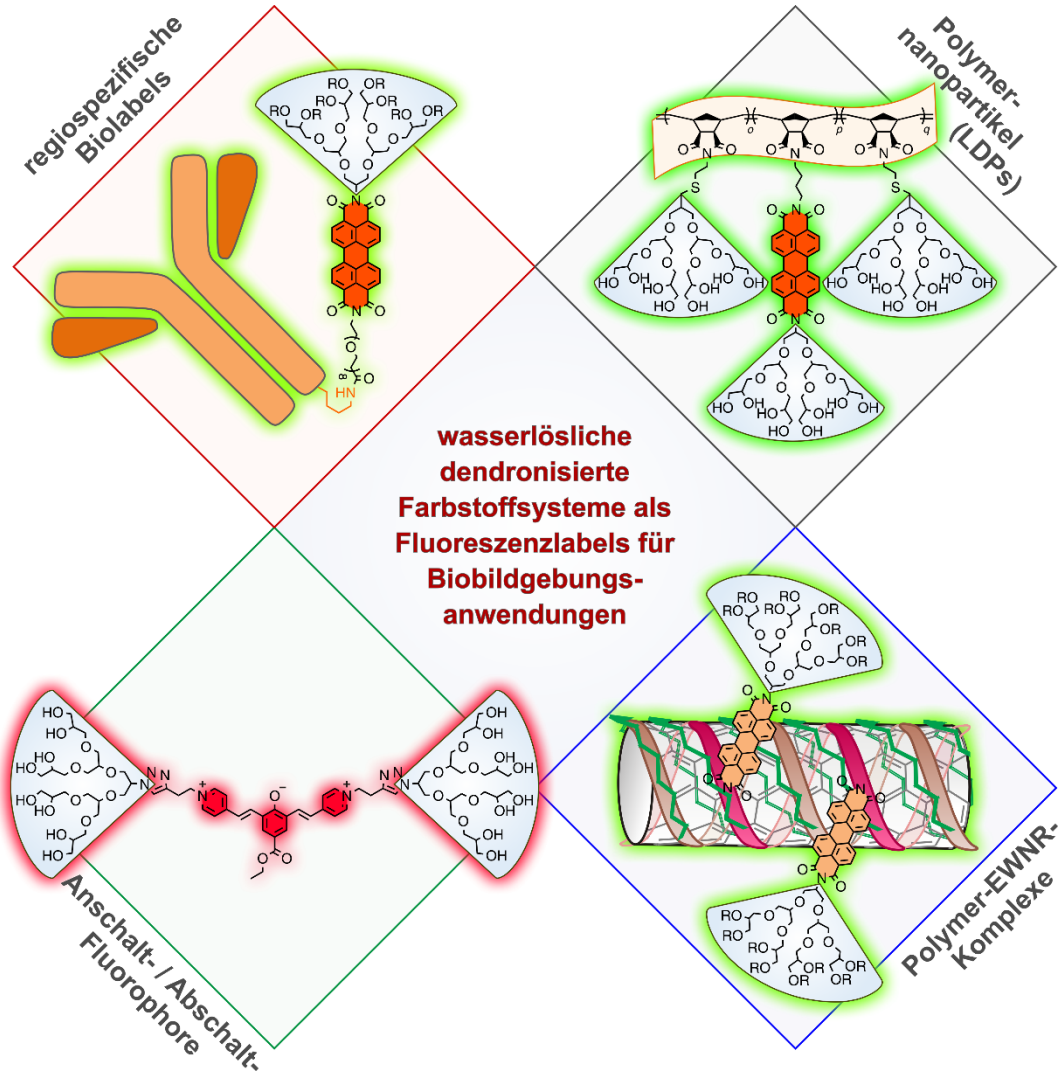

Übersicht über die vier in dieser Arbeit enthaltenen Projekte. Die Farbhervorhebung der Strukturen entspricht der Wellenlänge ihrer Emissionsmaxima (R = OH oder SO_4^-).

Contents

1 Introduction **1**

2 Theoretical Background **3**

2.1 Functional Dyes and Pigments ... 3

2.2 Perylene Dyes and Pigments ... 4

2.2.1 Perylene Bisimides ... 5

2.2.1.1 Imide-Substituted PBIs ... 7

2.2.1.2 Bay-Substituted PBIs ... 9

2.2.1.3 Ortho-Substituted PBIs ... 12

2.3 Fluorescence and Phosphorescence ... 15

2.3.1 Förster Resonance Energy Transfer ... 17

2.4 Fluorescence Bioimaging ... 19

2.4.1 Fluorescent Organic Nanoprobes in Bioimaging ... 20

2.4.1.1 Single-Walled Carbon Nanotubes in Bioimaging ... 20

2.4.1.2 Fluorescent Polymer Nanoparticles in Bioimaging ... 23

2.4.2 Fluorescent Labels and Staining Agents in Bioimaging ... 26

2.4.3 Water-Soluble PBIs ... 28

2.4.3.1 Aggregation Patterns of PBIs ... 31

2.4.3.2 Water-Soluble PBIs as Site-Specific Biolabels ... 33

2.5 Dendritic Site Isolation of Fluorophores ... 35

3 Motivation and Objectives **39**

4 Publications **41**

4.1 Noncharged and Charged Monodendronised Perylene Bisimides as Highly Fluorescent Labels and their Bioconjugates ... 41

4.1.1 Author Contributions ... 42

4.2 Linear Dendronized Polyols as a Multifunctional Platform for a Versatile and Efficient Fluorophore Design ... 57

4.2.1 Author Contributions ... 58

4.3 Fluorescent Polymer–Single-Walled Carbon Nanotube Complexes with Charged and Noncharged Dendronized Perylene Bisimides for Bioimaging Studies ... 67

4.3.1 Author Contributions ... 68

4.4 Enhancement of Fluorescent Properties of Near-Infrared Dyes using Clickable Oligoglycerol Dendrons ... 81

4.4.1 Author Contributions ... 82

5 Summary and Conclusion **89**

6 Future Perspectives **97**

7 Bibliography **101**

Appendix **115**

A.1 SI *Chem. Eur. J.* 2017, *23* (20), 4849-4862 115

A.2 SI *Polym. Chem.* 2018, *9* (15), 2040-2047 145

A.3 SI *Small* 2018, *14* (28), 1800796 175

A.4 SI *Org. Biomol. Chem.* 2015, *13* (16), 4727-4732 213

List of Publications and Conference Contributions **239**

Curriculum Vitae **241**

1 Introduction

Dyes and pigments are an integral part of our daily lives that impart color to the environment and make it look more appealing. In prehistorical times natural colorants were used to color caves, fabrics, and pottery (Figure 1.1a).[1] Nowadays colorants cover a broad range of applications from textile, pharmaceutical, food, cosmetics, plastics, paint, and paper industry (Figure 1.1b).[2] The major difference between dyes and pigments is their solubility.

Dyes are mostly organic substances that dissolve in the used medium and adhere to the applied material through the formation of covalent bonds and noncovalent interactions.[3] According to a dye theory by O. N. Witt in 1876,[4] an organic dye consists of three components: the i) chromogen, ii) chromophore, and iii) auxochrome (Figure 1.2). The chromogen is a colored or colorless conjugated compound (e.g., one or more benzene rings), which can be rendered colored by the attachment of suitable substituents. One of these substituents is a chromophore, which is an unsaturated, usually electron-withdrawing group (e.g., -N=N-, -C=O) bearing the color. The other one is an auxochrome or antiauxochrome which is an electron-donating (e.g., -OH, $-NH_2$) or -accepting group (e.g., $-NO_2$, -C=O), respectively, intensifying the color of the chromophore.[2] Mesomeric interactions between auxochromic and antiauxochromic groups via the conjugated π-system have a bathochromic effect on the absorption maximum of the dye. In addition, these groups endow the dye with solubility and support the dye-substrate affinity.[5] Some common chromophores present in organic dyes are azo, anthraquinone, phthalocyanine, nitro, methin, or nitroso groups.[2]

Pigments are colored, colorless, or fluorescent finely ground solid particles or crystals of organic or inorganic nature.[2] They are insoluble materials that need to be dispersed in a carrier or binder, also called vehicle, for an application to the substrate. After the substrate treatment, the binder dries out and attaches a fine layer of pigments to the material. Due to their insolubility pigments remain physically and chemically unaffected by the

Figure 1.1. a) Ancient cave paintings of a bison painted with natural dyes and pigments. Reprinted with permission from Ref. [6] (© 2014 The Royal Chemical Society). b) Dye powders for textiles in various colors at a market stall. Reprinted with permission from Ref. [7] (© 2018 The Royal Society of Chemistry).

incorporated vehicle. While dyes impart color solely by selective light absorption, pigments can impart color by selective light absorption and reemission via light scattering or reflection of certain wavelengths. Generally, dyes are more widely applicable than pigments due to a higher substrate compatibility, color brilliance, and color strength, but are also more susceptible towards photobleaching, heat exposure, and chemical agents. Therefore, dyes are typically used for coloring textiles, paper, and foodstuffs, whereas pigments are used for paints, plastics, and cosmetics. Dyes and pigments can be divided into natural colorants obtained from plants, animals, or minerals and synthetic colorants generated by chemical processes.

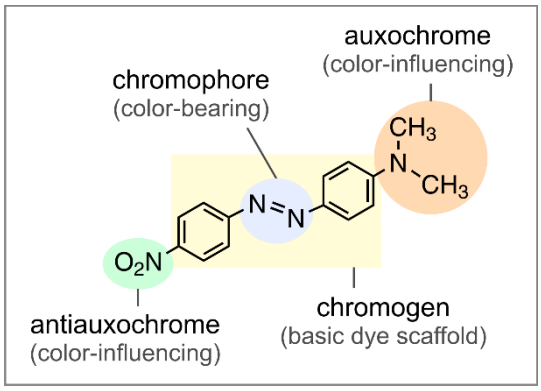

Figure 1.2. Chemical structure of an organic dye molecule consisting of a conjugated chromogen (benzene rings), a color-bearing chromophore (azo group), and two color-influencing groups, the auxochrome (dimethylamine group) and antiauxochrome (nitro group), shown as an example of 4-nitro-4'-(*N,N*-dimethylamino)-azobenzene. Adapted with permission from Ref. [5] (© 2003 Wiley-VCH Verlag GmbH & Co. KGaA, Weinheim).

Ever since prehistorical times, mankind has utilized natural dyes like red iron oxide obtained from red soil, sepia derived from cuttlefish, or Indian yellow generated from the urine of cows.[8] Some of the natural dyes were hard to obtain or expensive to produce. Tyrian purple also referred to as royal purple is gained from the sea snail Murex brandaris. An amount of 12,000 snails was required to obtain approximately 1.4 g of the dye, which is why only eminent royal and church dignitaries could afford this color.[9] A revolution in colorant history began with the discovery of synthetic dyes like Berlin Blue produced by J. J. Diesbach in 1706,[10] mauveine produced by W. H. Perkin in 1856,[11] or synthetic indigo produced by A. Baeyer in 1878.[12] Besides their conventional use as coloring agents, dyes and pigments are nowadays used for their technological function, which opened up the new class of functional dyes and pigments.[13]

2 Theoretical Background

2.1 Functional Dyes and Pigments

Functional dyes are not utilized for their aesthetic coloration but for their functional activity determined by the physical, chemical, and electronic properties of the chromophore. They can be classified by five features or activities, including light absorption or emission, photochemical or photoelectric activity, and light-induced polarization.[13] The design of these functional dyes allows them to interact with electromagnetic radiation, pH, electricity, heat, pressure, and frictional forces.[14] Since the color of functional dyes is not of primary importance, they cover a broad range of wavelengths from 300 to 1,500 nm extending from the near ultraviolet (NUV, $<$ 400) via the visible (Vis, 400-700 nm) to the near infrared (NIR, $>$ 700 nm) region of the electromagnetic spectrum.[14] Therefore, colorless molecules that absorb in the NUV or NIR not visible to the human eye are also assigned to this dye class. They are used for specific applications in areas such as high-tech electronics, photoreprography, laser technology, biochemical analytics, and medical diagnostics.[13]

One of the most important functional pigments found in nature is chlorophyll shown in Figure 2.1a. It converts light energy into chemical energy stored in molecular bonds of carbohydrates to fuel the plants' biological processes. During photosynthesis, carbon dioxide and water are rearranged to carbohydrates (e.g., sugars) and oxygen with the help of sunlight (bottom in Figure 2.1a). Therefore, chlorophyll regulates the atmospheric oxygen level and supplies plants and organisms with the energy necessary for their lives.[15] Another class of functional pigments are carotenoids, which are used as colorants in foodstuffs. They absorb light energy for photosynthesis in plants and protect chlorophyll from photodamage; β-carotenes also act as antioxidants and precursors of vitamin A in living organisms.[16]

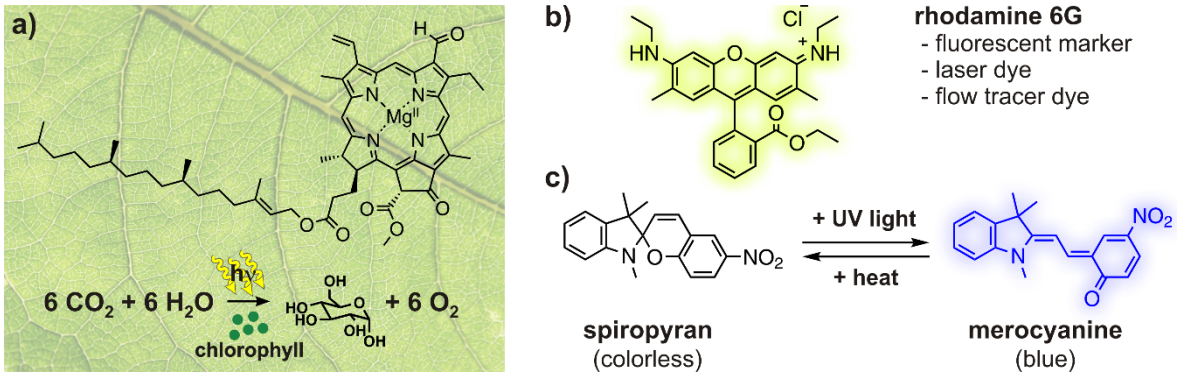

Figure 2.1. Photochemically active functional dyes and pigments. a) Structure of leaf pigment chlorophyll b, which converts light energy into chemical energy during photosynthesis. Bottom: reaction of photosynthesis, which converts carbon dioxide and water into sugar and oxygen, promoted by sunlight. Leaf background from Ref. [17] (© 2018 Pixabay). b) Structure of the functional dye rhodamine 6G and its applications. c) Photochromic functional dye based on a spiropyran system for high-tech applications.

A common synthetic functional dye is rhodamine 6G depicted in Figure 2.1b. Due to its emitting properties and photostability, it is used as dye or gain medium in lasers,[18] fluorescent marker in microscopy studies,[19] and tracer dye of waters in float tracing methods.[20] An example for a functional dye with photochromic activity is spiropyran shown in Figure 2.1c. Spiropyran is an UV-absorbing, colorless compound, that becomes intensively colored by light absorption and regenerates thermally in the absence of light. Its reversible turn-on/turn-off mechanism based on an electrocyclic reaction by UV photoexcitation makes the dye popular in light filters, window panes, sunglasses, and light monitors.[13]

The class of functional pigments includes colored or colorless as well as pearlescent, luminescent, or phosphorescent particulate compounds of organic or inorganic nature with anti-corrosive, electrically or thermally conductive, or special effect features.[21] The most significant applications for functional pigments are surface coatings followed by plastics, inks, and cosmetics. Particularly in automotive industry, special effect pigments with thermochromic, photochromic, or fluorescent properties are popular due to their infinitive array of colors and light effects. Typically, functional dyes and pigments consist of polyunsaturated or polycyclic aromatic compounds, such as perylene dyes, which have become an emerging research topic in recent decades.

2.2 Perylene Dyes and Pigments

Perylenes are planar, polycyclic, aromatic hydrocarbons based on the framework of two naphthalene units linked in the peri positions (Figure 2.2a). They were first isolated by R. Scholl in 1910[22] and represent the smallest member in the family of rylene dyes. Rylenes dyes are naphthalene oligomers, also referred to as poly(peri naphthalene)s (PPNs, Figure 2.2b). In the homologous series of rylenes, additional naphthalene units are added to the perylene scaffold ($n = 0$) along the long molecular axis resulting in the higher rylene homologs termed terrylene ($n = 1$), quaterrylene ($n = 2$), pentarylene ($n = 3$), and hexarylene ($n = 4$). The highest rylene homolog that has been synthesized to date is the octarylene bisimide.[23, 24] The absorption and emission properties of rylenes correlate to the size of the dye scaffold with longer wavelengths for higher rylene homologs (Figure 2.2c).[25, 26] In contrast, the fluorescence quantum yields (FQYs) drastically decrease from 94 to 5% from perylene to quaterrylene due to the enhanced π-stacking of the extended aromatic core system. Derivatives of terrylene (TBI) or quarterrylene (QBI) have been used as key fluorophores in single-molecule studies or as NIR absorbers in laser marking technologies due to their red-shifted absorption.[27-29] A striking achievement by Müllen *et al.* was the

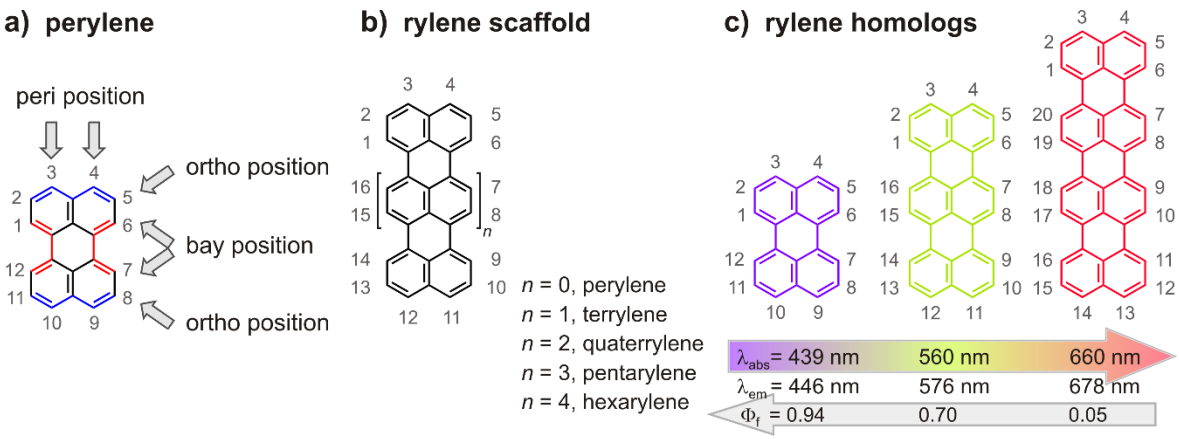

Figure 2.2. a) Structure and substitution patterns of perylene. b) Rylene scaffold and the corresponding denotation of higher rylene homologs determined by the number *n* of naphthalene units. c) Higher rylene homologs and their absorption and emission maxima covering a range of ≈ 220 nm as well as their FQYs.[25]

preparation of highly fluorescent nanoparticles by surface decoration of polyphenylene dendrimers with rylene derivatives.[30-33] Depending on the chromophoric alignment, the particles could serve as single-photon sources; additional introduction of donor and acceptor dyes into the particles led to light-harvesting complexes.

Perylene dyes possess outstanding chemical, thermal, and photochemical stability and are available in large scale for low costs. The major drawback of perylenes, however, is their poor solubility, which has hampered them from extensive use. Owing to the ability to functionalize the dye in various positions, a variety of highly soluble perylene-based derivatives has been developed. The three common substitution patterns of the perylene scaffold include the outer peri positions (3, 4, 9, 10), bay positions (1, 6, 7, 12), and ortho positions (2, 5, 8, 11), as depicted in Figure 2.2a. The substitution at the peri positions with imide functions gives the respective perylene mono- or bisimides, which possess an increased photostability due to the electron withdrawing character of the imides.[34]

2.2.1 Perylene Bisimides

The leading representative among the perylene derivatives is perylene-3,4,9,10-tetracarboxylic bisimide (PBI). Initially, PBIs were applied as high-performance pigments in the coloration of automotive paints, synthetic fibers, and engineering resins due to their insolubility but variety of colors in a solid state.[21, 35] PBI pigments hold a pronounced crystallochromic behavior that is caused by the correlation of crystal packing and absorption maximum (color) in the solid state. The various structures of the imide substituents in the PBI periphery lead to a different crystal packing, which in turn affects the degree of orbital overlap of adjacent molecules. A better orbital overlap results in a bigger bathochromic shift

in absorption, yielding a wide palette of pigment colors between black and red (right side in Scheme 2.1).[35-37]

The first technical synthesis of PBI pigments was patented by M. Kardos in 1913.[38, 39] Since then, the manufacturing process of PBI pigments remained almost unchanged as shown in Scheme 2.1.[21] First, 1,8-ethylenenaphthalene **1** is oxidized to naphthalene-1,8-dicarboxylic anhydride **2** under catalysis of vanadiumpentoxid. Subsequent imidization of **2** with ammonia gives naphthalene-1,8-dicarboxylic imide **3**, which is dimerized via an oxidative coupling to perylene-3,4,9,10-tetracarboxylic bisimide (PBI) **4** in the presence of molten alkali at high temperatures over 200 °C. Hydrolysis of PBI **4** with sulfuric acid yields perylene-3,4,9,10-tetracarboxylic bisanhydride (PBA) **5**, which undergoes a condensation reaction with primary aminated aliphatic or aromatic substituents to give the corresponding organo-soluble imide-functionalized PBIs **6**. The poor solubility of PBIs is caused by the strong aggregation tendency of the aromatic core via intermolecular π-π stacking interactions. By specific substitution in the imide or core positions of the dye framework, the solubility behavior as well as the optical properties including the absorption and emission maximum can be controlled (Figure 2.3). The availability of highly soluble PBIs has extended their application to fields such as laser dyes,[40, 41] photovoltaic cells,[42] fluorescent solar collectors,[43] or organic light-emitting devices (OLEDs).[44] The versatile synthetic modifiability of these functional dyes has led to extensive research on PBIs in scientific fields such as supramolecular chemistry,[45] organic electronics,[46] and cellular research.[47]

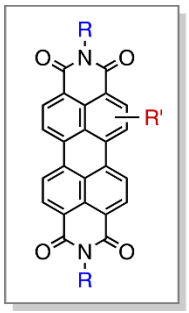

control of properties by substitution:

R controls:
- solubility
- aggregation
- photostability

R' controls:
- solubility
- absorption maximum (color)
- emission maximum

Figure 2.3. Chemical structure of PBI with different substitution patterns controlling the properties of the dye.

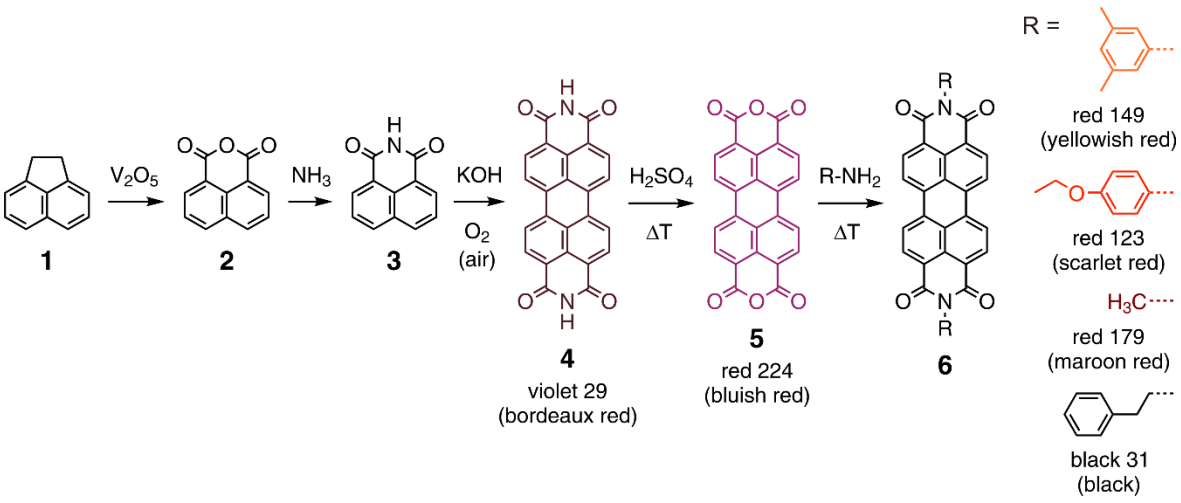

Scheme 2.1. Technical synthesis and color index of commercially available pigments based on PBA **5** and PBIs **6** including their colors.

2.2.1.1 Imide-Substituted PBIs

The first organo-soluble PBIs pioneered by Langhals *et al.* in the 1980s were archived by introducing sterically demanding linear or cyclic alkyl substituents or ortho-substituted aryl substituents in the imide positions (Figure 2.4a).[48-50] Particularly the so-called "swallowtail" substituted PBI **7** (see insert in Figure 2.4b) with secondary branched 1-hexylheptyl residues offered excellent solubility ($>$ 100 g/L), fluorescence properties, and photostability in common organic solvents.[48] These features made them suitable compounds for applications as laser dyes[40] or reference standards in relative FQY measurements.[51] The absorption and emission spectra of swallowtail PBI **7** represent the characteristic band shape typically obtained for imide-substituted PBIs (Figure 2.4b). The absorption spectrum shows a vibronic fine structure with three major absorption bands belonging to the stated electronic transitions and a high molar absorption coefficient of around 90,000 M^{-1} cm^{-1}.[51] The corresponding emission spectrum is nearly a perfect mirror image of the absorption with a small Stokes shift of 9 nm and a FQY of unity in common organic solvents.[50-55] The spectral similarity among imide-substituted PBIs is due to the electronic decoupling of the imide

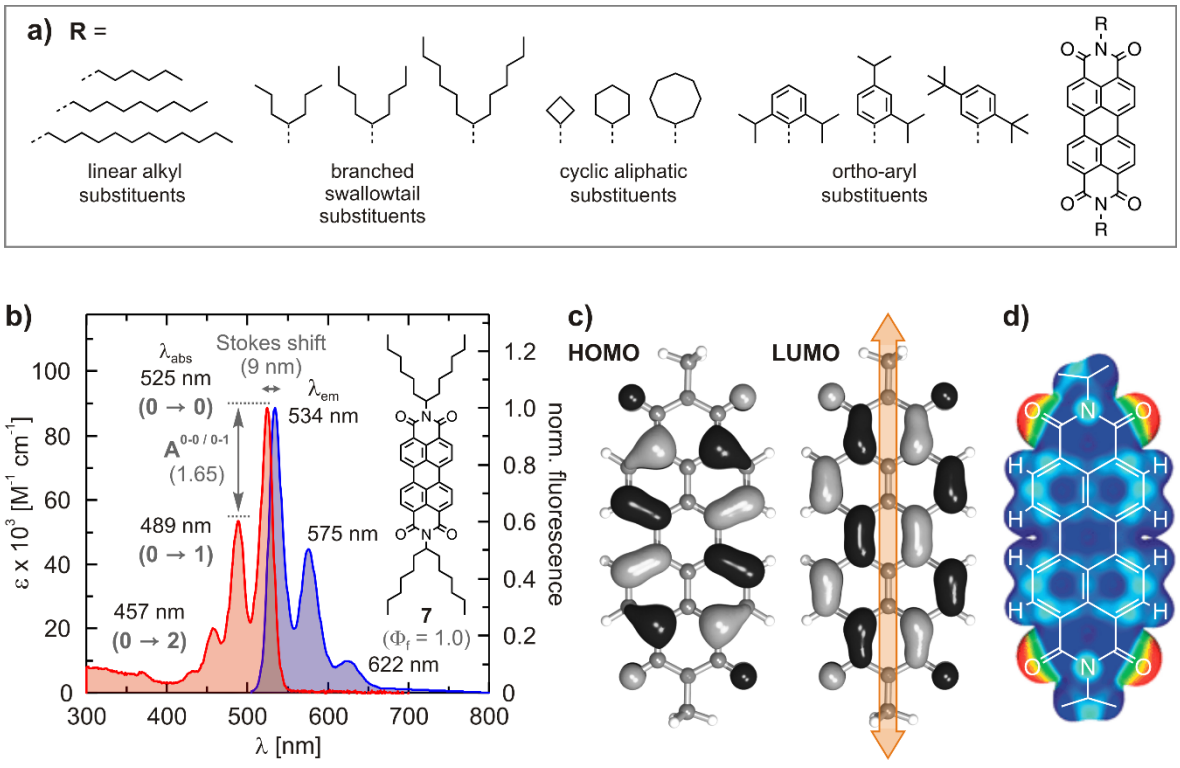

Figure 2.4. a) Sterically demanding imide substituents of organo-soluble PBIs. b) Absorption (red) and normalized emission (blue) spectra of swallowtail PBI **7** at 1 µM in DCM. Absorption maxima belonging to the stated vibronic transitions and optical properties including emission maxima, peak ratio $A^{0\text{-}1/0\text{-}2}$, Stokes shift, and FQY. c) Frontier orbitals of *N,N'*-dimethyl PBI according to DFT calculations. The arrows indicate the orientation of the $S_0 \rightarrow S_1$ transition dipole moment along the long molecular axis. Adapted with permission from Ref. [46] (© 2011 American Chemical Society). d) Electrostatic potential surface of *N,N'*-dimethyl PBI from DFT calculations indicating electron-deficient (blue) and -rich (red) areas. Adapted with permission from Ref. [56] (© 2009 The Royal Society of Chemistry).

substituents from the π-conjugated system of the chromophore. The decoupling is caused by orbital knots at the highest occupied molecular orbital (HOMO) and lowest unoccupied molecular orbital (LUMO) in both imide nitrogens. The orbital knots are represented by the frontier orbitals for the electronic transition between the ground state (S_0) and first excited state (S_1) in Figure 2.4c.[57] The symmetry of the molecular orbitals suggests a dipole moment of the $S_0 \rightarrow S_1$ transition polarized along the long molecular axis.[36, 58] The influence of imide substituents on the frontier orbital energies of the PBI is limited to inductive effects that cause only small spectral shifts in absorption and emission (< 5 nm).[59] Therefore, imide substituents are mainly utilized to introduce moieties that provide solubility,[48, 50] suppress aggregation,[52, 60] or tune the functional properties of the condensed matter.[45, 56] The solubility and aggregation behavior can be controlled by the type and size of the substituents.

However, there are two examples in which imide substituents exert an influence on the optical properties of the chromophore. While the HOMO-LUMO band gap remains unchanged by imide substitution,[57] the energy of both frontier orbitals increases with the electron-donating effect of the substituents. When the orbitals of the substituents are located above the electronic ground state of the PBI, a photoinduced electron transfer (PET) from the electron-rich substituent to the electron-deficient PBI might occur involving fluorescence quenching effects.[61, 62] Also aryl-substituted PBIs exhibit fluorescence quenching, when the substituents in the imide positions are not fixed in an orthogonal conformation with, e.g., *iso*-propyl or *tert*-butyl groups in the ortho positions of the substituent. The resulting non-radiative deactivation process was attributed to a torsional vibration of the aryl group around the R-N bond described as "loose bolt effect".[50, 53] Due to these effects, only moderate FQYs have been reported for electron-rich phenoxylated PBIs[53, 61] ($< 5\%$) and simple phenylated PBIs[58] (70%), whereas, for example, 2,4-di-*tert*-butylpheny substituted PBIs showed an excellent FQY of 100%.[53]

The electrostatic potential surface of *N,N'*-dimethyl PBI shows a pronounced quadrupole moment with the highest electron density located at the four carbonyl oxygens and the lowest density in the bay regions (Figure 2.4d).[45] The resulting electron deficiency of the central PBI core creates a high electron affinity, which delivers an additional binding strength that can be used to assemble higher-order superstructures. The planar π-conjugated PBI surfaces can undergo strong Van der Waals interactions that lead to one-dimensional self-assembled stacks.[63] The optical properties of the π-π aggregates may differ widely as a consequence of individual intermolecular dye interactions (Figure 2.5a). Würthner *et al.* conducted extensive research on supramolecular PBI architectures.[45] They showed the correlation between the structural assembly and fluorescence properties for monomeric,

dimeric, and polymeric chirally substituted PBIs **8** in solution (Figure 2.5b).[45, 64] The chiral side chains influence the chemical equilibrium of the M/P aggregate conformations on a higher level of organization with left-handed (M) helices for dimeric and right-handed (P) helices for polymeric columnar stacks (Figure 2.5a).

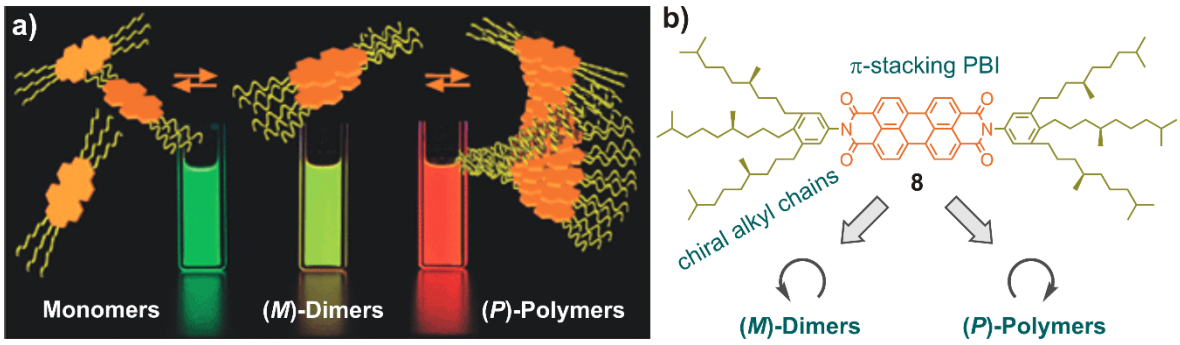

Figure 2.5. a) Aggregation equilibria of PBIs bearing alkylated phenyl substituents in both imide positions and their characteristic fluorescence in solution. Adapted with permission from Ref. [56] (© 2009 The Royal Society of Chemistry). b) Chemical structure of PBI **8** bearing phenyl substituents with chiral alkyl chains, which influence the chemical equilibrium of the aggregates.

2.2.1.2 Bay-Substituted PBIs

In contrast to the imide substituents, bay substituents can have a significant impact on the electronic, structural, and optical properties of PBIs. The bay substitution with electron-donating or -withdrawing residues can vary the absorption maximum from the complete visible up to NIR region. This variation is caused by shifting the HOMO and LUMO of the fluorophore through interactions with the orbitals of the bay substituents. Π-donor substituents have a stabilizing effect on the HOMO and π-acceptor substituents a destabilizing effect on the LUMO. This effect is often associated with the loss of the vibronic fine structure and results in a bathochromic shift of the absorption and emission maxima. The substitution with electron withdrawing groups such as F, Cl, or Br results in a small bathochromic shift in absorption (< 5 nm) for analogous halogenated PBIs relative to their unsubstituted parent due to the weak π-donor strength of the halogens.[62] Electron-donating substituents such as phenoxy, pyrrolidino, or other cyclic amines raise the HOMO to a greater extent than the LUMO.[65-70] The resulting bathochromic shift in absorption and emission is proportional to the π-donor strength of the respective substituent. This effect is demonstrated by PBIs equipped with moderate donating phenoxy (**10**) and stronger donating methoxy groups (**11**) in respect to their unsubstituted parent **9** (Figure 2.6a). Substitution with a stronger π-donor like nitrogen yields an even bigger modulation of the electronic band gap, which leads to a bathochromic shift of up to 170 nm towards long

absorption wavelengths of about 700 nm. The dramatic red shift is caused by a quadrupolar charge transfer from the nitrogens to the perylene,[71-73] which results in a pronounced solvatochromism and a decrease in FQY in the case of pyrrolidino di-bay-substituted PBIs.[62] Also the substitution with carbon in form of aryl or alkynyl substituents through catalytic couplings yields a red shift in absorption due to the extension of the π-conjugated dye system.[74, 75] The extent of the shift depends on the character of the substituent bound to the carbon.

In addition, bay substituents can cause a sterically induced twist of the two naphthalene moieties forcing the substituents out of the PBI plane. The torsional angle of the twist depends on the number and steric bulk of the substituents.[56, 69] For example, the torsional angle between the two naphthalene planes of tetramethoxy PBI **11** was determined with 31° (Figure 2.6b).[76] Although the twist of the PBI core potentially leads to a hypsochromic shift, the above mentioned effects leading to a bathochromic shift often dominate.[46] The twisted core and bulky substituents prohibit a tight molecular packing and thus strongly increase the solubility of the PBIs by lowering aggregation.[46, 77] Normally, bay-substituted PBIs mainly aggregate in dimers, which is why they are not suitable to form extended π-stacking architectures.[78] However, no distortion was observed for planar fluorine,[79, 80] cyanine,[81] or diphenylphenoxy[82] 1,7-substituted PBIs proving that bay substitution does not necessarily involve a core twist.

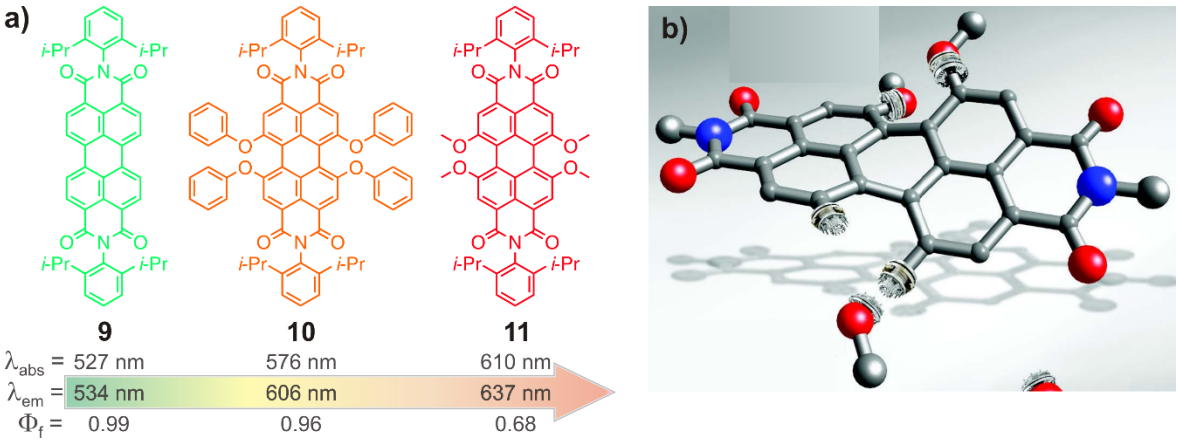

Figure 2.6. a) Chemical structures of core-unsubstituted PBI **9** and core-substituted PBIs bearing four phenoxy (**10**) or methoxy substituents (**11**) in the bay positions as well as their corresponding absorption and emission maxima and FQYs. b) Schematic molecular structure of tetramethoxy-bay-substituted PBI **11** twisted in the naphthalene units. Adapted with permission from Ref. [76] (© 2016 The Royal Society of Chemistry).

Bay-substituted PBIs are synthesized by nucleophilic substitution or transition metal-catalyzed cross couplings of the halogenated PBI key intermediates as displayed in Scheme 2.2. 1,6,7,12-tetrachloro (**12**) or 1,7-dibromo (**13**) PBIs are obtained by imidization of the corresponding halogenated PBA **5**. Dibrominated PBI **13** is often obtained in a mixture of

1,7- (major) and 1,6-dibromo (minor, ca. 10-20%) regioisomers.[66, 83] Bay substitution was first accomplished by Seybold and coworkers at BASF in 1989 through nucleophilic displacement of chlorine by phenolate yielding tetraphenoxy PBI **14**.[84] Straightforward nucleophilic substitution of 1,7-dibromo PBI **13** with fluoride,[79] phenol,[34] pyrrolidine,[71] or cyanide nucleophiles[81, 85] leads to the corresponding bay-substituted PBIs **15** to **18** with distinct optical and electronic properties. Palladium-catalyzed C-C couplings such as Sonogashira,[86, 87] Suzuki,[74, 88] and Stille[89, 90] reactions have also been employed to synthesize alkynyl- and aryl-functionalized PBIs **19** and **20**, respectively.

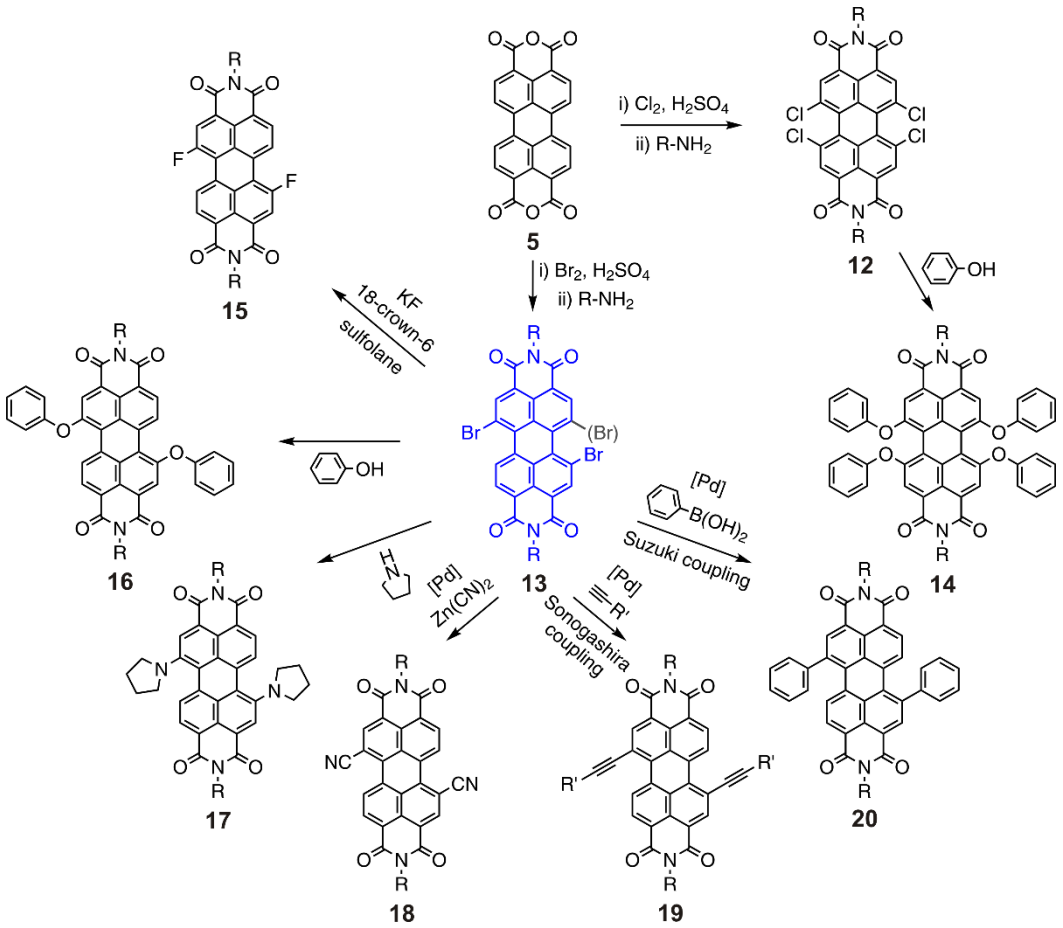

Scheme 2.2 Synthetic strategies towards various bay-substituted PBIs starting from dibromo PBI **13**.

Recently, Spenst and Würthner demonstrated an interesting turn-on/turn-off fluorescence mechanism using bay-phenoxylated PBIs (Figure 2.7a).[91] They prepared para-xylylene-bridged PBI cyclophanes **21** as host molecules for the complexation of a series of electron-poor or -rich guests molecules shown in Figure 2.7b. The guest encapsulation into the rigid PBI cavity was carried out by the formation of a 1:1 arylene@PBI cyclophane complex. The resulting FQYs of the various arylene@PBI cyclophane complexes and the free host molecule PBI **21** are depicted in Figure 2.7b. It was found that the complexation

with electron-poor guests like anthraquinone, 9-fluorenone, or biphenyl resulted in an increased fluorescence intensity with FQYs up to 100%. In contrast, the complexation of electron-rich guests like pyrene, anthracene, or perylene led to a drastic fluorescence quenching with FQYs far below that of the uncomplexed host ($\Phi_f = 21\%$). The fluorescence increase was ascribed to a reduced electronic coupling of the two PBI chromophores by intercalation of the electron-poor guest molecule between their cofacial π-surfaces.[92] By contrast, the fluorescence quenching was attributed to an intermolecular charge-transfer (CT) process from the HOMO of the electron-rich guest molecule to the HOMO of the photoexcited PBI cyclophane as described in the insert of Figure 2.7b. Additionally, electron-rich host-guest complexes displayed a significant red-shifted emission of up to 60 nm to a maximum of 690 nm, indicating emission originating from CT states. Thus, guests with an energetically lower-laying HOMO compared to that of host **21** boosted the emission by reduced PBI-PBI coupling, while guests with a higher-laying HOMO erased the emission by host-guest CT interactions. Therefore, these PBI cyclophanes could be applied as dual turn-on/turn-off fluorescent probes for the sensing of electron-poor and electron-rich guest molecules.

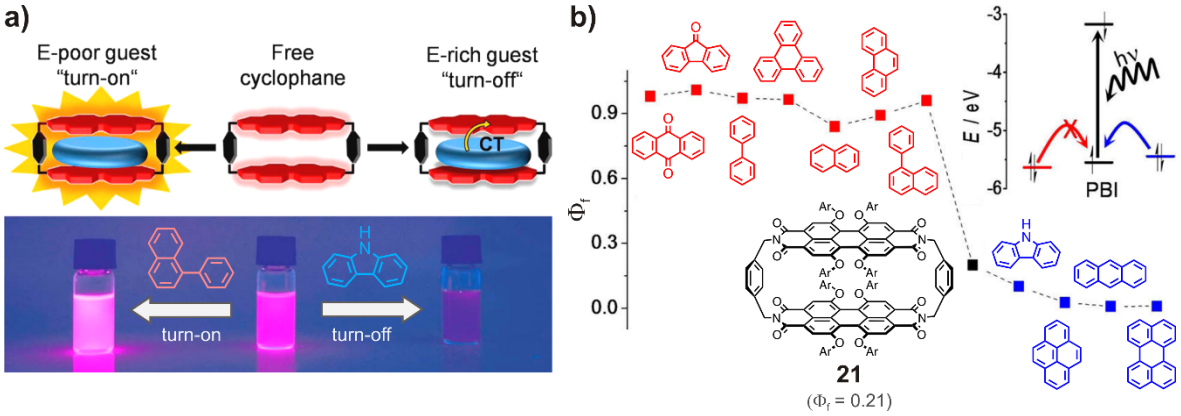

Figure 2.7. a) Schematic illustration of the turn-on/turn-off fluorescence mechanism of PBI cyclophane **21** upon complexation with electron-poor and electron-rich aromatic guests (top). Photograph of the turn-on/turn-off fluorescence (bottom). Adapted with permission from Ref. [45] (© 2015 American Chemical Society). b) Plot of the FQYs of the different host-guest complexes. Electron-poor guests are depicted in red and electron-rich guests in blue, the free para-xylylene-bridged PBI cyclophane host molecule is shown in black. Inset: schematic illustration of the oxidative fluorescence quenching mechanism by formation of an arylene@PBI cyclophane complex with electron-rich guest molecules.

2.2.1.3 Ortho-Substituted PBIs

In contrast to the classic functionalization patterns in the peri and/or bay positions of the PBI scaffold, which have been known since the 1980s, substitution in the ortho positions has only been explored in recent years. A substitution of the ortho over the more reactive bay positions was achieved by a C—H activation and addition strategy with transition metal catalysts that were ortho-directed by the carbonyl oxygens of the imides (Murai–Chatani–Kakiuchi protocol).[93, 94]

In 2009, Osuka *et al.* reported the direct ruthenium-catalyzed reaction of PBI with terminal alkenes or arylboronates resulting in alkyl[95] (**22**) or aryl[55] (**23**) 2,5,8,11-tetrasubstituted PBIs (Scheme 2.3). Interestingly, alkyl and aryl ortho substituents showed different effects on the optical properties of the PBIs. Ortho-alkylated PBIs **22** exhibited optical properties similar to their unsubstituted precursor **6** with high FQYs up to 94%.[95] Also the absorption spectra of aryl-substituted PBIs **23** resembled the fine-vibronic structure of core-unsubstituted PBIs **6** with slightly blue-shifted maxima, due to the orthogonal tilt of the aryl groups to the PBI core. However, similar to bay substituents, electron-donating ortho substituents such as MeO-phenyl or bromo-phenyl led to fluorescence quenching of the dye with FQYs between 0 to 15%, whereas PBIs with electron-withdrawing substituents such as (trifluorometyl)phenyl exhibited high fluorescence properties with FQYs of 75%.[55] In comparison, the corresponding core-unsubstituted parent PBI **6** featured a FQY of 98%.

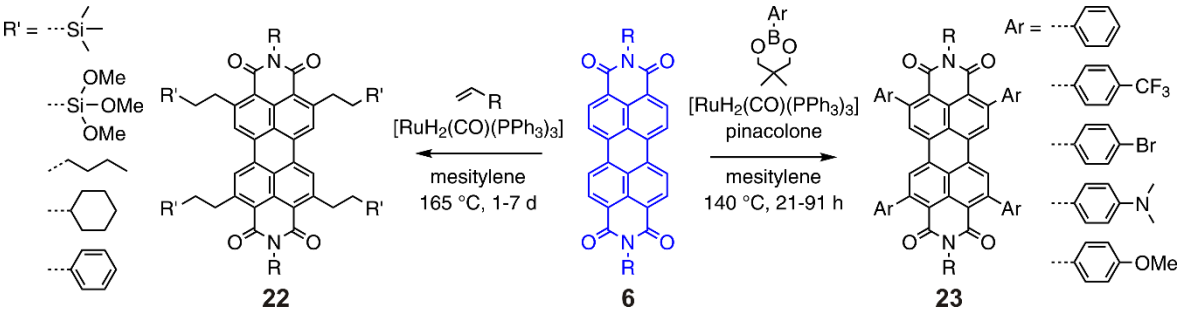

Scheme 2.3. First synthetic pathways towards alkylated (**22**) and arylated (**23**) ortho-substituted PBIs.

In 2011, Shinokubo *et al.* performed the iridium-catalyzed borylation of PBIs **6** that were post-functionalized to ortho-pyridinium (**25**) or ortho-hydroxylated (**26**) PBIs (Scheme 2.4).[96] Tetrahydroxy PBIs **26** exhibited a 13 nm blue-shifted absorption maximum due to the formation of intramolecular hydrogen bonds between the carbonyl and hydroxyl groups. The hydrogen bonds increased the electron-withdrawing nature of the carbonyl groups, stabilizing the HOMO energy level and increasing the HOMO-LUMO band gap. At about the same time, Müllen *et al.* introduced the ruthenium-catalyzed borylation of PBIs. The resulting tetraboronate PBIs **24** were used as key intermediates for tetrasubstituted PBIs

bearing benzonitrile (**27**), or chloro (**28**), bromo (**29**), iodo (**30**), or cyano groups (**31**) in the ortho positions.[97] In 2017, the direct synthesis of tetraiodinated PBIs **30** was reported, thereby replacing the borylation step for the post-functionalization of PBIs. Similar to tetraboronate PBIs **24**, tetraiodinated PBIs **30** served as significant precursors for a variety of ortho-tetrasubstituted PBIs bearing phenylacetylenes (**32**), phenyl groups bound directly (**33**) or via different heteroatoms (**34**), or alkylamines (**35**).[98, 99] The above-mentioned ortho-substituted PBIs featured diverse absorption maxima in the visible range between 446 and 555 nm and high FQY up to 95%.[95] It should be noted that while the bay substitution often involves a propeller-like twist of the PBI core due to the steric strain of the substituents, the ortho substitution retains a planar PBI scaffold due to the steric separation of the substituents. The planarity of ortho-functionalized PBIs makes them ideal building blocks for the construction of conjugated polymers. Starting from tetraiodinated PBI **30**, two different types of microporous conjugated polymers were constructed based on the network of phenylacetylene or diphenylacetylene ortho-substituted PBIs.[99]

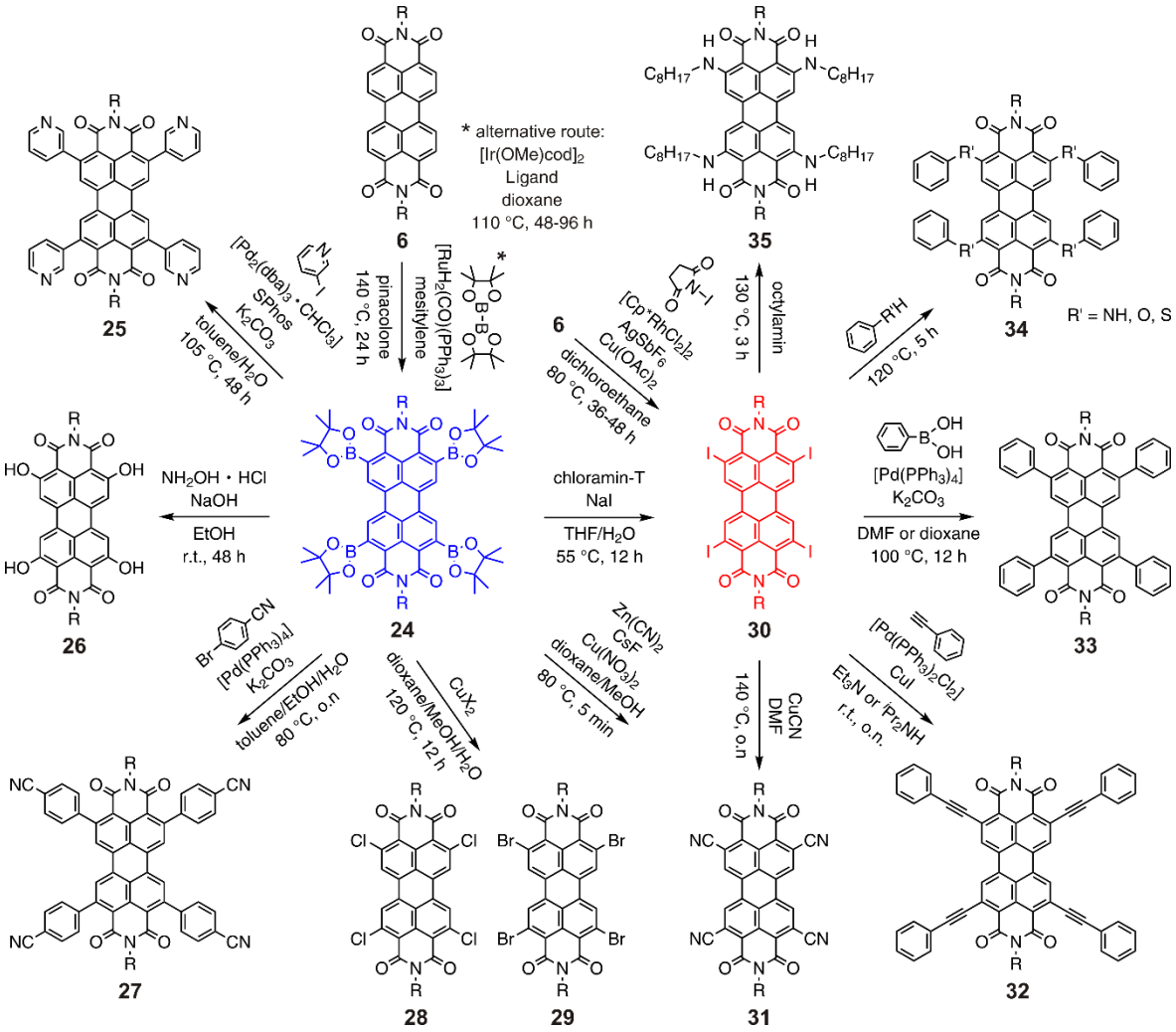

Scheme 2.4. Tetraborylated (**24**) and tetraiodinated (**30**) ortho-substituted PBIs as precursors for a variety of post-functionalization.

2.3 Fluorescence and Phosphorescence

Luminescence is the emission of light by a substrate in form of a body-cold radiation caused by chemical reactions, electrical or mechanical energy, or subatomic motions. Fluorescence and phosphorescence are photoluminescence phenomena emerging from the excitation and deactivation of electrons by photon absorption or emission. Emitted light typically has longer wavelengths and thus lower energy than absorbed light due to the partial dissipation of the absorbed energy, a phenomenon known as the Stokes rule.[5] The fluorescence spectrum is usually a reflection of the absorption spectrum, a fact known as the mirror image rule.

The absorption of energy in form of photons leads to the excitation of electrons from the lowest vibrational level of the electronic ground state (S_0) into any of the vibrational levels of the first or higher excited singlet states (S_1, S_2, S_3, etc.). The photon energy is quantized, allowing the electrons to occupy only discrete energy levels. First, rapid collisions between the molecules in solution lead to relaxation into the vibrational ground state of the respective excited state. The transition from higher excited singlet states S_2 or S_3 into the S_1 state usually occurs by non-radiative internal conversions due to the small energy gap between higher adjacent singlet states. The deactivation of the S_1 state can proceed via several competing non-radiative or radiative pathways illustrated by the Jablonski diagram in Scheme 2.5.[100] Non-radiative deactivation mechanisms of excited state electrons include: i) vibrational relaxation (VR) by dissipation of the excitation energy through collisions with the surrounding molecules (heat), ii) internal conversion (IC) by vibrational coupling of a higher to a lower excited state with equal multiplicity, iii) intersystem crossing (ISC) to an excited state with a different spin multiplicity that subsequently leads to a radiative or secondary non-radiative deactivation process, or iv) external conversion (EC) by interaction with a quencher molecule absorbing the excitation energy.[101] Generally, emission occurs from the lowest vibrational level of the first excited state (S_1 or T_1) to any of the vibrational levels of the ground state and is therefore independent of the excitation wavelength (Kasha-Vavilov rule[1]).[102] Radiative deactivation mechanisms comprise emission in form of: v) fluorescence by singlet-singlet ($S_1 \rightarrow S_0$) transitions or vi) phosphorescence by triplet-singlet ($T_1 \rightarrow S_0$) transitions of excited state electrons, in the latter case after prior ISC.

The major difference between fluorescence and phosphorescence is the lifetime of their excited states determining the duration of emission. While fluorescent materials lose their emission relatively swiftly after excitation within nanoseconds, phosphorescent materials retain their emission for a longer period from milliseconds up to several hours. During the intersystem transition, a singlet state is converted to a triplet state (or vice versa). This

[1] Photon emission (luminescence) occurs in appreciable yield only from the lowest excited state of a given multiplicity (S_1 or T_1). The emission wavelength and luminescence quantum yield are thus independent of the excitation wavelength.

singlet-triplet transition involves a quantum mechanically forbidden spin exchange enabled by a spin-orbit coupling. The spin reversal necessary to deactivate the excited triplet state is less probable and the radiative decay is thus relatively slow. The reversed intersystem crossing from a triplet to singlet state ($T_1 \rightarrow S_1$), caused by triplet-triplet annihilation[2] (P-type) or thermal activation (E-type), leads to emission of delayed fluorescence (DF) with lifetimes half as long or as long as observed in phosphorescence.[102] The efficiency of the fluorescence process can be defined by the FQY (Φ_f), which is the ratio of number of photons emitted to number of photons absorbed (Eq. 3.1).[100] The maximum FQY is equal to 1 meaning that each photon absorbed leads to a photon emitted.

$$\Phi_f = \frac{photons\ emitted}{photons\ absorbed} \tag{3.1}$$

Fluorescence is a concentration-dependent process in which high concentrations increase the possibility of inner filter effects through reabsorption processes,[3] the formation of non-fluorescent ground state dimers, and the emergence of fluorescent excited dimers (excimers[4]). The occurrence of fluorescence can be used as a nondestructive tool for *in vitro* and *in vivo* applications in life sciences. Fluorescent staining agents are used to image biological materials and fluorescent labels are applied to track biomolecules. Furthermore, fluorescence characteristics such as high sensitivity, spatial resolution, and local specificity provide the basis for steady state and time-resolved fluorescence spectroscopy and microscopy, which are used for sophisticated applications in genetics and cell biology.

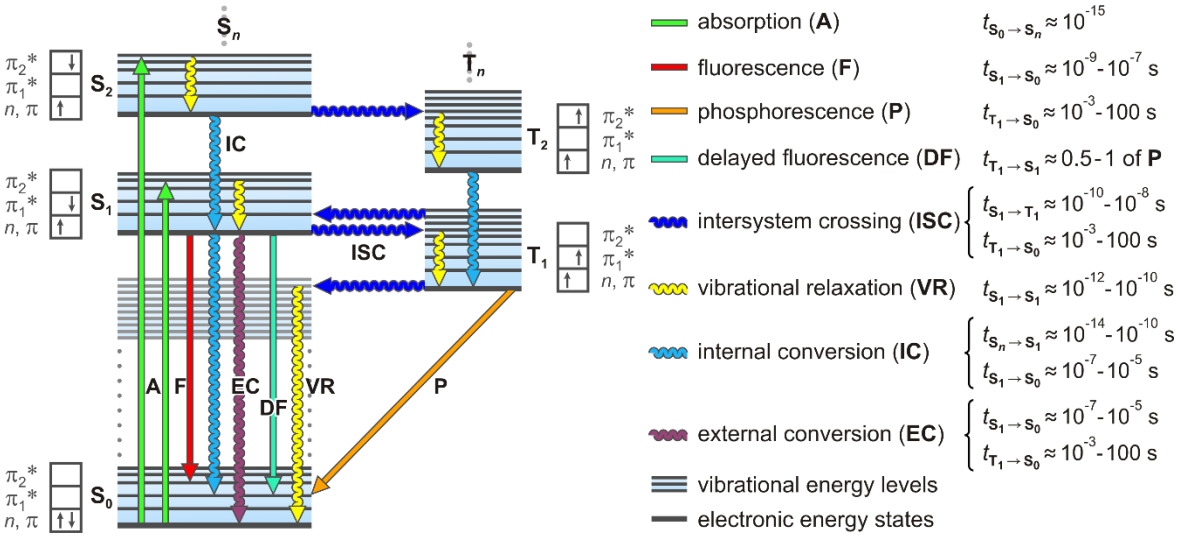

Scheme 2.5. Jablonski diagram (energy scheme) of a photoluminescent system describing the different relaxation mechanisms for excited state molecules. Solid arrows indicate radiative and wavy arrows non-radiative electronic transitions; *t* states the excited state lifetimes belonging to the various electronic transitions. Adapted from Ref. [103] (© 2018 Olympus Corporation).

[2] The collision between two molecules in the T_1 state produces an S_0 and S_1 singlet sate molecule.
[3] Reabsorption is a process in which the emitted radiation of a molecule is reabsorbed by another molecule extinguishing the short-wavelengths part of the spectrum.
[4] Excimers are formed by interaction of an excited monomer with a monomer in the ground state ($M^* + M \rightarrow (MM)^*$) leading to a new emission band at longer wavelengths.

2.3.1 Förster Resonance Energy Transfer

Förster resonance energy transfer (FRET), discovered by Theodor Förster in 1946, is a popular tool for probing intra- and intermolecular interactions over nanometer scale distances with applications in single-molecule experiments,[104] molecular motors,[105] biosensors,[106] and light-harvesting materials.[107] The phenomenon describes a non-radiative quantum mechanical process in which an electronically excited donor molecule transfers excitation energy to a nearby acceptor molecule via long-range dipole-dipole coupling interactions.[108] The non-radiative resonance energy transfer mechanism is demonstrated in the Jablonski diagram in Figure 2.8a. First, a donor molecule is excited by a photon and relaxes to the lowest vibrational level of the first excited singlet state (S_1) according to the Kasha-Vavilov rule.[102] When the conditions for the occurrence of FRET are met, the events of donor fluorescence and energy transfer to the acceptor compete for the decay of the excitation energy. In case an acceptor molecule is located within a minimal spatial radius, the excited electron returns to the ground state in a non-radiative manner without the emission of a photon. The excited state energy of the donor is transferred to an acceptor molecule, whose electrons are excited to a higher electronic state. Upon return to the electronic ground state (S_0), the acceptor emits a photon. This non-radiative energy transfer involving donor-acceptor dipole couplings is referred to as resonance. In the theory of resonance energy transfer, the excited donor fluorophore is treated as an oscillating dipole that can transfer energy to a second dipole having a similar resonant frequency resulting in coupled oscillators. The occurrence of FRET can be detected by quenching the donor fluorescence intensity (I_D) and reducing its fluorescence lifetime, which is associated with an increasing acceptor fluorescence intensity (I_A), also referred to as sensitized fluorescence.

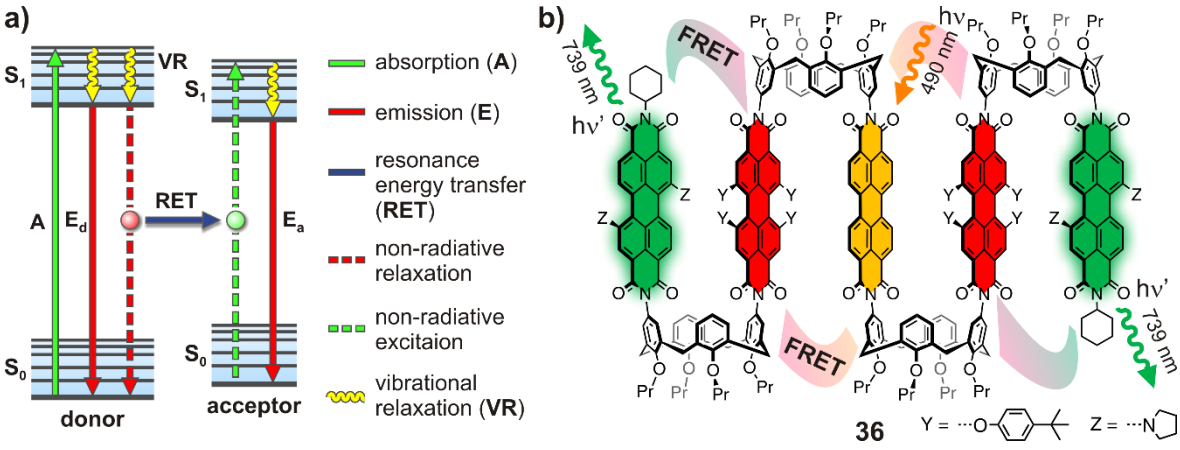

Figure 2.8. a) Jablonski diagram describing the FRET mechanism from a donor molecule to an acceptor molecule resulting in FRET. Solid arrows indicate radiative transitions, dashed arrows non-radiative coupled transitions, and wavy arrows non-radiative transitions. Adapted from Ref. [109] (© 2018 Olympus Corporation). b) Multi-chromophoric PBI-calix[4]arene array **36** displaying sequential FRET by excitation of the middle PBI yielding emission from the outer PBIs. Adapted with permission from Ref. [45] (© 2015 American Chemical Society).

A large acceptor to donor intensity ratio (I_A/I_D) is indicative of a high FRET efficiency that can be associated to a closer proximity or more favorable orientation of the fluorophores. It is noteworthy that the occurrence of FRET is not restricted to fluorescence but can also occur in connection with phosphorescence.[110]

The FRET efficiency (E_{FRET}) is the quantum yield of the energy transfer transition, corresponding to the fraction of energy transfer events that occur per donor excitation event. The formula for the FRET efficiency involves the Förster distance (R_0) of the donor-acceptor pair, which relates to the distance at which the energy transfer efficiency is 50%, and the actual donor-acceptor distance (r, see Eq. 3.2).

$$E_{FRET} = \frac{energy\ transfer}{donor\ excitations} = \frac{1}{1+\left(\frac{r}{R_0}\right)^6} \tag{3.2}$$

The FRET efficiency of the donor-acceptor energy transfer depends on the following criteria: i) the distance between the donor and the acceptor molecules located within 1 to 10 nm spacing, ii) the spectral overlap integral ($J(\lambda)$) between the donor emission spectrum and the acceptor absorption spectrum, iii) the relative orientation of the transition dipole moments of the donor emission and the acceptor absorption spectrum (preferably parallel), and iv) the FQY of the donor in the absence of the acceptor.[111] At distances below 1 nm other possible modes of energy or electron transfer might occur, which is why resonance energy transfer is limited to a 1 to 10 nm distance of two interacting molecules. Differently to Dexter energy transfer, which is based on the collisional exchange of electrons between two molecules separated in the range of a 1 nm distance, Förster energy transfer does not require a collision. FRET efficiency measurements can be utilized to determine if two fluorophores are located within a nanoscale distance to each other. There are three common ways of inferring the FRET efficiency, by measuring either the acceptor emission intensity over time or the donor fluorescence intensity (I) and donor fluorescence lifetime (τ), respectively, in the presence (I_{DA} or τ_{DA}) and absence (I_D or τ_D) of the acceptor (Eq. 3.3).

$$E_{FRET} = 1 - \frac{I_{DA}}{I_D} = 1 - \frac{\tau_{DA}}{\tau_D} \tag{3.3}$$

The transfer efficiency is inversely proportional to the sixth power of the donor-acceptor distance (see Eq. 3.2), which makes FRET highly sensitive to even small changes in distance.[112] The distance dependency provides an ideal method to quantify molecular dynamics and conformational changes of intrinsically or labeled fluorescent proteins.[113] By labeling sub-cellular structures with individual fluorophores, FRET can also be employed to examine the proximity of the labeled molecules within a living cell. An interesting case of a sequential FRET was observed for the multi-chromophoric PBI-calix[4]arene array **36** with five co-facially aligned PBIs in a row, where the excitation of the middle PBI (yellow, λ_{ex}= 490 nm) led to the emission of the outer PBIs (green , λ_{em}= 739 nm; Figure 2.8b).[114, 115]

2.4 Fluorescence Bioimaging

Fluorescence bioimaging has become a virtually indispensable tool for medical, pharmaceutical, and biochemical research. It relates to noninvasive methods to detect and visualize biological molecules, materials, and processes (*in vitro* and *in vivo*) with the help of appropriate fluorescent labels and staining agents. The imaging methods aim to interfere as little as possible with the biomolecule or process observed. The types of specimen that can be observed range from single biomolecules, such as proteins, antibodies, DNA, and virions over subcellular structures, and individual cells, up to tissues and entire multicellular organisms.[116] Fluorescent labeling of intracellular components like nuclei, mitochondria, cytoskeleton, and membranes enables the live-cell imaging of their localization within fixed and living preparations.[117] The current potential of fluorescence bioimaging of cells is shown in the microscopic image in Figure 2.9a. The illustrated bovine pulmonary artery endothelial cell (BPAE) was stained with various fluorescent probes to individually visualize its different cellular components such as mitochondria, cytoskeleton, and cell nuclei.

Recent progress in the field of optical microscopy opened up the possibility of real-time, 3-dimensional, and high-resolution imaging methods on a single-molecular level that helped uncover fundamental biological processes difficult to obtain from ensemble measurements.[118] Typical high-resolution imaging techniques are based on confocal laser scanning microscopy (CLSM) or total internal reflection fluorescence (TIRF) microscopy, which provide a resolution limit of approximately up to 0.2 µm.[118, 119] The method of choice for deep-tissue imaging is two-photon excitation (2PE) microscopy, which enables imaging down to 1 mm depth due to greatly reduced light scattering in biological tissue by multiphoton excitation.[120] If more detail is required, super-resolution techniques, such as structured illumination microscopy (SIM) or stimulated emission depletion (STED) microscopy, allow imaging of a magnitude in the range of 10 to 20 nm with a spatial

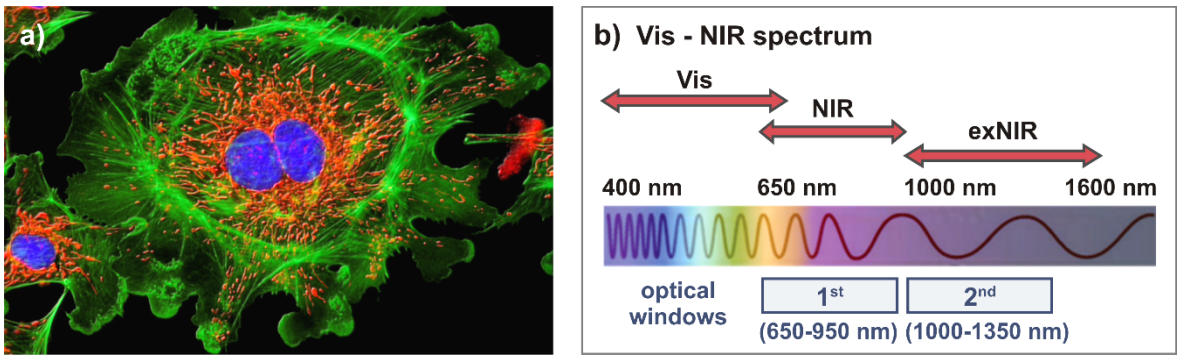

Figure 2.9. a) Microscopy image of BPAE cells, mitochondria stained with mitotracker red CMXros (red), filamentous actin with alexa fluor 488 (green), and nuclear DNA with DAPI (blue). Adapted from Ref. [121] (© 1995-2017 Michael W. Davidson and The Florida State University). b) Electromagnetic spectrum and relative wavelengths of the corresponding electromagnetic waves as well as spectral location of the first and second optical windows. Adapted from Ref. [122] (© 2007-2016 PennWell Corporation).

resolution far below the diffraction limit of light.[123] These new imaging techniques helped to examine a multitude of complex *in vivo* biological processes, including changes in receptor kinetics,[124] molecular or cellular signaling[125] and interactions,[126] as well as movements of molecules through membranes.[127] However, these methods place high requirements on the fluorophores used in terms of photostability or the number of photons emitted, which limits the appropriate fluorophores to a small amount. Fluorescent labels and staining agents that are commonly applied in bioimaging are mostly of organic nature with their fluorescence emission usually located in the visible region or in the first optical transparency window of tissue ranging from the red up to the NIR area (650-950 nm, Figure 2.9b).[128] New developments in the area of nanomaterials, including nanoparticles, -diamonds, -clusters, -wires, -graphenes, and -tubes, have revealed the potential of nanostructures as fluorescence probes for bioimaging in the second optical window (1,000-1,350 nm) located in the extend NIR region.[129, 130] NIR light (700-2,500 nm) is able to penetrate biological tissues, such as skin and blood, more efficiently than visible light, as these tissues scatter and absorb less light at longer wavelengths.[128] Therefore, NIR fluorescent probes are particularly valuable for bioimaging as they allow deep photon penetration into the tissue, minimize photodamage of biological specimen, and produce low autofluorescence from cell components.[131]

2.4.1 Fluorescent Organic Nanoprobes in Bioimaging

Over the past decades, fluorescent organic nanoprobes have emerged as novel imaging tools for monitoring biological processes in cells and organisms. Due to their diverse chemical structures, simple modification, and high FQYs, they have been intensively studied in biosciences as drug carriers and theranostic agents.[129] Modern fluorescent nanoprobes have even been used in complex up-conversion,[132] multiplex,[133] or two-photon emission[134] techniques. The focus of this work rests on photoluminescent single-walled carbon nanotubes (SWNTs) and fluorescent polymer nanoparticles (PNPs) as bioimaging probes.

2.4.1.1 Single-Walled Carbon Nanotubes in Bioimaging

SWNTs are nanoscale cylinders that consist of a sp^2-hybridized lattice of carbon atoms. They possess characteristics such as high mechanical robustness, outstanding thermal and electronic conductivity, as well as long emission wavelengths in the NIR.[135] These unique features make them popular materials in biomedical fields, e.g., as diagnostics and therapeutics or in tissue engineering and biosensing.[135] Their NIR emission and absorption

render them useful fluorescent[136] or photoacoustic[137] imaging agents, as shown in *in vivo* experiments with mice. SWNTs are excellent Raman probes because of their strong resonance Raman scattering and large scattering cross-section, which can be used to sense[138] and image[133] biological samples. The hollow structure and large aspect ratio of the tubes provide a suitable platform for the encapsulation[139] and surface immobilization[140] of drug molecules. The great potential of SWNT as theranostic agents has recently been demonstrated by McFadden *et al.* They reported triple-functionalized SWNTs with reporter molecules (monoclonal antibody), fluorescent markers (fluorescein), and medical drugs (doxorubicin) that enabled the detection, visualization, and treatment of cancer cells through the introduction of a single agent (Figure 2.10a).[141] The antibody- and fluorescein-conjugated bovine serum albumin (BSA) proteins were covalently conjugated to carboxyl groups of the oxidized SWNTs, whereas the doxorubicin drug molecules were loaded onto the tube surface via π-stacking and hydrophobic interactions.

Intensive studies on the biomedical suitability of SWNTs have revealed some adverse effects. The major drawbacks are due to the poor water solubility, cell permeability, biodistribution, and biocompatibility of SWNTs, thereby preventing the exploration of their full bioimaging potential. The toxicity of SWNTs is attributed, *inter alia*, to their large hydrophobic surface, aggregation tendency, and non-biodegradable nature.[142] The evoked toxic effects are primarily caused by membrane or DNA damage, oxidative stress, changes in mitochondrial activity, and altered intracellular metabolic pathways.[142] Surface passivation with polymers proved to be a suitable method to overcome these obstacles. The noncovalent functionalization of the nanotubes with phospholipid poly(ethylene glycol) (PL-PEG) improved the water solubility and biocompatibility of SWNTs (Figure 2.10b i).[143-145]

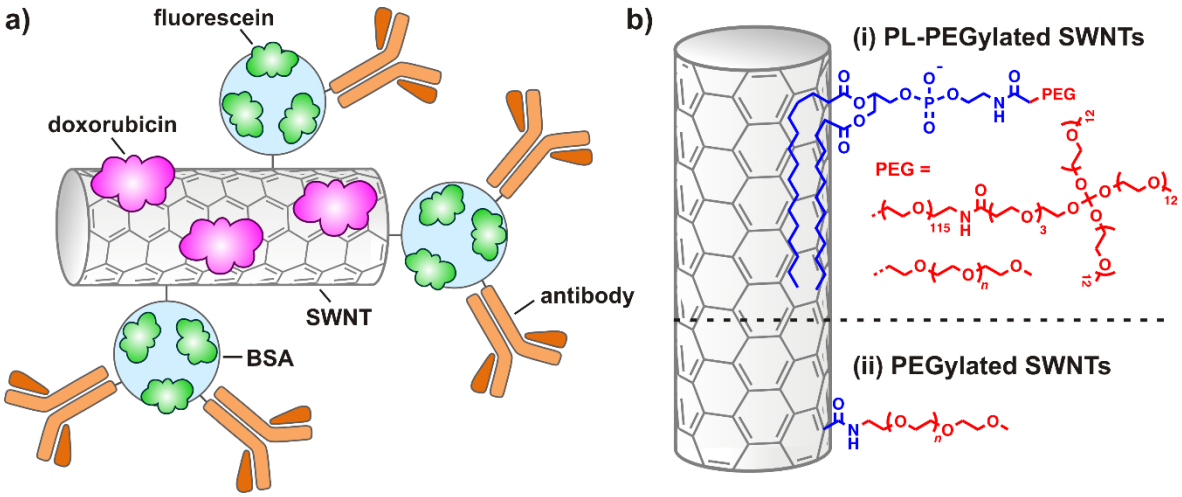

Figure 2.10. a) Triple-functionalized SWNT complex with BSA-conjugated antibodies and dyes as well as immobilized drugs for targeted cancer therapy. Adapted with permission from Ref. [141] (© 2009 Elsevier Ltd.). b) (i) Noncovalently PL-PEGylated SWNTs bearing branched or linear PEG chains. Adapted with permission from Ref. [144] (© 2008 The National Academy of Sciences of the USA). (ii) Covalently PEGylated SWNTs. Adapted with permission from Ref. [140] (© 2007 American Chemical Society).

The phospholipid binds to the nanotubes by virtue of hydrophobic interactions, and the PEG chains confer water solubility and biocompatibility. The PEG coating also reduces the non-specific binding of biomolecules to the tube surface, which alters their cellular interaction pathways and thus decreases cytotoxic effects. Noncovalent binding, however, might be sensitive to environmental factors, such as pH and salt concentration. As an alternative to noncovalently functionalized SWNTs, Dai *et al.* utilized covalently functionalized SWNTs with PEG chains conjugated to the sidewalls of the tubes (Figure 2.10b ii). The PEGylated SWNTs were stable in buffer and serum solutions and have been successfully applied in drug loading studies with doxorubicin.[140] In 2009, Welsher *et al.* demonstrated the bioimaging potential of PL-PEGylated SWNTs, which afforded high FQYs of 84% relative to cholate-suspended SWNTs. The PL-PEG SWNTs enabled whole-body *in vivo* imaging of mice as shown in Figure 2.11.[143] The NIR photoluminescence image taken 30 minutes after injection showed a clear staining of the vasculature beneath the skin as a result of SWNTs circulating in the blood (Figure 2.11c). The SWNTs also allowed deep-tissue imaging, as evident by photoluminescence signals from deeper anatomical regions, likely due to strong uptake into the reticuloendothelial system.

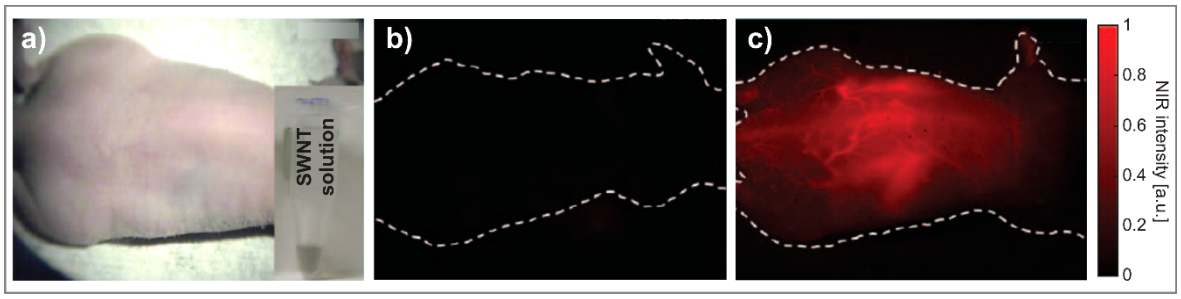

Figure 2.11. a) Nude mouse for *in vivo* treatment with PL-PEG SWNT complexes (insert). b) NIR image of an untreated mouse showing no autofluorescence. c) NIR image of a treated mouse showing strong photoluminescence from the PL-PEG SWNT complexes 30 min after injection. Adapted with permission from Ref. [143] (© 2009 Macmillan Publishers Limited).

In order to use the NIR luminescence of SWNTs for bioimaging, they must be highly suspended in aqueous solution. The suspension with surfactants, such as sodium dodecyl sulfate (SDS) and Triton X-100, gives highly dispersed SWNTs but impairs their already low biocompatibility.[135, 146] Due to the high critical micelle concentration (CMC) of these amphiphiles, an excess of surfactant is required, which might lyse the cell membranes and denature proteins.[145] The polymer wrapping method is a common practice to circumvent this issue.[147, 148] Thereby, polymers wrap around the tubes through noncovalent interactions and introduce water solubility and biocompatibility, while preserving the SWNTs' unique properties.[148] The polymer coating is stable even with changes in pH and other environmental effects. Recent studies showed that the combination of fluorescently labeled

polymers with fluorescein or cyanine dyes and intrinsically photoluminescent SWNTs leads to dual-fluorescent nanoprobes.[149-152] The concept of dual fluorescence could be used to create novel bioimaging probes with a broad optical readout for demanding imaging studies.

2.4.1.2 Fluorescent Polymer Nanoparticles in Bioimaging

In recent years, fluorescent polymer nanoparticles (PNPs) have attracted immense attention owing to their attractive characteristics for applications in bioimaging and -sensing as well as drug delivery.[153] Their large surface-to-volume ratio offers a suitable platform for surface modification with small organic dyes; the polymer matrix shields the fluorophores from their external environment, thereby preventing aggregation-induced quenching and photobleaching.[154, 155] These novel nanomaterials, which were originally inspired by advanced fluorophores and polymeric drug delivery vehicles, combine superior brightness with biodegradability and low toxicity.[156] Moreover, surface bioconjugation with, e.g., biotin, antibodies, or antigenic peptides allows target-specific labeling of cells, tissues, and entire organisms.[157] Optimal PNPs for bioimaging applications feature relatively small diameters in the range of 5 to 50 nm, which can be achieved by techniques such as microfluidics[158] or laser ablation.[159] An alternative to these quite demanding methods is the preparation of PNPs by intramolecular crosslinking of the polymeric backbone, a common method applied to star,[160] hyperbranched,[161, 162] or linear polymers.[163] Figure 2.12 illustrates the ideal properties of PNPs including controllable 1) size, 2) hardness, 3) solubility, 4) external and 5) internal functionality, 6) density/porosity, as well as their ability to be 7) scalable and 8) biocompatible. The integration of a single reactive functional moiety into the nanoparticle would broaden their potential application to target-specific bioconjugation[164] or controlled nanoscale assembly.[165] Typically, the main limitation of ONPs is their lack of water solubility and functionality for post-modification.

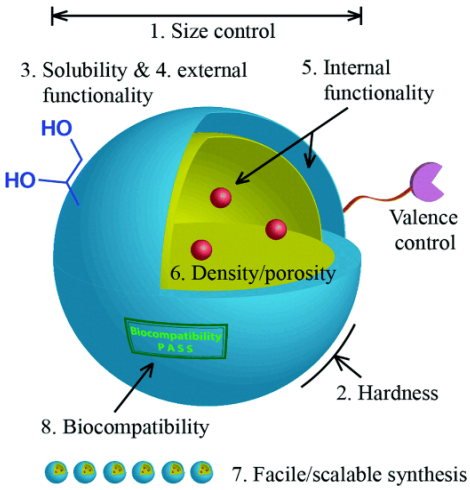

Figure 2.12. Schematic representation of an idealized polymer nanoparticle (PNP) and its desired properties. Reprinted with permission from Ref. [153] (© 2014 The Royal Society of Chemistry).

Zimmerman *et al.* reported water-soluble organic polymer nanoparticles (ONPs) **41** with a single kind of reactive group prepared by simple crosslinking of linear polymer chains.[153] The ONPs were generated from functionalized norbornene monomers equipped with *N*-hydroxysuccinimide

(NHS) esters and fluorescent dyes (Scheme 2.6a). The synthesis consisted of four steps, comprising ring-opening metathesis polymerization (ROMP), incorporation of a cross-linkable tri-*O*-allyl-TRIS unit, ring-closing metathesis (RCM), and final dihydroxylation of the alkene groups to render the ONPs water-soluble. The resulting particles turned out roughly spherical with diameters ranging from 5 to 50 nm. The ONP scaffold provided a protective carrier for the built-in functionalities, which was exemplified by fluorescein dyes. Fluorescein-conjugated ONPs showed significantly enhanced photostability over the free dyes and proved to be good imaging agents on HeLa cells with increased uptake into lysosomes. In a toxicity study, ONPs with smaller particles sizes (≈15 nm) showed improved cell viability compared to ONPs with larger particles sizes (≈47 nm). In a follow-up study, an advanced type of ONPs based on crosslinked dendronized polyols (CDPs) **46** was introduced.[166] CDPs were synthesized in a similar manner to ONPs but did not require the dihydroxylation step due to the use of PG dendrons (Scheme 2.6b).[166] The elimination of the dihydroxylation step using toxic potassium osmate renders CDPs more environmentally friendly and biocompatible imaging agents than ONPs. To verify the shielding effect of CDPs, they were synthesized with a variety of fluorophores, including coumarin, fluorescein,

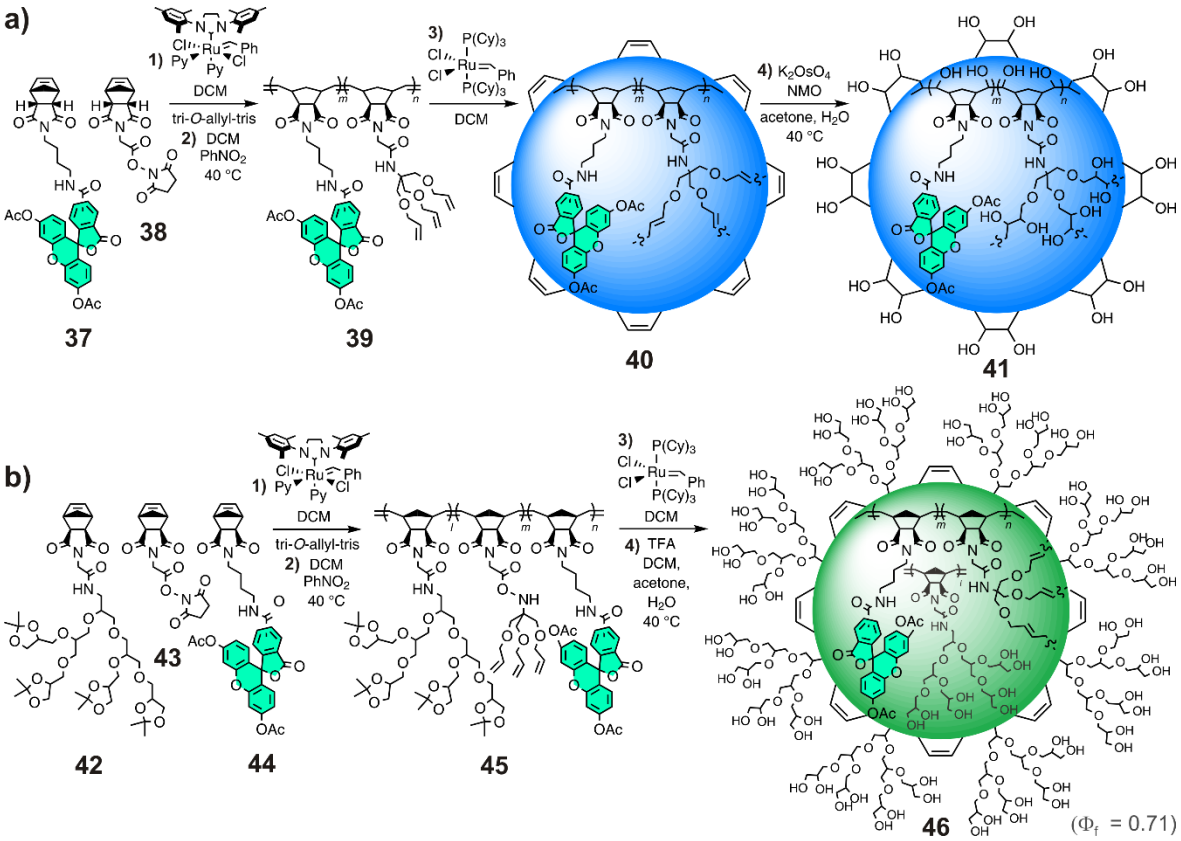

Scheme 2.6. Synthesis of fluorescent PNPs with fluorescein dyes (green) reported by Zimmerman *et al.* a) Organic nanoparticles (ONPs) **41** and b) crosslinked dendronized polyols (CDPs) **46** synthesized though several steps, including 1) ROMP, 2) introduction of a crosslinkable unit, 3) RCM, and 4) dihydroxylation (in ONPs) or acid-catalyzed hydrolysis (in CDPs). Adapted with permission from a) Ref. [153] (© 2014 The Royal Society of Chemistry) and b) Ref. [166] (© 2016 The Royal Society of Chemistry).

bodipy, PBI, and rhodamine. The polyol scaffold tremendously improved the brightness and photostability of the dyes, as shown in photobleaching studies between the CDPs and the free dyes. FQYs between 5 and 71% substantiate adequate dye shielding by the LDP scaffold. The various CDPs showed no cytotoxic effects in a cell viability assay and have been successfully applied as fluorescent imaging agents on HeLa cells. The good cell viability resulted from the small particle diameter (≈6 nm) and cytocompatible dendritic scaffold of the CDPs. These examples demonstrate that dye-conjugated polymers with internal crosslinkable units lead to bright PNPs suitable for cellular bioimaging studies.

Another type of PNPs applicable for bioimaging studies are highly fluorescent π-conjugated polymers.[167] McNeill *et al.* reported conjugated polymers based on polyfluorene (PF), poly(phenylene ethynylene) (PPE), and phenylenevinylene (PPV) with particle sizes in the range of 5 to 15 nm and FQYs between 1 and 40% (Figure 2.13a).[168, 169] These so-called conjugated polymer dots (CPdots) were available in a variety of colors, which opened up the possibility of multicolor fluorescence cell staining performed on macrophages (Figure 2.13b). The large number of tightly packed chromophores resulted in high emission rates and minimal photoblinking in single-particle imaging, which indicates the potential of CPdots for demanding bioimaging applications. However, a drawback that occurs with most conjugated polymers is their lack of hydrophilicity and the accruing poor bioavailability. In this regard, dendritic polyol-based PNP architectures are a good alternative because they are water-soluble and biocompatible.[170]

Besides the covalent conjugation of dyes on the particle surface, fluorescent PNPs can also be synthesized by noncovalent encapsulation of dyes into the particles.[171] Although the encapsulation method provides an easy procedure, it might result in undesirable dye leaching. Covalent linkage can resolve this problem but requires prior functionalization of the dyes with reactive or polymerizable groups.[156] The high brightness and photostability, abundant surface modification, and, most notably, low toxicity of fluorescent PNPs render them excellent fluorescent probes for demanding imaging techniques in biosciences.

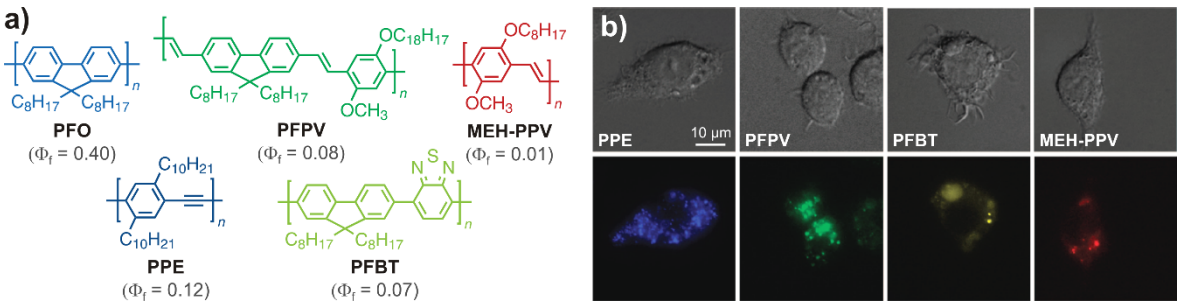

Figure 2.13. a) Chemical structures of fluorescent conjugated polymer dots (CPdots) in the colors of their emission wavelengths. B) Live-cell imaging of macrophages labeled with indicated CPdots. Brightfield channel (top) and fluorescence channel (bottom). Adapted with permission form Ref. [168] (© 2008 American Chemical Society).

2.4.2 Fluorescent Labels and Staining Agents in Bioimaging

In order to visualize selected biomolecules and subcellular structures, a fluorescent label or staining agent is required. Although there is a wide variety of fluorescent labels and agents available nowadays, advanced bioimaging techniques created the demand for novel high-performance fluorescent probes. An adequate fluorescent label ideally features the following characteristics: i) water solubility, ii) high brightness,[5] iii) high photophysical and chemical stability, iv) biocompatibility, v) absorption and emission maxima above 500 nm to minimize the autofluorescence of the cells and background noise of fluorescent impurities,[172] and vi) the availability of conjugatable monofunctionalized derivatives.[173] In addition, the label should not influence the structure and function of the biomolecule of interest.[174] Conventional organic fluorescent dyes often suffer from limitations such as poor hydrophilicity and photostability (photobleaching and -blinking), low brightness and quantum yield, insufficient stability in biological systems, and low detection sensitivity.[175] For example, xanthene dyes like fluorescein[176] and rhodamine[177] tend to turn into their non-fluorescent leuco-form via undesired alkylation or acylation, which ultimately leads to photobleaching.

The origin of fluorophore instability can be explained by the photophysical processes, which a fluorophore undergoes. A fluorophore in its first excited singlet state usually rapidly circles between the S_0 and S_1 states, which results in fluorescence emission (for more detail see Chapter 2.3). The fast time scale on the order of nanoseconds hardly allows reactions with quenchers such as oxygen.[178] A fluorophore in its T_1 state has a significantly longer lifetime, which makes it more vulnerable towards oxidative and reductive degradation processes. These processes can be mediated by solvent impurities (e.g., metal ions), molecular oxygen (O_2), compounds belonging to the attached biomolecule, or even by another fluorophore.[178] These oxidative or reductive electron transfer processes result in the formation of non-fluorescent cationic or anionic radical species of the fluorophore ($R^{\cdot+}$ and $R^{\cdot-}$).[179] Molecular oxygen, whose ground state is a triplet state ($^3O_2$), is an effective quenching agent for triplet state fluorophores and a damaging reactant for biological specimen.[180] Electron transfer from a triplet fluorophore to molecular oxygen generates a superoxide radical ($O_2^{\cdot-}$) and a non-fluorescent cationic form of the fluorophore ($R^{\cdot+}$). Energy transfer from a triplet fluorophore to molecular oxygen generates excited singlet oxygen ($^1O_2$), a strong oxidizing agent (Scheme 2.7a). Reactions with superoxide radicals and singlet oxygen, alongside other forms of reactive oxygen species (ROS), involving the hydroxyl radical ($HO^{\cdot}$), hydroperoxyl radical ($HO_2^{\cdot}$), and hydrogen peroxide (H_2O_2), can lead to

[5] Product of the molar absorption coefficient ε and FQY Φ_f divided by 1,000.

photobleaching of fluorophores[181, 182] and phototoxic effects on biomolecules and cells.[183, 184] ROS are a natural byproduct of the cellular metabolism and are involved in the regulation of many physiological and pathological processes of the cell.[185] However, oxidative stress conditions, e.g., by UV light or heat exposure can increase the level of ROS and promote cellular proliferation and differentiation down to cell death.[186] To protect the fluorophores and biomolecules from irreversible damage by ROS, reducing anti-fading agents[187] or oxygen-scavenging enzymes[188] are added to the imaging solution during cell experiments.

Scheme 2.7b provides a simplified diagram for three different kinetic regimes that bias the performance of a fluorophore. In air-saturated solutions, reactions between molecular oxygen and T_1 are rapid, which results in considerable ROS formation and fast photobleaching (Regime 1). When no molecular oxygen is present, radical states of the fluorophore can be rapidly formed through electron transfer with its surrounding (Regime 2). The $R^{\cdot+}$ and $R^{\cdot-}$ radicals are non-emissive and can be long-lived resulting in pronounced photoblinking and -bleaching. Triplet state quenchers (TSQ) and reducing and oxidizing agents (ROX) can quench T_1 and radical states of the fluorophore and restore its ground state. When such quenching processes occur rapidly, triplet and radical states are short, which results in nonblinking and long-lasting fluorescence (Regime 3).

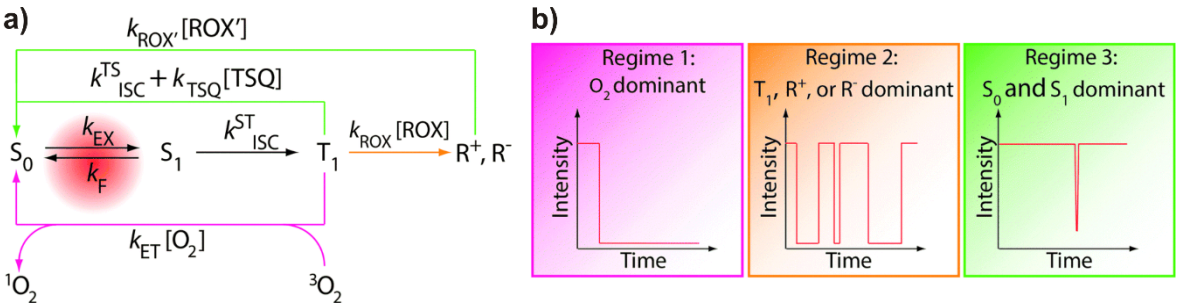

Scheme 2.7. a) Diagram describing the nature of fluorophore instabilities. b) Corresponding kinetic regimes showing the fluorescence intensity over time. TSQ: triplet state quencher; ROX and ROX′: reducing or oxidizing agents. In Regime 1, the fluorophore photobleaches quickly. In Regime 2, the fluorophore blinks frequently. In Regime 3, the fluorophore rarely blinks and lasts long. Adapted with permission from Ref. [178] (© 2014 The Royal Society of Chemistry).

Figure 2.14 gives an overview of classical fluorescent dyes covering the visible to the far-red range of the electromagnetic spectrum with wavelengths between 400 and 770 nm. Fluorophores employed in single-molecule[189] or super-resolution[190, 191] microscopy studies are predominantly based on rhodamine, fluorescein, oxazine, cyanine, BODIPY, or DCDHF (2-dicyanomethylene-3-cyano-2,5-dihydrofuran) dyes (see grey boxes in Figure 2.14). Those fluorophores are typical imaging agents for cells, tissues, and animals with fluorescence emission in the first optical window located at wavelengths between 650 and 950 nm.[128] Current trends in fluorescence probe technology aim to extend the emission of fluorescent probes into the far-red and near-infrared due to higher penetration depth, better image

contrast, and reduced photobleaching and -toxicity by longer wavelengths.[174] Owing to their long emission wavelengths, high photostability, and good biocompatibility, PBIs are ideal systems as fluorescent labels, which led to research on water-soluble PBI derivatives.

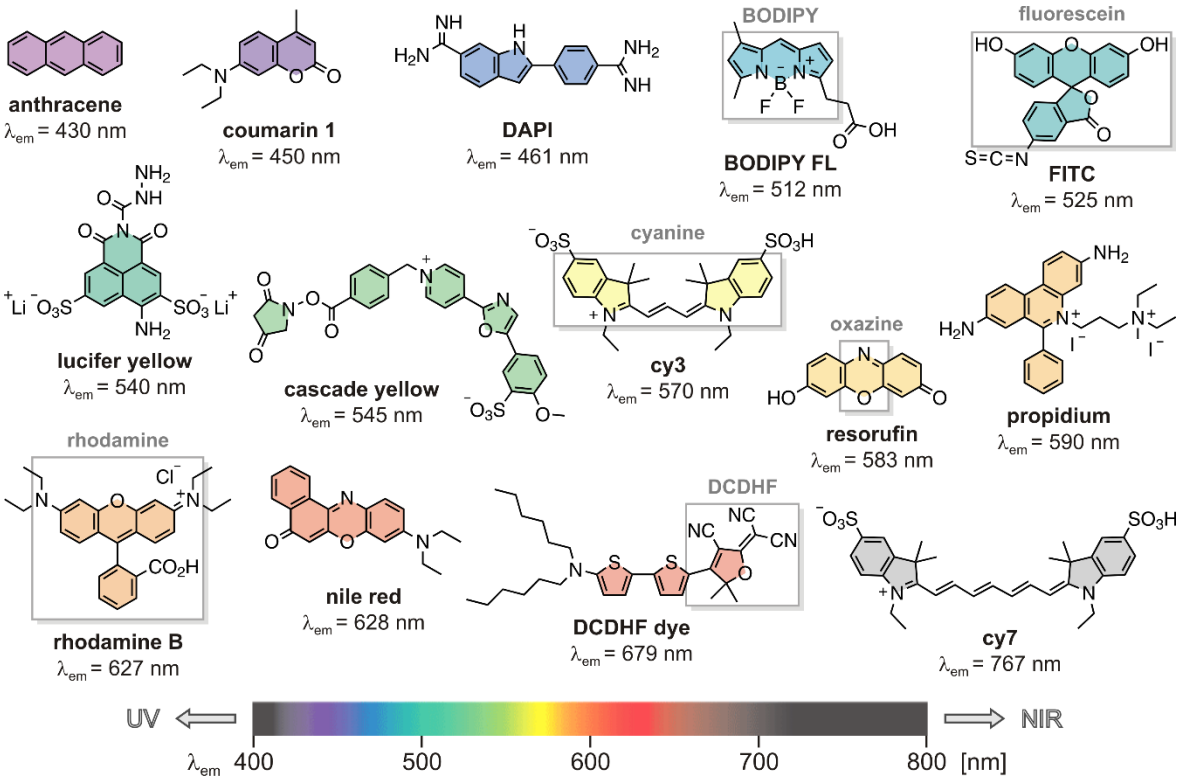

Figure 2.14. Common fluorescent probes for bioimaging studies covering the visible to the far-red range of the electromagnetic spectrum (bottom). The gray boxes highlight the key structures of the dyes.

2.4.3 Water-Soluble PBIs

The introduction of water solubility onto PBIs is a critical issue due to their strong tendency of aggregation, which is additionally enhanced in an aqueous environment by the hydrophobic effect.[192] In recent years, considerable progress has been made by introducing solubilizing substituents in the imide and/or bay positions of the hydrophobic dye core.

The very first approaches towards water-soluble PBIs were achieved by the introduction of charged or uncharged residues symmetrically attached in both sides of the imide positions on core-unsubstituted PBIs. In the late 1980s and early 1990s, Langhals *et al.*, Ford *et al.*, and Schnurpfeil *et al.* used small ionic aliphatic or aromatic residues such as aromatic sulfonate **47**,[193] potassium carboxylate **48**,[194] and quaternized nitrogens **49**[195] as solubilizing imide groups. Later on, a number of other PBIs with temporary or reversibly charged substituents was published, including phosphate tensides **50**,[196] spermine residues **51**,[197] guanidinium moieties **52**,[198] Newkome-type carboxylates **53**,[199] quaternized TRIS

amines **54** and **55**,[200] and sulfated polyglycerol (PG) dendrons **56** (Figure 2.15a).[201] Besides the utilization of charged imide substituents, a range of polar uncharged imide substituents was introduced as solubilizing agents. These polar uncharged substitutes include poly(ethylene glycol) chains **57**–**60**,[202-205] crown ethers **61**,[206] cyclodextrins **62**,[207] amide swallowtails **63**,[208] TRIS amine residues **64**,[209] mannose grafted dendrimers **65**,[210] and PG dendrons **66**[211] (Figure 2.15b). Although the mentioned substituents could render PBIs water soluble, many of them failed to sufficiently suppress the aggregate formation of the respective PBIs to maintain the optical properties of the monomeric dyes. Apart from these approaches, water-soluble PBIs have been archived by encapsulation with large dendritic structures of higher generations to give PBI-cored dendritic star polymers or high molecular weight PBI dendrimers in different core-shell architectures and charge densities variants.[212]

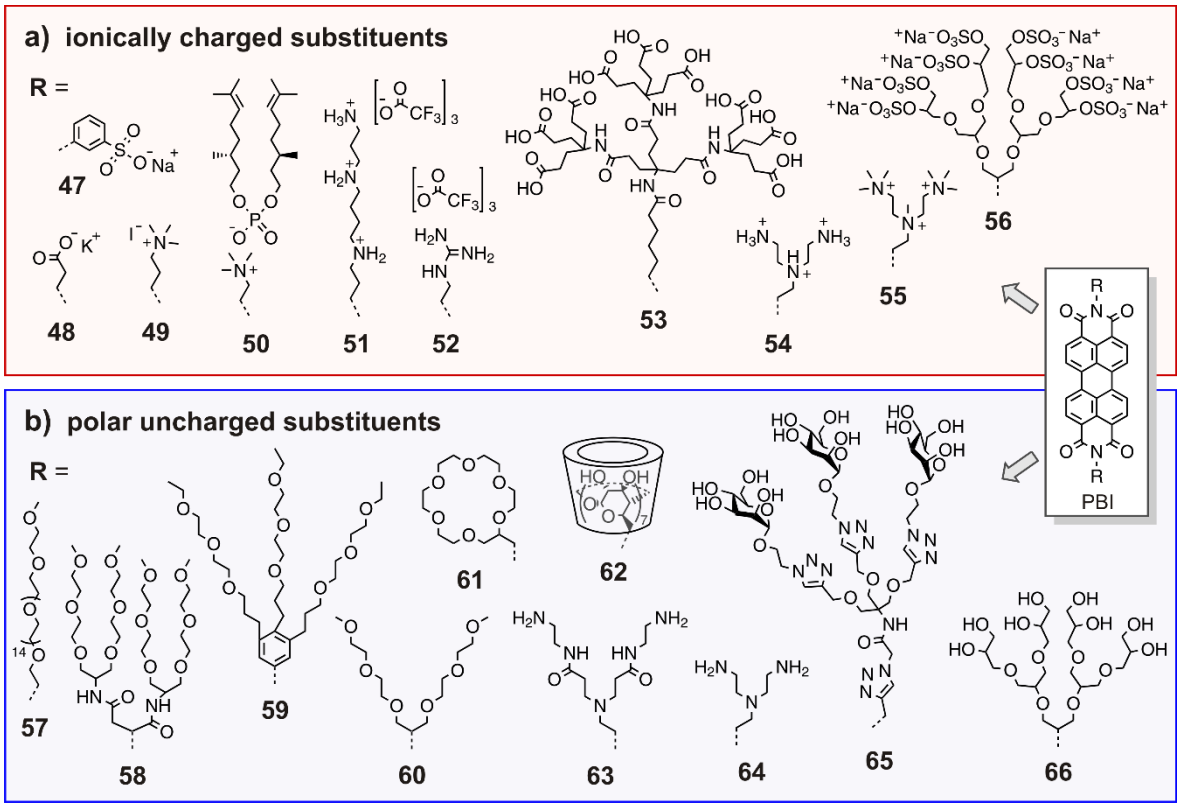

Figure 2.15. Typical a) temporary or reversibly ionically charged and b) polar uncharged imide substituents introduced symmetrically on both sides of the dye core to yield water-soluble PBIs.

Haag *et al.* showed that PBIs retain their outstanding FQYs in water, when aggregation is efficiently suppressed by sterically demanding PG dendrons in both imide positions of the PBI core (**67**, Figure 2.16a). The FQYs of the dendronized PBIs improved with increasing dendron generation from [G1] to [G4] from 33 to 98% (Figure 2.16b).[211] The FQYs of lower-generation dendronized PBIs could be further improved by introducing ionic sulfate groups into the dendron periphery (**68**), resulting in a steric and electrostatic

shielding effect; a powerful combination as evident by high FQYs between 92 and 99%.[201] For molecular bioimaging studies, however, small-size and low-weight fluorescent labels are required, which do not affect the function and shape of the biomolecule after conjugation.[213]

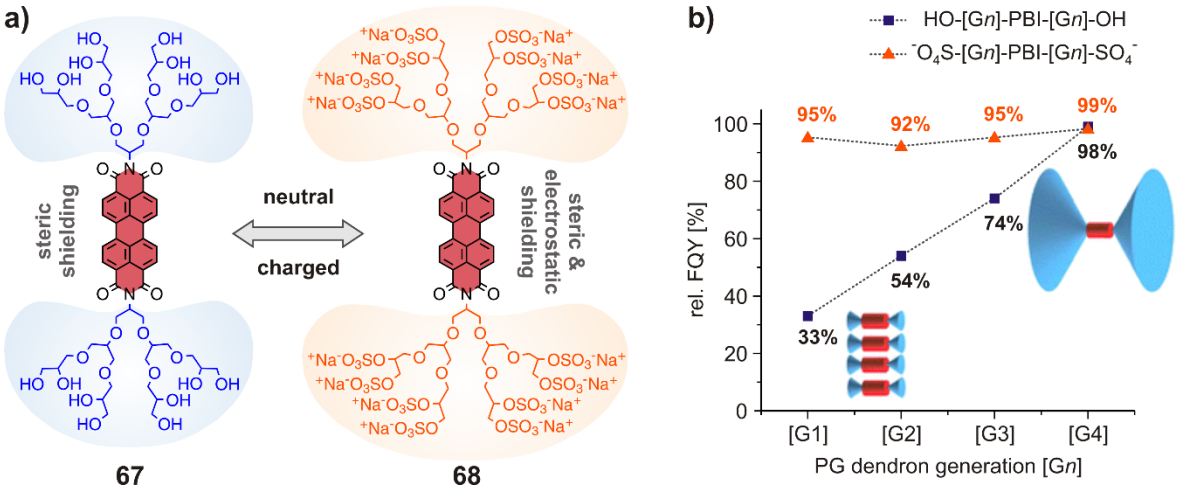

Figure 2.16. a) Structures of neutral hydroxylated (**67**) and charged sulfated (**68**) dendronized PBIs exemplarily shown for [G2]. b) Corresponding relative FQYs of neutral and charged PBIs from [G1] to [G4] measured in water. Adapted with permission from Ref. [211] (© 2010 The Royal Society of Chemistry) and Ref. [201] (© 2016 American Chemical Society).

The above-mentioned works pioneered by the groups of Würthner, Hirsch, and Haag, to name a few, were reported in the years between 2005 and 2016. Beforehand in 2004, Müllen *et al.* reported highly water-soluble PBIs by introducing ionic aromatic residues of low molecular weight including phenoxy substituents with carboxylate residues **69**, sulfonic acid residues **70**, pyridinium salts **71**, or quaternary ammonium salts **72** at the bay positions (Figure 2.17).[214, 215] The resulting PBIs revealed moderate to high FQYs in aqueous solution between 7 and 98%, which for the first time enabled an application of PBIs as fluorescent labels. Later developed PBI-based fluorescent labels were commonly based on the motive of tetraphenoxylated PBI **70** or tetrapyridinium PBI **71b** modified with a monofunctional group in the imide position for site-specific labeling. Indeed, **71b** was the first PBI used as a cellular staining agent, as demonstrated on cardiac fibroblast cells.[173] The high FQYs of these bay-functionalized PBIs are the result of a reduced π-stacking tendency due to the distortion of the PBI core induced by the phenoxy substitutes along with the Coulombic repulsion forces of the charged groups (also see Chapter 2.2.1.2). Although PBIs **70** and **71b** are mostly present as dimers, and thus not molecularly dissolved, the geometry of their aggregates induces only minimal fluorescence quenching, which manifests in high FQYs.[216] These works demonstrate that the introduction of dendritic substituents in the imide positions or small ionic substituents in the bay positions leads to highly fluorescent water-soluble PBIs. These findings paved the way for an application of PBIs as fluorescent probes.

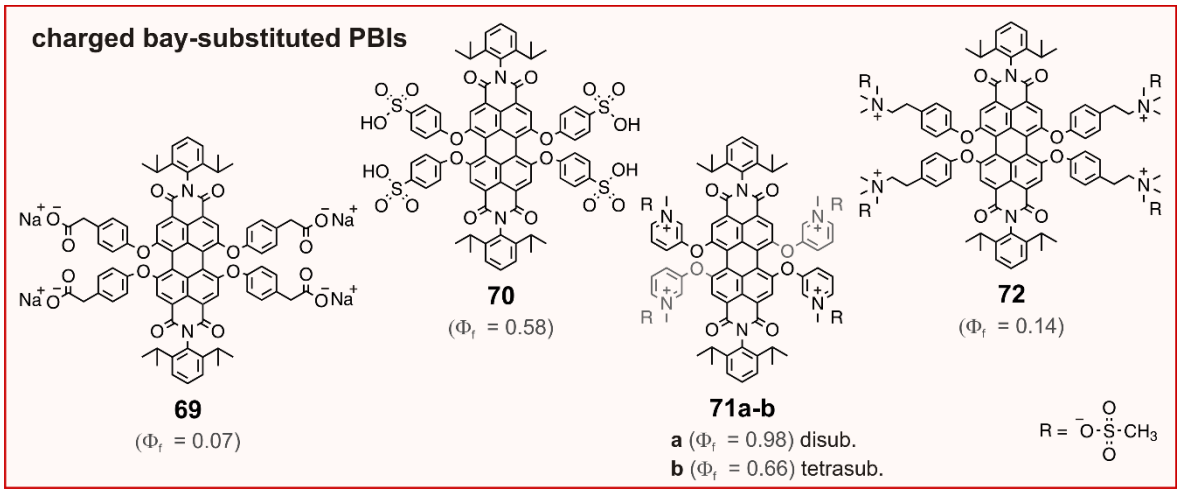

Figure 2.17. Structures of water-soluble PBIs with small ionically charged substituents in the bay positions. Note that PBI **71** exists in a disubstituted (**71a**) and tetrasubstituted (**71b**) version.

2.4.3.1 Aggregation Patterns of PBIs

The increased aggregation tendency of PBIs in aqueous solution leads to drastic changes in the spectral features of the dye.[45] The theory of molecular excitons, published by M. Kasha in 1963, describes the excitonic interactions of the transition dipole moments of chromophores with respect to their geometrical arrangement upon photoexcitation.[217] The theory differentiates between two types of aggregates, J-aggregates and H-aggregates, which lead to different spectral shifts.[218] J-aggregates, named after their discoverer E. E. Jelley in 1936,[219] exhibit a bathochromic shift (red shift) of the absorption band with respect to that of the monomer. They are also referred to as Scheibe-aggregates, as G. Scheibe independently reported on this topic in 1937.[220, 221] By contrast, H-aggregates, named after the term "hypsochromic", exhibit a hypsochromic shift (blue shift) of the absorption band with respect to that of the monomer. The formation of J- and H-aggregates is caused by different arrangements of adjacent molecules within an aggregate, which in turn leads to different interactions of their transition dipole moments.[218, 222] While most J-aggregates are highly fluorescent, H-aggregates are predominantly low or non-fluorescent. Depending on the substitution pattern, PBIs can take on either of the aggregation types, whereas their aggregates generally have lower FQYs than their monomers.[223, 224] The spectral changes observed for H- and J-type assemblies can be explained by Kasha's theory for the simple case of a PBI-PBI dimer (Figure 2.18a). In a dimer aggregate, the energy of the excited state is reduced relative to that of the monomers due to the energy gained by the Van der Waals interaction (ΔE_{VdW}). Dipole couplings of the dye units yield an energetic splitting ($\Delta\varepsilon$, Davydov splitting) of the dimers' excited singlet state in two different excitonic states,

one of higher and one of lower energy.[45, 225] Depending on the spatial arrangement (slip angle Θ) between the transition dipole moments, the photoexcitation from the ground state is allowed into only one of the excitonic dimer states. In J-aggregates, the transition dipole moments are arranged in a collinear manner ($\Theta < 54.7°$), which only allows the transition to the lower energy state involving a bathochromic shift of the absorption band (to lower energies) with respect to the monomer. In H-aggregates, the transition dipole moments are stacked in a parallel manner ($\Theta > 54.7°$), which only allows the transition to the higher energy state leading to a hypsochromically shifted absorption band (to higher energies) with respect to the monomer. In the latter case, the transition to the allowed state, which is higher in energy than the forbidden state, shows no fluorescence due to rapid internal conversion processes to the non-emitting lower state in which the radiative decay is forbidden.[226] An alignment of the dipole moments at the so-called magic angle ($\Theta = 54.7°$) does not involve an energetic splitting of the dimers' excited state, and indeed the spectra of these dimers are indistinguishable from those of their monomers.[45]

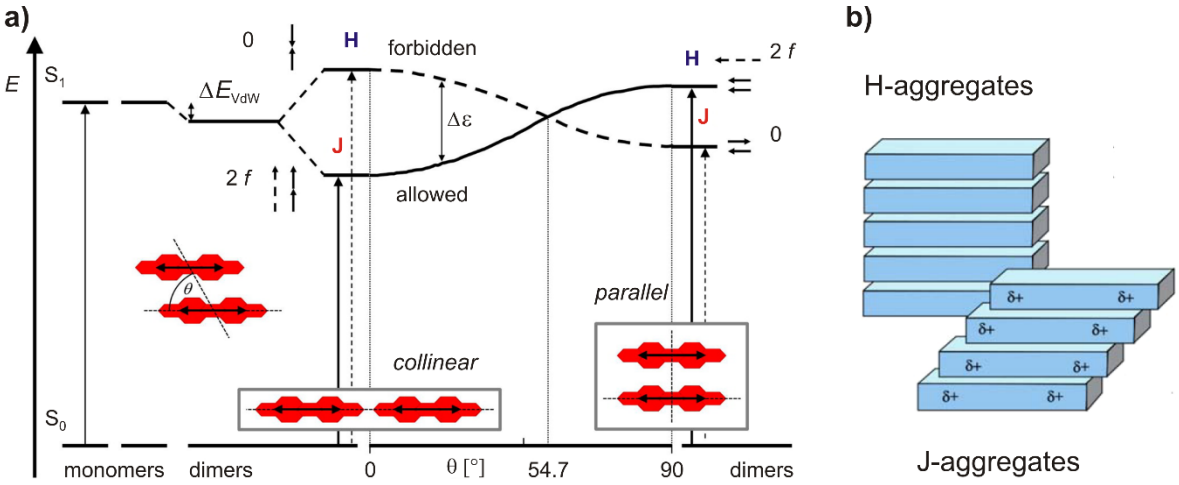

Figure 2.18. a) Schematic energy diagram for a PBI dimer system with coplanar transition dipoles leading to J- or H-aggregates. Transition dipole moments are depicted as black, solid double arrows; solid arrows indicate allowed transitions and dashed arrows indicate forbidden transitions. Adapted with permission from Ref. [45] (© 2015 American Chemical Society) b) Molecular stacking of non-fluorescent H- and highly fluorescent J-aggregates. Adapted with permission from Ref. [227] (© 2010 The Royal Society of Chemistry).

The different molecular stacking behavior of H- and J-aggregates is depicted in Figure 2.18b. In H-aggregates, the molecules form untilted stacks or stacks with a small tilt angle arranged in a face-to-face manner. In J-aggregates, the molecules are stacked in an offset end-to-end arrangement resulting in significantly tilted aggregates. A tilted stack is a compromise between the maximum overlap of π–π systems and the repulsive electrostatic forces of partial charges in the molecular orbitals. The crucial angle at which end-to-end interactions dominate over face-to-face interactions is 54.7°.[227]

2.4.3.2 Water-Soluble PBIs as Site-Specific Biolabels

Various water-soluble PBI-based fluorescent probes have been reported that function as non-covalently bound staining agents by cellular uptake,[228-231] charge interactions,[232] hydrophobic assembly,[233] hydrogen bonds,[234] or binding affinity.[207] Merely a few among the reported PBIs to date function as covalently bound labels using a single monofunctional group for target-specific bioconjugation. However, to explore biomolecular activities on a single-molecule level, the introduction of target-specific fluorescent reporters at specific sites of a biomolecule is of crucial importance.

Since the early 2000s, several monofunctionalized PBI-based fluorescent labels have been developed for site-specific labeling of proteins, enzymes, DNA, and steroids. Most of them are Müllen-like core-substituted PBIs bearing tetraphenoxy substituents with charged sulfonate or pyridinium groups (Figure 2.19a and b). These labels possess moderate FQYs between 15 and 58% in aqueous solution and have been successfully applied in bioimaging. For example, PBI **73** with a maleimide and PBI **74** with an NHS ester function were applied for labeling thiol and amine groups of phospholipases (PLA1), respectively, to track single-enzyme activities on native substrates.[235] In a different study, the activated acid function of PBI **74** was attached to a single-stranded DNA (ssDNA).[236] Here, the fluorescence of

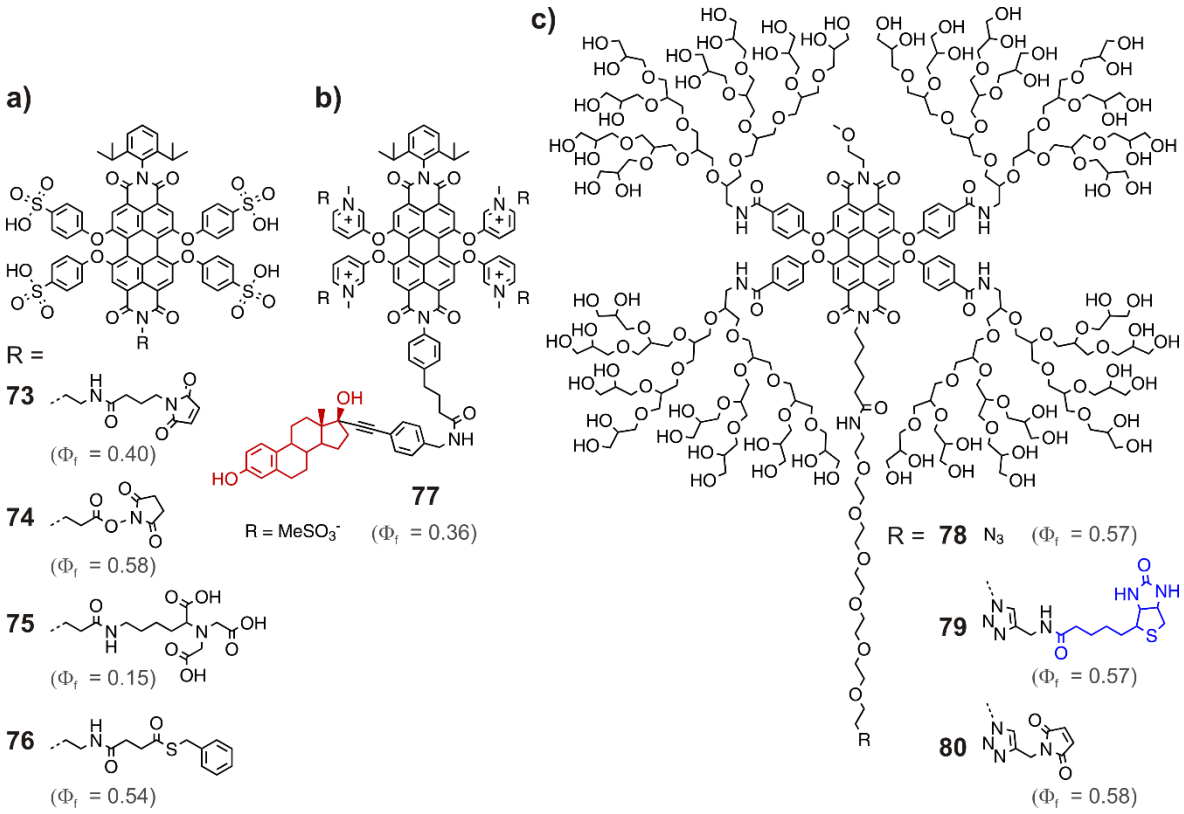

Figure 2.19. Water-soluble monofunctionalized PBIs for biolabeling of a) enzymes and ssDNA, b) estrogen hormone 17β-estradiol (red) and c) BSA, CoA, as well as bacterial and mammalian cell surfaces via biotin-streptavidin (biotin in blue) or CoA-ACP binding, respectively.

PBIs could be controlled through photoinduced electron transfer upon addition of reductants and oxidants, resulting in either photoblinking or stable emission of the dyes. Monofunctionalized PBIs with a nitrotriacetic acid moiety **75**[237] and thioester functional group **76**[238] were employed for site-selective labeling of histidine-tagged ATP synthase and cysteine-containing proteins in light-harvesting complex II (LHCII), respectively. Positively charged PBI **77** was labeled with an entire 17β-estradiol unit to serve as receptor-directed biolabels for determining the presence of estrogen receptors in any kind of cell (Figure 2.19b).[239]

In addition to the charged labels, Zimmerman *et al.* reported the first uncharged labels **78**-**80**, which possess FQYs from 57 to 58% (Figure 2.19c). The site-isolated PG-dendronized PBI **78** bears a single reactive azide group that can be click-coupled to yield biotin and maleimide derivatives **79** and **80**.[240] Biotinylated PBI **79** served as label on the surface of living bacterial cells (E. coli) through biotin-streptavidin linkage with extracellular λ receptor proteins. After preincubation with streptavidin, highly target-specific staining was observed on the bacterial surface, whereas in the absence of streptavidin no detectable staining occurred (Figure 2.20a and b). In control experiments, extracellular labeling with the ionic PBI-biotinylated analog **81** (Figure 2.20e) revealed unselective staining of the bacteria, both with and without streptavidin preincubation (Figure 2.20c and d). These results underscore the importance of neutral labels for target-specific binding studies. Maleimide PBI **80** was used to conjugate Cys-carrying bovine serum albumin (BSA) and coenzyme A (CoA). The latter was used to label ACP-tagged fusion proteins on the surface of living mammalian cells (HeLa), which can be enzymatically conjugated to CoA via acyl carrier proteins (ACP). These examples demonstrate the potential of monofunctionalized PBIs as site-specific labels for targeted imaging of various biomolecules.

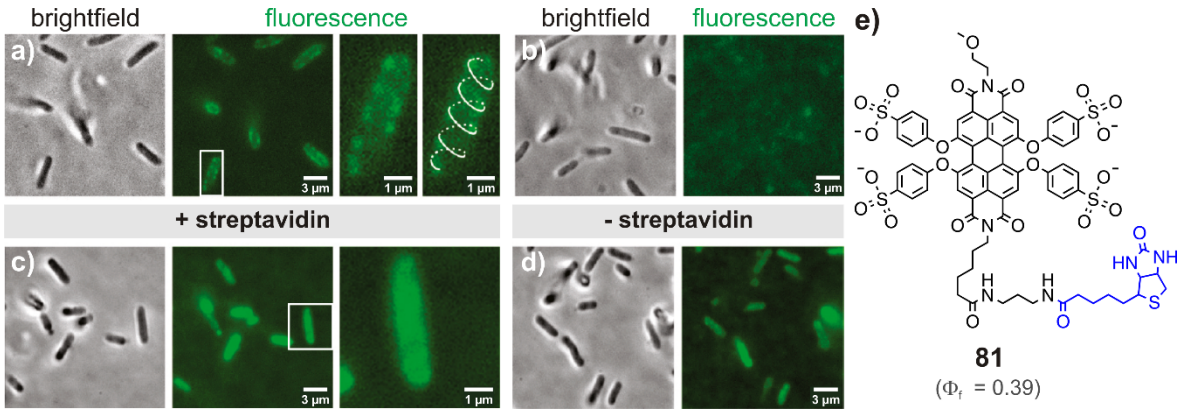

Figure 2.20. Fluorescent labeling of λ receptors on the surface of E. coli bacteria cells stained with PBI **79** a) with and b) without streptavidin preincubation. The white box in the middle panel was enlarged in the right panel, which shows the helical pattern of surface-bound λ receptors for one bacterial cell. As a control, cells were labeled with ionic PBI **81** c) with and d) without streptavidin preincubation, revealing unspecific binding. Adapted with permission from Ref. [240] (© 2011 American Chemical Society). e) Ionic non-dendronized PBI **81** with a biotin group (blue) for control experiments.

These bay-substituted labels were successfully applied in bioimaging studies. However, the bay positions are those that enable fine-tuning of the optical properties of PBI dyes. By using the bay substitution pattern for aggregate suppression, the broad spectrum of accessible wavelengths that can be achieved with PBIs is narrowed. A substituent in the imide position that introduces water solubility and simultaneously suppresses the aggregation tendency would be ideal since the optical properties remain unaffected and can be individually fine-tuned. As mentioned, polymeric architectures like dendrons and dendrimers constitute suitable compounds for the encapsulation of fluorophores to enhance their performance.

2.5 Dendritic Site Isolation of Fluorophores

Dendrimers are roughly spherical, three-dimensional, well-defined architectures that consist of highly ordered oligomeric or polymeric branches, so-called dendrons, with numerous peripheral end groups.[241] Dendrimeric architectures offer desirable molecular properties such as uniform size and shape (monodispersity) as well as variable functionalization and controllable density of surface groups (multivalency). Due to their excellent properties, dendritic molecules are used in various scientific fields such as catalysis, optoelectronics, as well as medical diagnostics and therapeutics.[242] Although most dendrimers and dendrons consist of a hydrophobic backbone, they can be easily rendered water-soluble by surface functionalization with hydrophilic peripheric groups such as sugars,[243] oligo-[244] or poly(ethylene glycols),[245] hydroxyl groups,[246] or charged residues.[247] Polyglycerol- (PG) based dendrimers and dendrons are particularly suitable compounds for biological applications as they offer good biocompatibility and high drug-loading capacities.[248]

The increasing importance of highly fluorescent probes has led to the application of dendritic structures as solubilizing agents and aggregation suppressors for the site-isolation of dyes.[212] These, dendronized fluorophores are defined by three segments: i) a central fluorophore core, ii) an interior dendritic structure built up by the dendron branches, and iii) a peripheric surface with numerous functional groups.[249] The resulting dendronized fluorophores are core-shell architectures with a hydrophobic dye core and hydrophilic dendritic shell. Efforts have been made to improve the water solubility of fluorophores such as squaraines **82**,[250] monomeric **83**[251] or polymeric **84**[252] fluorenes, and metalloporphyrins coordinated with palladium **85**[253] or zinc **86**.[254] Figures 2.21 and 2.22 provide an overview of these [G0]- to [G4]-dendronized fluorophores and their FQYs measured in aqueous solution or, in case of Zn porphyrins, their reduction potentials E_{red} measured in THF.

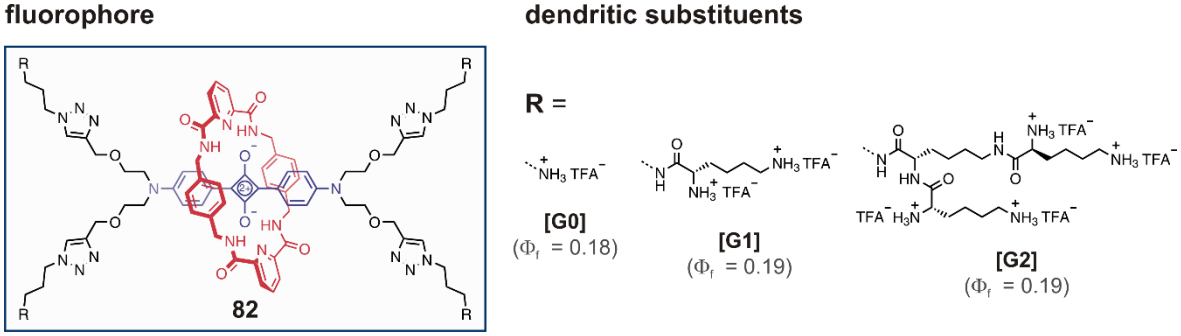

Figure 2.21. Squaraine rotaxanes with [G0] - [G2] dendritic polyamine substituents and their corresponding FQYs in aqueous solution.

The squaraine dye in Figure 2.21 is part of a rotaxane scaffold. Therefore, the dendritic polyamines serve not only as encapsulating units but also as stoppers to keep the squaraine axis within the macrocycle, resulting in squaraine rotaxanes **82**.[250] Fluorenes **83** gave an impressive example of water-soluble, two-photon-active fluorescent probes encapsulated within shielding layers of phosphorus-based dendrimers (Figure 2.22).[251] The [G2]-derivatized fluorene was successfully applied in bioimaging studies of vascular tissue of rats. Pd-tetrabenzoporphyrin complexes **84** with polyglutamate dendrons were reported as NIR probes for *in vivo* oxygen imaging of tissue by a phosphorescence-quenching mechanism.[253] The importance of dendronization became obvious on polyfluorenes **85** bearing phenylene-based dendrons with peripheral cationic amino groups exhibiting stunning FQYs of up to 94%.[252] Apart from biasing the luminescence performance, dendritic encapsulation also has an impact on the electrochemical properties of a dye. Redox-active porphyrin metal complexes such as the naturally occurring heme complex are part of cytochrome c that plays an important role in the electron transport chain between different protein complexes. The redox properties of porphyrin dyes were manifold investigated by Diederich *et al.*, who encapsulated the dye into a dendritic microenvironment of Newkome poly(ether amide) dendrons in different generations.[254-257] They found that the reduction potential of Zn porphyrin **86** became more negative as the generation of the attached dendrons increased from [G1] (E_{red} = -1.69 V) to [G3] (E_{red} = -1.9 V).[254] The diminished potential was attributed to the increased influence of the Newkome dendrons, which enhanced the electron density around the central porphyrin core and impeded the addition of electrons.

These examples show that the dendronization of dyes significantly improves their water solubility and optical performance as evidenced by retained or improved FQYs and modified reduction potentials. This opens a new generation of highly fluorescent probes with a multivalent periphery, which may be modified with cellular receptors, therapeutic agents, or targeting groups or ligands for sophisticated biological studies in the future. Moreover, dendritic fluorophores represent a good alternative to commonly used semiconductor quantum dots (QD) because of their versatile surface modification and scalable size.

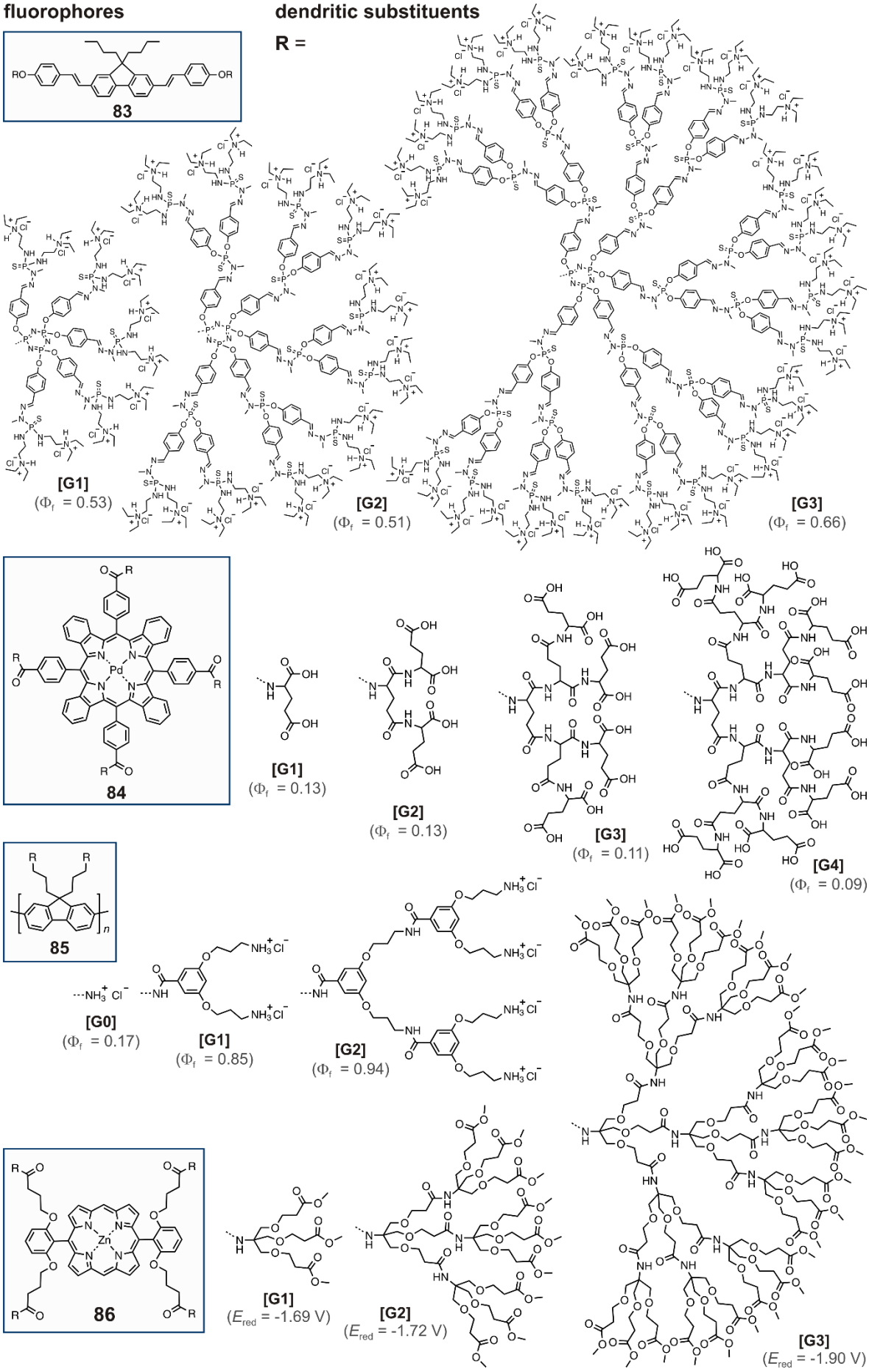

Figure 2.22. Dendronized fluorophores with [G0] - [G4] dendrons and their FQYs Φ_f or redox energies E_{red}.

3 Motivation and Objectives

Perylene bisimides represent an extraordinary class of functional dyes with excellent photophysical properties including outstanding FQYs, high photochemical stability, and long emission wavelengths. These features along with their good biocompatibility and simple chemical modifiability make them ideal fluorescent probes for bioimaging applications. Although many PBIs have been reported for a variety of applications, the synthesis of water-soluble, highly fluorescent, and monofunctionalized PBIs applicable as biolabels still poses a challenging task. The major drawback of PBIs is their pronounced aggregation tendency in aqueous media that leads to fluorescence quenching of the dyes and thus hampers their widespread application in bioimaging studies. To overcome this obstacle, the site isolation with sterically demanding groups represents a promising strategy for suppressing their aggregate formation. Multi-branched polyglycerol (PG) dendrons offer good biocompatibility, rapid cellular uptake, and easy modifiability of their hydrophilic headgroups.[248] Therefore, these bulky structures are ideal systems for the solubilization and site isolation of hydrophobic dyes as demonstrated on both-sided PG-dendronized PBIs.[211]

In order to establish new concepts for the construction of PBI-based fluorescent labels, the following objectives shall be pursued in this thesis:

1) Synthesis, photophysical characterization, and biological evaluation of water-soluble, highly fluorescent, monofunctionalized PBIs as target-specific labels for biomolecules.

2) Synthesis of dendronized PBI monomers for the incorporation into water-soluble, biocompatible polymer nanoparticles in form of linear dendronized polyols (LDPs), which are applicable as fluorescent bioimaging agents.

3) Noncovalent functionalization of single-walled carbon nanotubes (SWNTs) with water-soluble PBI-conjugated polymers to form supramolecular polymer-SWNT complexes for fluorescence bioimaging studies in two optical windows.

The general structure of the targeted PBIs can be divided into three components, whereas each component fulfills a certain purpose for the functionality of the respective label (Figure 3.1a). The main component is the core-unsubstituted PBI chromophore imparting fluorescence and color to the labels. The chromophore scaffold shall be unsymmetrically substituted with a PG dendron on one side and a linker with a monofunctional group on the other side of the imide positions. The dendron serves a two-fold purpose by introducing

water solubility through its multiple hydrophilic headgroups and suppressing aggregation due to its sterically demanding structure. To further suppress the aggregation tendency of the labels, the PG dendron shall be modified with ionic sulfate groups. The third component is a linker with a single reactive group serving as a coupling-active moiety for the conjugation of biomolecules or other components such as linear polymers. As conjugatable groups an activated acid function for target-specific bioconjugation, an *exo*-norbornene unit for polymerization, and a propargyl group for click coupling shall be introduced (Figure 3.1b).

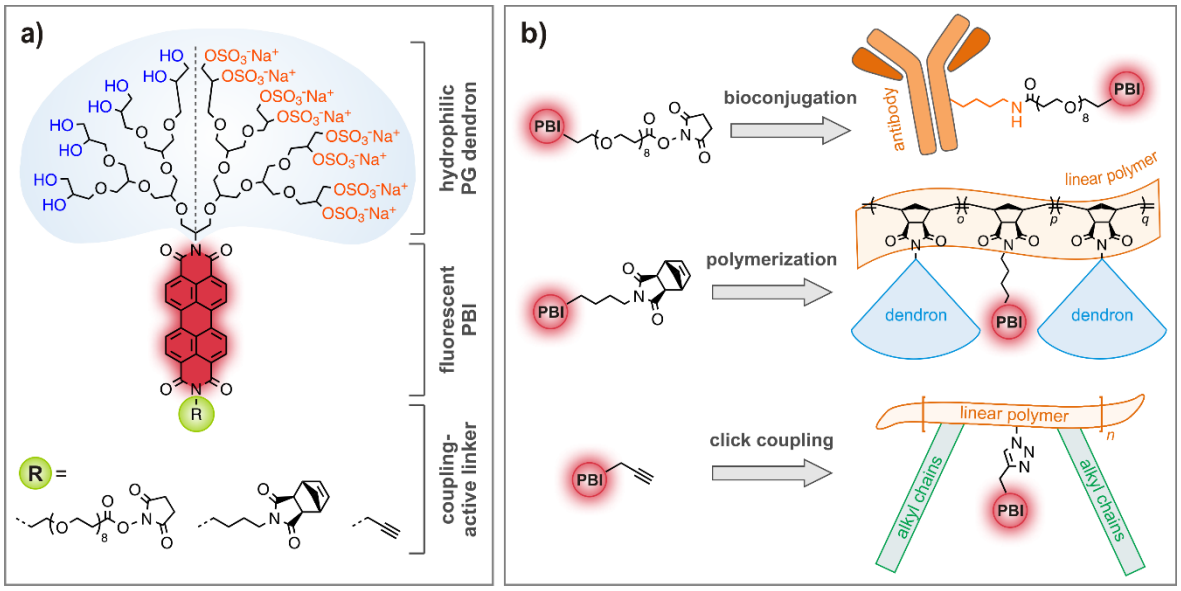

Figure 3.1. a) General structure of PG-dendronized PBI labels with various linker functions, exemplarily shown for [G3]. b) Cartoonlike illustration of the targeted coupling reactions.

It has been reported that the substitution with charge-neutral PG dendrons in only one side of the imide positions is not sufficient to completely suppress the aggregation of perylenes in an aqueous environment.[258] However, the combination of steric hindrance and ionic charge proved to be an effective tool to retain the fluorescence properties of PBIs in aqueous media. This was demonstrated by the introduction of charged sulfate groups in the periphery of both-sided dendronized PBIs, which led to highly fluorescent labels even in case of lower-generation dendronized PBIs.[201] Taking these findings into account, it shall be investigated whether the introduction of ionic sulfate groups in the dendron periphery can also prevent the aggregation of mono-dendronized PBIs. In all three cases, a clear correlation between the fluorescence properties of the dendronized PBIs and their dendron generation or extent of charge shall be established. In addition, not only the influence of charge on the optical properties, but also on the biological environment shall be examined. In summary, the main objectives of this work shall be the chemical synthesis, optical characterization, and biological analysis of neutral and charged PG-dendronized PBIs for bioimaging studies.

4 Publications

4.1 Noncharged and Charged Monodendronised Perylene Bisimides as Highly Fluorescent Labels and their Bioconjugates

Katharina Huth, Timm Heek, Katharina Achazi, Chirsitan Kühne, Leonhard H. Urner, Kevin Pagel, Jens Dernedde, and Rainer Haag

Chem. Eur. J. **2017**, *23* (20), 4849-4862.

An electronic version of the article is available under DOI: 10.1002/chem.201605847.

The Supporting Information is included in Appendix A.1.

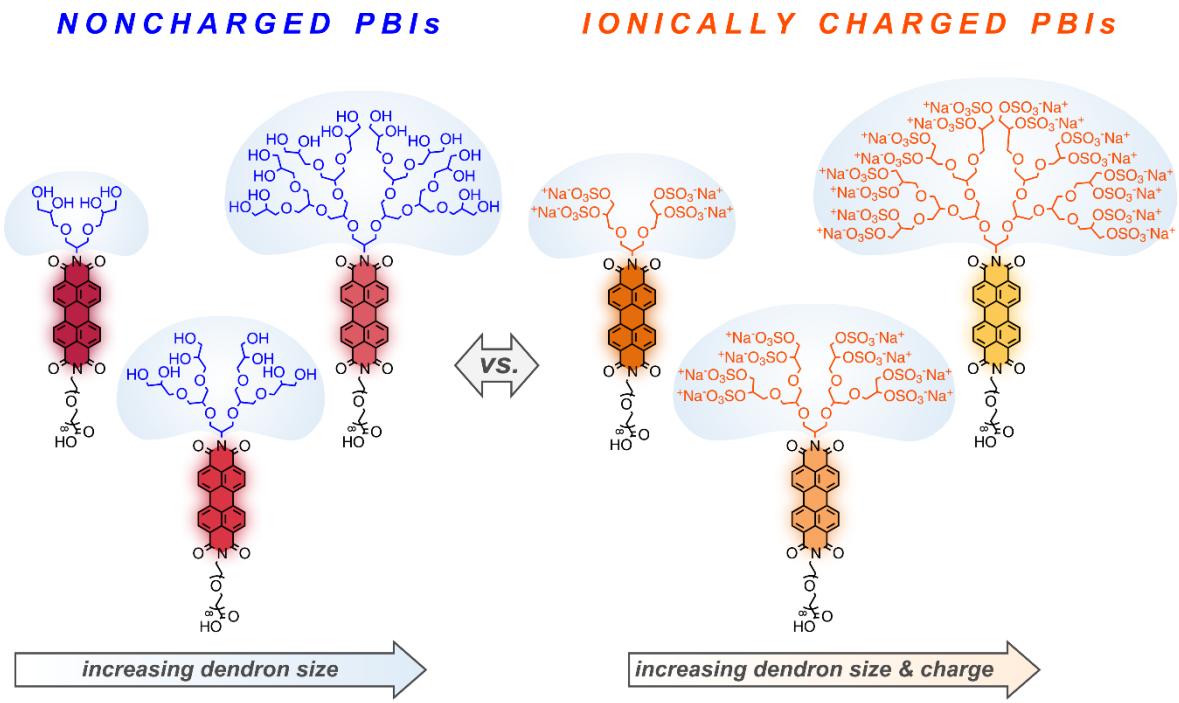

Figure 4.1. Chemical structures of the two sets of PG-dendronized monofunctionalized PBIs from dendron generation [G1] to [G3] in a noncharged hydroxylated (left) and charged sulfated (right) version as site-specific fluorescent labels for an antibody. Sulfated labels feature improved optical properties and higher intracellular staining efficiencies than their hydroxylated analogs due to an additional electrostatic shielding by the Coulombic repulsion forces of the ionically charged dendron. Graphical abstract adapted with permission from Ref. [259] (© 2017 Wiley-VCH Verlag GmbH & Co. KGaA, Weinheim).

4.1.1 Author Contributions

The PG-dendronized monofunctionalized PBI labels and antibody conjugates were synthesized, characterized, and photophysically evaluated by me. The basic concept of this project with dendronized PBIs as fluorescent labels for the antibody cetuximab was provided by Timm Heek. The purification of the PBI-antibody conjugates and examination of epidermal growth factor receptor (EGFR) expression on the cells was performed by Jens Dernedde. The biological evaluation of the conjugates including receptor-binging, cellular uptake, flow cytometry analysis, and toxicity studies were conducted by Christian Kühne, Katharina Achazi, and Paul Hillmann, respectively. Leonhard H. Urner conducted the customized MS analysis of the polycharged labels. Kevin Pagel contributed to the final version of the manuscript by some corrections and content-related details. The project was supervised by Rainer Haag, who provided scientific guidelines and suggestions to this project. The data analysis and evaluation as well as the manuscript writing were conducted by me. All coauthors corrected and proofread the manuscript and contributed to its final version.

4.2 Linear Dendronized Polyols as a Multifunctional Platform for a Versatile and Efficient Fluorophore Design

Ying Li,‡ Katharina Huth,‡ Edzna S. Garcia, Benjamin J. Pedretti, Yugang Bai, Gretchen A. Vincil, Rainer Haag, and Steven C. Zimmerman

Polym. Chem. **2018**, *9* (15), 2040-2047.

An electronic version of the article is available under DOI: 10.1039/C8PY00193F.

The Supporting Information is included in Appendix A.2.

‡ These authors contributed equally.

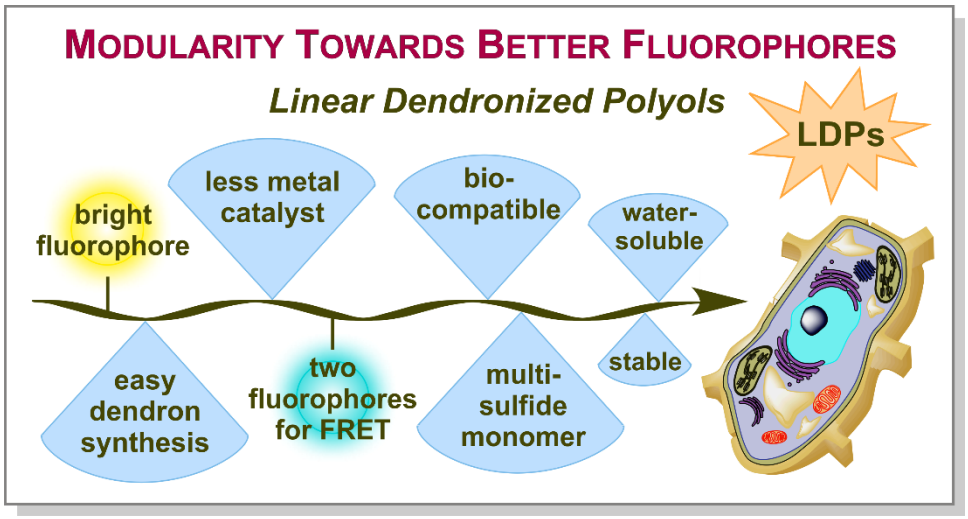

Figure 4.2. Properties of the fluorescent polymer nanoparticles based on linear PG-dendronized polyols (LDPs) applicable for bioimaging studies. The polymer scaffold protects the covalently attached fluorophores from photobleaching and improves their optical performance. Benefiting from the modular system of the LDPs, their optical properties can be fine-tuned by incorporating different combinations of dendron and fluorophore monomers. Graphical abstract adapted with permission from Ref. [260] (© 2018 The Royal Chemical Society).

4.2.1 Author Contributions

I synthesized the imide-substituted acetal-protected PG-dendronized PBIs in three generations from [G1] to [G3], which were used as precursors for the advanced PBI fluorophore monomers. Ying Li provided the concept of this project and performed the majority of the monomer and polymer syntheses and characterization, optical measurements, and biological assays. Edzna S. Garcia helped with the dendron monomer synthesis, photostability studies, and manuscript editing. Benjamin J. Pedretti helped with the synthesis of the dendron monomers and photostability studies. Yugang Bai and Gretchen A. Vincil synthesized several fluorophore monomers. Data analysis and processing as well as manuscript writing were performed equally by both first authors, Ying Li and myself. The majority of data plotting as well as the creation of the schemes and figures was performed by me. The project was carried out under the supervision of Steven C. Zimmerman, who was involved in the concept development and manuscript writing of the project. Rainer Haag corrected the manuscript and contributed some content-related details. All coauthors proofread the manuscript and contributed to its final version.

Please note that the counting method of the dendron generation [Gn] differs between the Zimmerman and Haag groups. In the Haag-way of counting, glycerol is considered [G0], whereas in the Zimmerman method it counts as [G1]. In the corresponding manuscript the Zimmerman counting method was utilized, while in the present thesis the Haag counting method was applied.

4.3 Fluorescent Polymer–Single-Walled Carbon Nanotube Complexes with Charged and Noncharged Dendronized Perylene Bisimides for Bioimaging Studies

Katharina Huth,‡ Mareen Glaeske,‡ Katharina Achazi, Georgy Gordeev, Shiv Kumar, Raúl Arenal, Sunil K. Sharma, Mohsen Adeli, Antonio Setaro, Stephanie Reich, and Rainer Haag

Small **2018**, *14* (28), 1800796.

An electronic version of the article is available under DOI: 10.1002/smll.201800796.

The Supporting Information is included in Appendix A.3.

‡ These authors contributed equally.

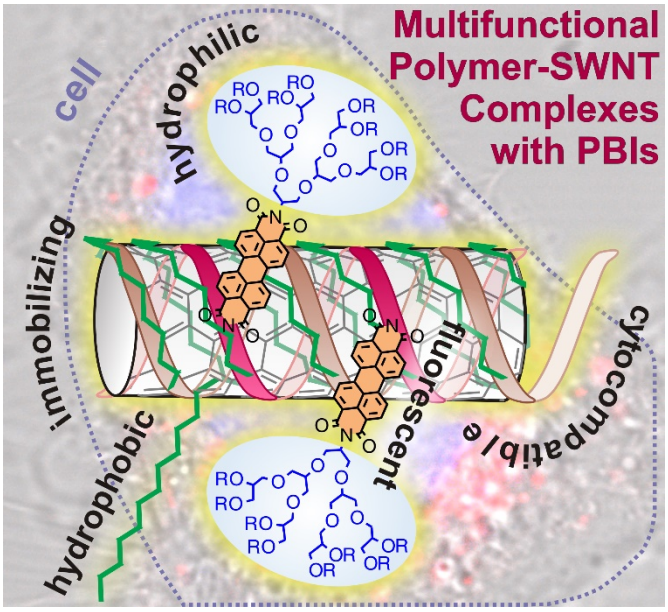

Figure 4.3. Schematic structure of the fluorescent polymer-SWNT complexes with neutral (R = OH) or charged (R = SO_4^-) PG-dendronized PBIs for bioimaging studies in the 1st and 2nd optical transparency window of tissue. The dual-fluorescent complex allows the direct imaging of the SWNTs' cellular uptake via the PBI and SWNT emission and strongly improves the cytocompatibility of the nanotubes. Graphical abstract adapted with permission from Ref. [261] (© 2018 Wiley-VCH Verlag GmbH & Co. KGaA, Weinheim).

4.3.1 Author Contributions

I synthesized the free dyes consisting of PG-dendronized PBIs, the alkylated polymer, and the dye-polymers. Furthermore, I performed the characterization of the compounds and polymers as well as the photophysical investigation of the free dyes and dye-polymers. In addition, I provided several conceptual ideas to the project and guided it into a biological direction. Shiv Kumar synthesized the polymer backbone under supervision of Prof. Sunil K. Sharma. Mareen Gläske carried out the complex formation and the dispersibility study of the polymer-SWNT complexes; she also contributed several conceptual ideas to the project. Intracellular Raman and photoluminescence (PL) measurements were performed by Georgy Gordeev. Raúl Arenal conducted high resolution transmission electron microscopy (HRTEM) and electron energy loss spectroscopy (EELS) on the polymer-SWNT complexes. The biological studies were performed by Katharina Achazi and Eliza Quaas. The manuscript was written and prepared equally by both first authors, Mareen Gläske and myself. The project was supervised by Rainer Haag, Stephanie Reich, Mohsen Adeli, and Antonio Setaro, who provided scientific guidelines and suggestions. All coauthors corrected and proofread the manuscript and contributed to its final version.

4.4 Enhancement of Fluorescent Properties of Near-Infrared Dyes using Clickable Oligoglycerol Dendrons

Orit Redy-Keisar, Katharina Huth, Uwe Vogel, Bernd Lepenies, Peter H. Seeberger, Rainer Haag, and Doron Shabat

Org. Biomol. Chem. **2015**, *13* (16), 4727-4732.

An electronic version of the article is available under DOI: 10.1039/C5OB00299K.

The Supporting Information is included in Appendix A.4.

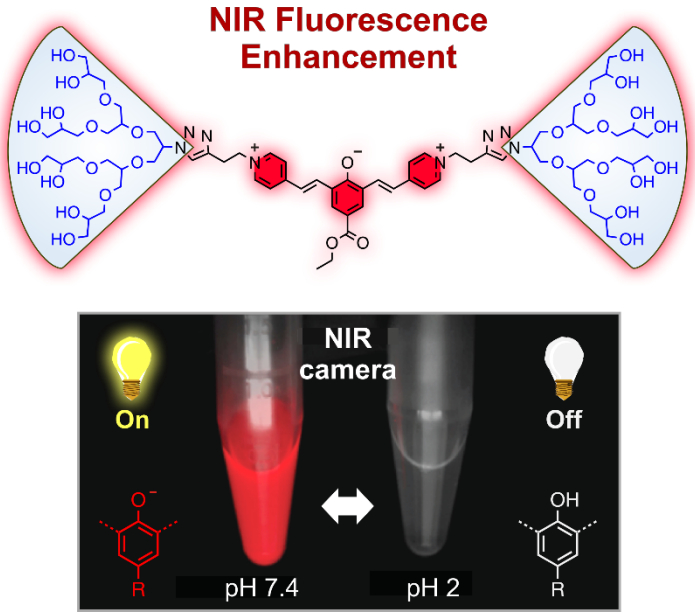

Figure 4.4. The site-isolation of NIR-emitting cyanine derivatives with [G1]- or [G2]-oligoglycerol dendrons leads to enhanced water solubility and fluorescence properties. The phenolic structure of the dyes enables a pH-driven turn-on/turn-off fluorescence mechanism upon deprotonation to its phenolate/quinone form (left) or protonation to its phenol form (right). The resulting turn-on/turn-off fluorescence can be imaged with an NIR camera due to a color change from red to black. Graphical abstract adapted with permission from Ref. [262] (© 2015 The Royal Chemical Society).

4.4.1 Author Contributions

The second generation azidated [G2]-N_3 acetal-protected oligoglycerol (OG) dendron was synthesized and characterized by me under supervision of Rainer Haag. Orit Redy-Keisar synthesized and optically characterized the OG-dendronized cyanine derivatives. The manuscript was written by Orit Redy-Keisar and proofread and corrected by me. Uwe Vogel conducted the uptake studies on macrophage cells under supervision of Bernd Lepenies and Peter H. Seeberger. Doron Shabat supervised the project and provided scientific guidelines and suggestions. All coauthors corrected and proofread the manuscript and contributed to its final version.

5 Summary and Conclusion

This thesis presents new approaches for the construction of water-soluble, highly fluorescent, and site-specific PBI-based labels for bioimaging applications. The core-unsubstituted PBI labels are equipped with a PG dendron on one side and a coupling-active linker on the other side of the imide positions. The monofunctional linker bears a single reactive group that can easily be conjugated to biomolecules or other components such as linear polymers. Site isolation with PG dendrons is an effective tool to retain the outstanding fluorescence properties of PBIs in aqueous solution. Nevertheless, neutral hydroxylated PG dendrons can only mediate high FQYs if higher dendron generations (≥ [G3]) are used.[211] For biological studies, the molecular size and weight of a label is a crucial point.[175] Small-size and low-weight fluorophores are of great interest since they are less likely to affect the structure and function of the labeled biomolecule. To make lower-generation dendronized PBIs (≤ [G2]) accessible for high FQYs in polar aqueous media, ionically charged sulfate groups were introduced on the dendron headgroups. However, the introduction of charge into biological systems is a critical issue, as it inevitably arouses the concern of nonspecific binding to cell components through attractive electrostatic interactions.[240] Molecular recognition, on the other hand, relies on target-specific attractive interactions between two partner molecules and may therefore be beneficial to, e.g., induce receptor-mediated cellular uptake.[263] In this thesis, the various projects on PBI-based: 1) biolabels, 2) polymer nanoparticles, and 3) polymer-SWNT complexes as well as an example of the dendritic site isolation of an NIR fluorophore are discussed.

The first project is concerned with the synthesis, optical characterization, and biological analysis of a series of [G1]- to [G3]-dendronized PBI biolabels equipped with a coupling-active PEG linker bearing an activated acid function in form of an NHS ester (see Chapter 4.1). The dendronized and monofunctionalized labels were prepared in a straightforward six-step synthesis. To further suppress the aggregation behavior of the neutral hydroxylated labels, the dendron headgroups were modified with charged sulfate groups. While HO-[G1]- and HO-[G2]-PBIs were only partially soluble in water, higher-generation HO-[G3]-PBI and the entire series of $^{-}O_4S$-[Gn]-PBIs (n = 1-3) were very soluble. To find the best candidate for biolabeling, the aggregation behavior of the neutral and charged PBI labels was compared by means of concentration-dependent absorption and emission measurements in water. Hydroxylated PBIs exhibited a concentration-dependent absorption behavior with a transition from strongly aggregated to more disaggregated PBIs upon dilution with FQYs between 12 and 73%. In contrast, sulfated PBIs showed a mostly concentration-independent monomeric absorption behavior with FQYs between 81 and

100%. Since the labels should be used in a biological environment, their optical performance was additionally examined in PBS (phosphate-buffered saline) as a physiological solvent. The optical properties in PBS gave the same trend observed in water with reduced molar absorption coefficients, $A^{0\text{-}0/0\text{-}1}$ peak ratios, and FQYs due to the higher ionic strengths of the buffer solution. The reduction was a result of charge screening effects that led to contact ion pairing, which reduced the Coulombic repulsion forces among the PBIs and thus restored their aggregate formation. The combination of steric and electrostatic shielding proved to be a powerful tool for suppressing the H-type aggregation of PBIs, as evident by 100% FQY of the sulfated [G2]- and [G3]-labels in both solvents, PBS and water. The effective aggregate suppression by the multiple sulfate groups (≥ 8) allowed for the reduction of one dendron generation from [G3] to [G2], while retaining the PBIs' excellent 100% FQY. This finding reduces the synthetic effort necessary to generate highly fluorescent monomerized PBIs in water. The biological performance of the labels was probed upon bioconjugation to the therapeutic antibody cetuximab via an amide bond coupling to lysine side chains (Figure 5.1a). An optical comparison study between the free dyes and the dye-cetuximab conjugates revealed an increased aggregation tendency of the dyes after bioconjugation as obvious by strongly aggregated absorption patterns and reduced FQYs. Despite the partial quenching, hydroxylated and sulfated [G3]-PBI-cetuximab still exhibited FQYs of 55 or 66%, respectively, which were more than sufficient for the targeted bioimaging studies. The biological suitability of the dye-cetuximab conjugates was evaluated by *in vitro* binding, toxicity, and uptake studies. Receptor-binding studies showed an unaffected target-recognition of the antibody after labeling. A cytotoxicity assay confirmed the good cytocompatibility of the dye labels. Cellular uptake studies and flow cytometry analysis revealed two key findings: first, higher-generation dendronized PBIs showed superior

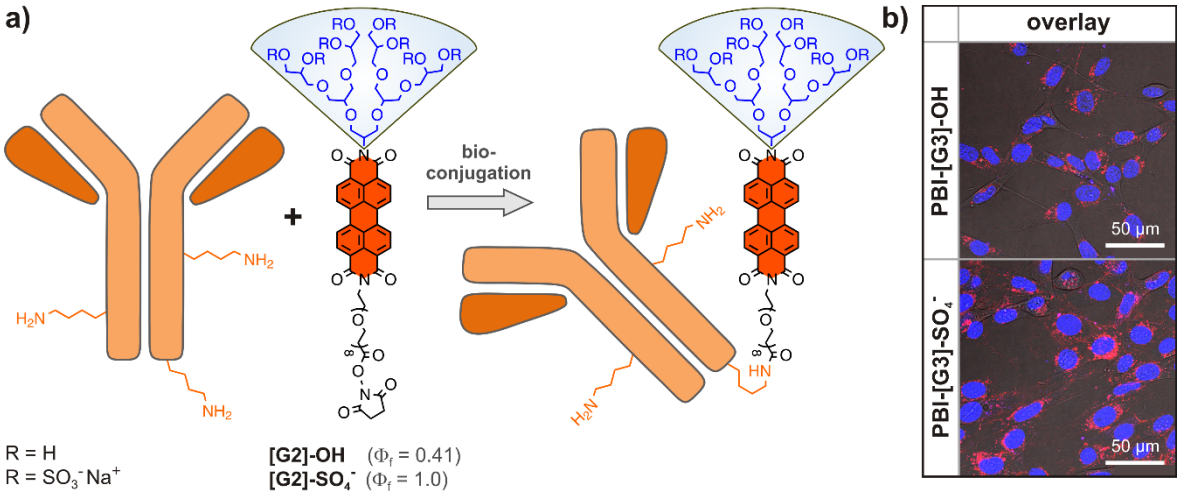

Figure 5.1. First project about noncharged and charged PBIs as target-specific fluorescent labels. a) Bioconjugation reaction of an antibody with PBI-[G*n*]-OR (*n* = 1-3), exemplarily shown for [G2]. b) Cellular uptake study of PBIs (red) into HER14 cells; cell nuclei are stained in blue.

intracellular fluorescence signals over lower-generation dendronized PBIs ([G_{high}] > [G_{low}]) and, second, sulfated PBIs exhibited superior intracellular fluorescence intensities over hydroxylated PBIs ($^{-}O_4S$ > OH, Figure 5.1b). The good cytocompatibility and bioimaging performance render the highly fluorescent, dendronized, monofunctionalized PBI labels suitable candidates for target-specific labeling of biomolecules.

In the second project, dendronized PBIs were incorporated into polymer nanoparticles consisting of linear dendronized polyols (LDPs), which were applied as fluorescent staining agents in cellular studies (see Chapter 4.2). To investigate the impact of enhanced dendronization, hydroxylated PBI monomers **P[G*n*]** (n = 1-3) in three different generations were prepared. The dendronized PBI monomers were equipped with an *exo*-norbornene linker, which allowed their incorporation into a polymer backbone (left side in Figure 5.2a). The polymer synthesis between dendron and fluorophore monomers was conducted in two steps, comprising ring-opening metathesis polymerization (ROMP) and acid-catalyzed hydrolysis of the acetal protecting groups. The resulting water-soluble, fluorescent, polymeric LDPs were small in diameter (< 6 nm), which is beneficial for cellular studies. The polymers were synthesized with a molar feed ratio of dendron monomer **[G2]** and dendronized PBI monomer **P[G*n*]** of 20 : 2. Despite the 10-fold excess of dendron monomers over fluorophore monomers, the FQYs of the resulting LDPs-**P[G*n*]** could be improved by a factor of ≈ 8 with increasing generation of the dendronized PBIs from [G1] (Φ_f = 7.8%) to [G3] (Φ_f = 23%). This result shows the importance of covalent dendritic site isolation since the mere dendritic environment of the LDP scaffold was not sufficient to prevent fluorescence quenching of the dyes. In addition to LDPs containing one fluorophore, LDPs with two different fluorophores were prepared to achieve new photophysical properties and probe the modularity of the polymer platform (Figure 5.2a). The resulting bi-fluorophoric LDPs[6] afforded large Stokes shifts caused by the occurrence of FRET. As FRET pairs, fluorophore monomer **P[G3]** and one out of three donor fluorophores including **C**oumarin, **F**luorescein, and **B**odipy were used. The FRET efficiency between the two fluorophores was determined by the ratio of the acceptor and donor emission intensities (I_A/I_D), with a higher emission ratio indicating a higher FRET efficiency. The highest FRET efficiency among LDP-**P[G3]C** (E_{FRET} = 0.27), LDP-**P[G3]F** (E_{FRET} = 0.61), and LDP-**P[G3]B** (E_{FRET} = 0.93) was observed for the PBI-bodipy pair (Figure 5.2b). Bodipy is a rather small molecule compared to coumarin and fluorescein, which might have enabled a closer proximity of the acceptor and donor fluorophores, resulting in higher FRET efficiency. The bi-fluorophoric LDP of PBI and fluorescein was also prepared in a block-copolymerized version[7] synthesized

[6] Feed ratio of bi-fluorophoric LDPs: 20 **[G2]**, 2 **P[G3]**, and 2 **C**, **F**, or **B**.
[7] Feed order and ratios of LDP-**P[G3]F-block**: i) 5 **[G2]**, ii) 10 **[G2]**, 2 **P[G3]**, 2 **F**, and iii) 5 **[G2]**.

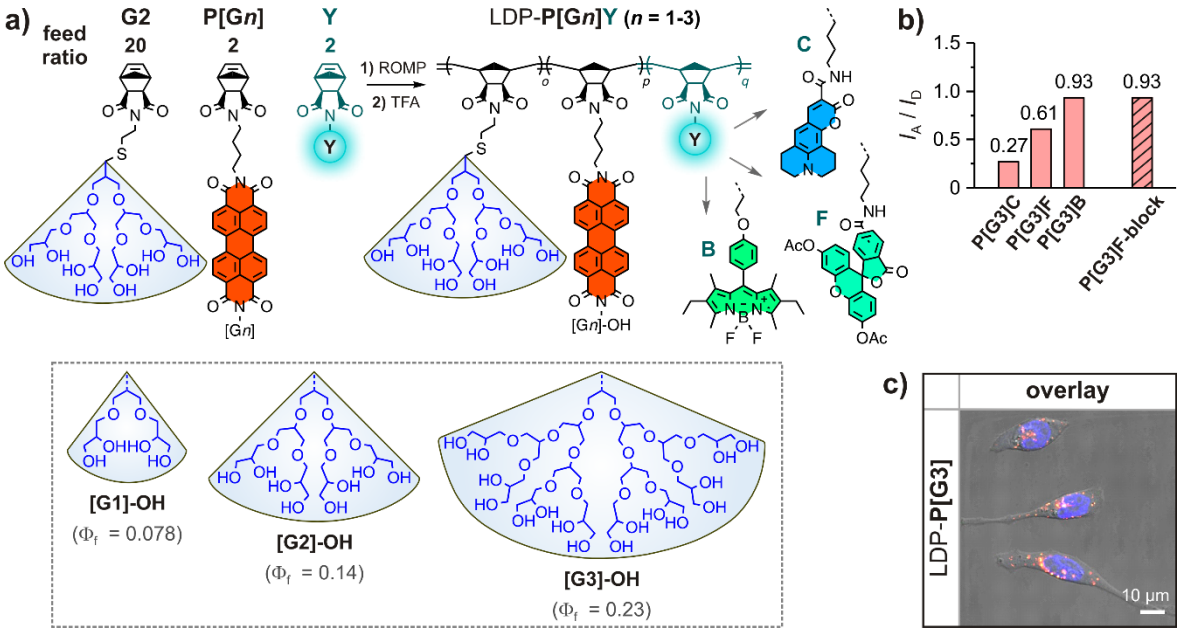

Figure 5.2. Second project about linear dendronized polyols (LDPs). a) Synthesis of mono- or bi-fluorophoric LDPs containing **P**BI-**[G*n*]** (n = 1-3). The second fluorophore **Y** shown in dark green is either **C**oumarin, **F**luorescein, or **B**odipy and was exclusively introduced for the FRET study. b) FRET efficiency of bi-fluorophoric LDPs and LDP-**block** with acceptor **P[G*n*]** and donor **C**, **F**, or **B**. c) Cellular uptake study of LDP-**P[G3]** (red) into HeLa cells; cell nuclei are stained in blue.

with the same monomers and feed ratios as regular LDPs but with a different monomer feed order. Interestingly, LDP-**P[G3]F-block** (E_{FRET} = 0.93) provided a higher FRET efficiency than regular LDP-**P[G3]F** (E_{FRET} = 0.61). The increase in FRET efficiency suggests a more compact structure of LDP-**block**, allowing for a closer proximity of the two kinds of fluorophores within the polymer backbone. A cytotoxicity study of LDP-**P[G3]** confirmed the good cytocompatibility of the PBI-conjugated polyols; a cellular uptake study performed on HeLa cells showed a bright intracellular staining pattern of the fluorescent LDPs predominantly localized around the cell nucleus (Figure 5.2c). The good cytocompatibility and intracellular staining efficiency render the water-soluble, FRET-capable LDPs suitable fluorescent staining agents for bioimaging studies. In addition, the large Stokes shift of bi-fluorophoric LDPs reduced spectral overlap between absorption and emission, allowing accurate fluorescence detection with reduced background interference. Compared to previously published ONPs[153] and CDPs[166] (see Chapter 2.4.1.2), LDPs required less synthetic effort and toxic ruthenium catalyst due to the elimination of the crosslinking step. These improvements also make them a more practical and biocompatible platform than these crosslinked nanoparticles.

The third project dealt with the preparation and photophysical characterization of polymer-single-walled carbon nanotube (SWNT) complexes with dendronized PBIs for bioimaging studies in two optical windows (see Chapter 4.3). The supramolecular complexes

consisted of neutral hydroxylated or charged sulfated dendronized PBIs conjugated to alkylated polymers. The polymers noncovalently functionalized the SWNTs by wrapping around their scaffold. The design of the complexes consisted of several functional subunits, whereas each fulfilled a certain purpose: i) the hydroxylated or sulfated PG dendrons introduced hydrophilicity and prevented dye-quenching, ii) the PBIs served as fluorescent labels, iii) the alkyl chains ensured the hydrophobic attachment to the SWNTs, iv) the cytocompatible polymer solubilized and coated the tubes, and v) the SWNTs were the general immobilization platform. In addition to the alkylated dye-conjugated polymer, a simply alkylated polymer was prepared to enhance the coating of the tubes while keeping a constant dye concentration. The complexes were prepared by horn sonication of the two polymers and SWNTs in aqueous solution (Figure 5.3a). In absorption and emission measurements, sulfated complexes ($\Phi_f = 5.1\%$) showed superior optical properties over their neutral analogs ($\Phi_f = 4.3\%$). Photoluminescence excitation (PLE) measurements proved a high dispersibility of the SWNT complexes and no signs of energy transfer processes between the dyes and nanotubes. These two key findings excluded the undesired appearance of possible fluorescence quenching effects that are triggered by either aggregation or energy transfer processes. The biological suitability of the complexes was investigated by cytotoxicity and cellular uptake studies on HeLa cells. The cytocompatibility of the synthesized polymers towards commercial surfactants was assessed using sodium dodecyl sulfate (SDS) and Pluronic. The cytotoxicity assay revealed a good cell viability of the polymer-wrapped SWNT complexes and low viability up to cell death of surfactant-solubilized or pristine SWNTs. In microscopy studies and flow cytometry analysis, the sulfated complexes showed an improved intracellular fluorescence signal over their hydroxylated analogs (Figure 5.3b). The higher staining efficiency was caused by two

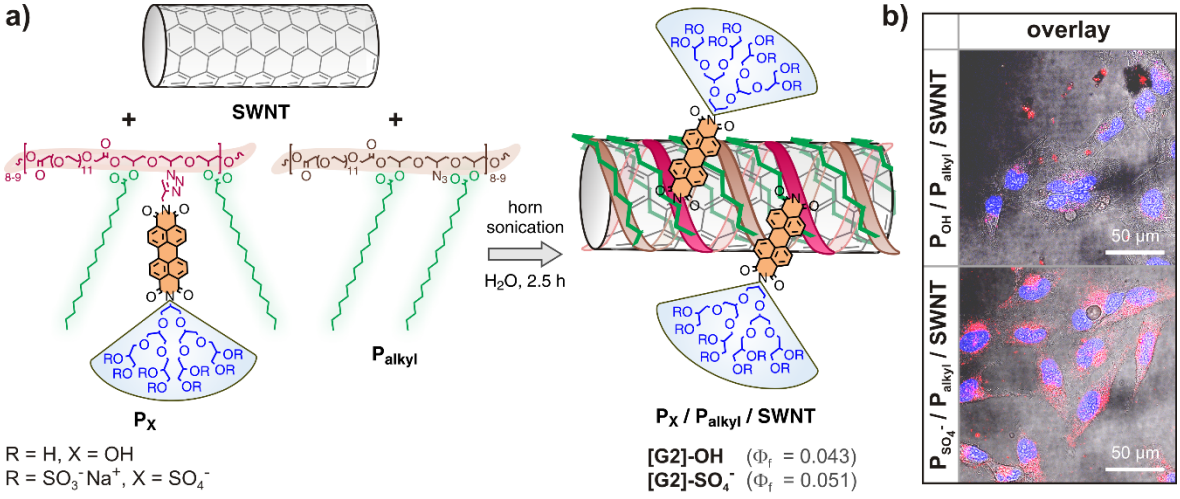

Figure 5.3. Third project about PBI-polymer-SWNT complexes. a) Preparation of the hydroxylated or sulfated complexes. b) Cellular uptake study of the complexes (red) into HeLa cells; cell nuclei are stained in blue.

factors: an enhanced shielding ability by the electrostatic repulsion forces of ionically charged complexes and an improved receptor-mediated uptake through scavenger receptors on the cell surface.[263] However, the bright intracellular staining signals only confirmed the uptake of the PBIs, as the spectral range and resolution scale of the microscope only allowed for the detection of the PBI emission. To ensure that the observed intercellular fluorescence originated from the unperturbed polymer-SWNT complexes, Raman spectroscopy in combination with photoluminescence (PL) measurements was performed on cellular internalized complexes. The PL signals of both, the PBI and SWNT emission, along with the spatial distribution of the SWNT Raman G band, closely resembled the shape of the cell under study. This discovery confirmed the successful cellular internalization of the entire polymer-SWNT complexes via the PBI and SWNT emission using the 1st and 2nd optical windows. Consequently, the complexes allowed for the direct imaging of the SWNTs' cellular uptake through a broad readout in two optical windows. The combination of nanometer size, dual fluorescence, and high cytocompatibility makes these polymer-SWNT complexes valuable systems for a variety of bioimaging studies.

Inspired by the reduced aggregation tendency of PG-dendronized PBIs, Shabat and coworkers tested the effect of dendronization on NIR-emitting cyanine derivatives synthesized in a [G1] and [G2] version (see Chapter 4.4). In the fourth project, the dendronized dyes were optically characterized at different pH values, and their photostability verified upon internalization into macrophages. The cyanine derivatives were based on a donor-two-acceptor π-electron system consisting of a phenol group (latent donor) and two pyridinium groups (acceptors, also termed picolinium groups). The deprotonation of the phenol led to the formation of a phenolate or quinone form (active donor), that was able to donate a π-electron pair to one of the two pyridinium acceptors via charge transfer. While the phenol form of the dye is non-fluorescent, the phenolate form emanates strong NIR

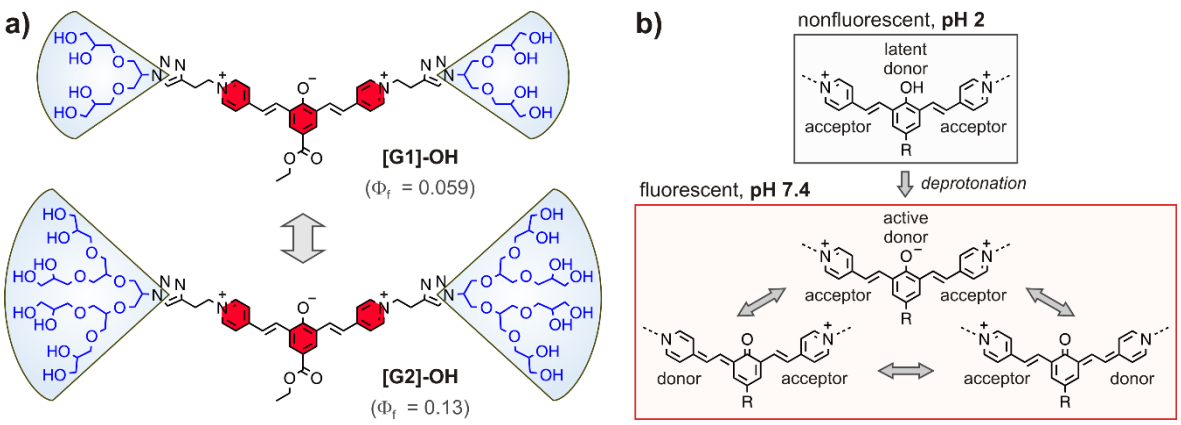

Figure 5.4. Fourth project about PG-dendronized cyanine derivatives. a) Structures of [G1]- and [G2]-cyanine derivatives. b) Donor-two-acceptor π-electron system of the dye.

fluorescence. In optical measurements, the [G1]-cyanine derivative ($\Phi_f = 5.9\%$) suffered from poor water solubility leading to aggregation. By contrast, the [G2]-cyanine derivative ($\Phi_f = 13\%$) showed good water solubility and enhanced fluorescence properties due to increased dendritic shielding (Figure 5.4a). The turn-on/turn-off fluorescence mechanism was demonstrated on the [G2]-cyanine derivative upon deprotonation of the phenol group by a change in pH. At acidic pH 2, the dye yielded no NIR emission and exhibited a blue-shifted absorption band, indicating the presence of its protonated form. At neutral pH 7.4, the dye exhibited a strong NIR emission and a red-shifted absorption emanating from its quinone form (Figure 5.4b). The appearance of NIR fluorescence was associated with a color change from black to red that could be visualized with an NIR camera. The large Stokes shift of the quinone of about 200 nm indicated a low potential for fluorescence self-quenching. In two different photostability studies, the [G2]-cyanine derivative outperformed conventional cy5 and cy7 dyes and exhibited good bioimaging potential in the staining of macrophages. The turn-on/turn-off fluorescence mechanism, large Stokes shift, and high photostability make the [G2]-dendronized cyanine derivative a suitable NIR fluorescent probe for biological assays.

In summary, these studies showed that the site isolation of fluorophores with hydroxylated PG dendrons constitutes a promising way to introduce water solubility and reduce aggregate formation. The introduction of charged sulfate groups in the dendron periphery exerted a positive effect on the optical properties of the dyes. A comparative study between the neutral and charged PBIs revealed superior intracellular staining efficiencies of sulfated labels over their hydroxylated analogs. The charged labels featured a reinforced aggregate suppression and improved cellular uptake due to the ionic sulfate groups. The diminished aggregation is due to the Coulomb repulsion forces of the negatively charged sulfates, which prevent intermolecular π-π stacking of the dyes. The improved uptake relies on the ability of heparan sulfate mimics, such as dendritic PG sulfates (dPGS), to interact with cell surface-bound scavenger receptors that mediate the uptake of polyanionic ligands.[264] In comparison, neutral labels showed inferior intracellular fluorescence signals due to weaker shielding capacity in combination with poorer cellular uptake caused by their neutral charge, related protein-resistant properties, and weak nonspecific interactions with biological systems.[263] For this reason, charged labels provided a higher intracellular fluorescence intensity than their neutral counterparts. However, regardless of the state of charge (neutral or ionic), the cellular staining efficiency of the labels improved with increasing dendron generation. This finding indicates that the combination of steric and electrostatic shielding is an efficient tool for the site isolation of PBIs. Therefore, it is not surprising that in each of the projects, the best bioimaging candidate was the fluorophore

with the most sterically demanding and, in the case of charged labels, highly charged dendron species. The result of this dual shielding effect became evident by excellent FQYs of up to 100%. Remarkably, such high FQYs have not previously been reported for either core-substituted or core-unsubstituted neutral or charged PBIs in aqueous media. The biological suitability of the PBI labels was successfully demonstrated by fluorescence imaging studies on cells using PBI-conjugated: i) antibodies, ii) polymer nanoparticles, and iii) polymer-SWNT complexes. The neutral and charged labels were tolerated well by the utilized cell lines and showed no cytotoxic side effects. Adverse effects due to the use of sterically demanding and/or charged labels or could not be established in the studies carried out.

In conclusion, it was demonstrated that the introduction of hydrophilic, sterically demanding PG dendrons and monofunctional linkers onto core-unsubstituted PBIs leads to water-soluble, highly fluorescent, site-specific dye labels suitable for bioimaging applications. In order to obtain high intracellular fluorescence signals and improved cellular uptake, the introduction of charged sulfate groups in the dendron periphery is mandatory. The presented PG-dendronized PBIs constitute a novel generation of labels and set new benchmarks for the design of future PBI-based fluorophores for bioimaging studies.

6 Future Perspectives

The results of this work demonstrate the versatile bioimaging application of dendronized monofunctionalized PBIs. The biomarkers possess emission maxima located in the green range of the electromagnetic spectrum (544-552 nm). However, for bioimaging purposes an emission in the first optical window (650-1,350 nm) is of interest, where light has its maximum penetration depth. Bay substitution has proven to be a useful tool to shift the emission of PBIs into the far-red up to the NIR region.[235] Hence, the absorption and emission of the presented PBI labels could be red-shifted by introduction of sulfonyl phenoxy or pyridinium groups in the bay positions.

The size of a label is an important criterion, as bulky fluorophores might influence the structure and function of the biomolecule after labeling. Other ways to generate water-soluble, highly fluorescent, monofunctionalized PBIs could be investigated without the use of sterically demanding PG dendrons. For that purpose, hydrophilic groups like PEG chains, cyclodextrins, crown ethers, etc., could be tested to generate small-size and low-weight PBI biolabels ($M_W \leq 1$ kDa) for delicate biomolecules such as small peptides or nucleotides.

Cetuximab offers multiple lysine residues per antibody that are able to undergo labeling. However, for single-molecule studies, mono-selective binding of one dye molecule per biomolecule is of interest. Blood plasma proteins like human serum albumin (HSA) or bovine serum albumin (BSA) exhibit a single reactive cysteine group (Cys34) that allows mono-selective labeling. In addition to albumin, recombinant proteins or defined cRGD (cyclic Arg-Gly-Asp) peptides could be applied in bioconjugation studies on a single-molecule level. In addition to a linker with an NHS ester function, a linker with a maleimide function could be generated to label a variety of biomolecules containing Lys or Cys residues.

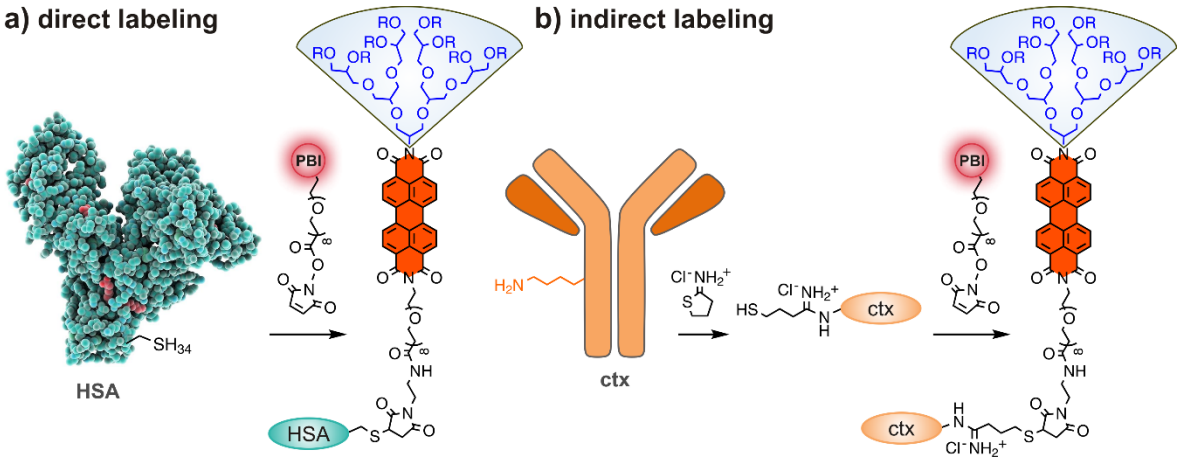

Figure 6.1. Maleimide-functionalized PBI labels for a) direct labeling of Cys residues of blood protein human serum albumin (HAS) or b) indirect labeling of Lys residues of antibody cetuximab (ctx) by means of Traut's reagent. HAS protein reprinted from Ref. [265] (© 2018 FineArtAmerica.com).

In fact, the maleimide function would offer the advantage of being able to bind Cys and Lys residues, the latter by means of Traut's reagent (2-iminothiolane, see Figure 6.1).

Charge plays an important role in the cellular uptake and biodistribution of a label. The use of sulfated dendronized PBIs was inspired by polyanionic dendritic polyglycerol sulfates (dPGS). Manifold sulfated compounds such as dPGS are highly water-soluble multivalent systems that exert an intrinsic anti-inflammatory effect on sore tissue by reducing the inflammatory response.[266] Polycationic systems, on the other hand, bearing protonated amine groups have a strong affinity for negatively charged cell membranes. This binding affinity results in high cellular uptake[267] and allows for noncovalent binding of negatively charged polyelectrolytes such as DNA or nuclear proteins.[47] Comparative studies between positively and negatively charged ionic compounds revealed a charge-dependent cellular uptake and metabolism for oppositely charged species.[263] However, the use of charged labels entails the risk of non-specific binding interactions with cell components. A profound comparative study between positively, neutrally, and negatively charged PBIs could reveal the best candidate, which could be chosen as a benchmark label for future bioimaging studies.

Dendronized dialkylated perylene-based dyes have shown great potential as markers of the disordered lipid domains of cellular membranes.[258] The incorporation of an alkyl-cholesterol anchor unit in the linker position of mono-dendronized PBIs should generate amphiphilic dyes that might be able to reach the liquid-ordered domains in the lower lying part of the membrane. These so-called lipid raft domains influence the membrane fluidity and play an important role in fundamental cellular surface processes like membrane protein and receptor trafficking.[268] These lipid rafts, which naturally contain cholesterol, are more ordered and tightly packed than the surrounding bilayers. The incorporation of steroidal PBIs into the lipid raft domains could enable a firmer and deeper anchorage of the labels into the more rigid part of the membrane (Figure 6.2b). Since the plasma membrane is highly negatively charged, it would be interesting to test the effect of positively, neutrally, and negatively charged dendronized PBIs (Figure 6.2a). The penetration of the membrane with these dendronized steroidal PBIs could be monitored by time-resolved fluorescence spectroscopy and would most likely result in membrane and vesicle staining by virtue of highly fluorescent single-embedded PBIs.

Furthermore, the polar hydroxylated headgroups and hydrophobic tail of these amphiphilic PBIs could provide a suitable interior for the encapsulation of hydrophobic drug molecules, e.g., dexamethasone or doxorubicin in form of micelles. The resulting core-shell architectures could be probed as potential drug delivery systems by release studies on cells.

It can be assumed that the micelles break open on the cell surface, thereby releasing the active substances, which could then be absorbed into the cells. Due to the use of a dye-based drug delivery system, the drug release could be monitored by membrane staining of the fluorescent PBI-makers. A comparative study of steroidal PBIs in different dendron generations could provide information on the degree of hydrophilicity needed to form stable micelles; the differently dendronized [Gn]-PBI-cholesterols (n = 1-3) could furthermore produce micelles of various sizes for the encapsulation of a wide range of molecules.

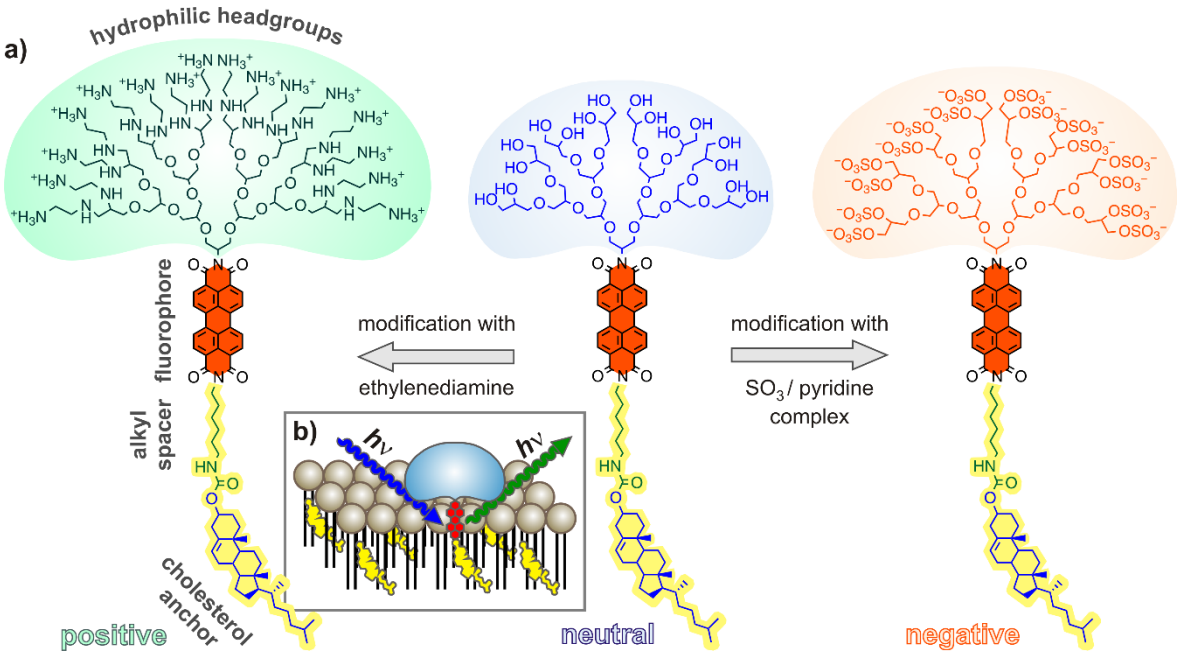

Figure 6.2. a) Positively, neutrally, and negatively charged [G3]-dendronized PBI markers with an alkyl linker and cholesterol anchor unit for fixation in the lipid raft domains of cell membranes. b) Cartoonlike representation of the insertion of the fluorescent PBI marker into the lipid raft domains of the membrane, which naturally contain cholesterol (yellow).

7 Bibliography

[1] H. Valladas, J. Clottes, J. M. Geneste, M. A. Garcia, M. Arnold, H. Cachier, N. Tisnerat-Laborde, *Nature* **2001**, *413*, 479.

[2] A. Gürses, M. Açıkyıldız, K. Güneş, M. S. Gürses in *Dyes and Pigments*, 1st Ed., Springer International Publishing AG, Switzerland, **2016**.

[3] R. Pohorecki, J. Bridgwater, M. Molzahn, R. Gani, C. Gallegos in *Chemical Engineering Education and Main Products*, EOLSS Publishers Company Limited, **2010**.

[4] E. Noelting, *Ber. Dtsch. Chem. Ges.* **1916**, *49*, 1751-1832.

[5] H. Zollinger in *Color Chemistry. Synthesis, Properties and Applications of Organic Dyes and Pigments*, 3rd revised Ed., Wiley-VCH Verlag GmbH & Co. KGaA, Weinheim, **2003**.

[6] P. Ball, *The Royal Society of Chemistry* **2014**, https://www.chemistryworld.com/feature/the-colourful-science/7448.article [March 3rd, 2018].

[7] A. Horan, *Royal Society of Chemistry* **2018**, http://www.rsc.org/Membership/Networking/InterestGroups/OrganicDivision/organic-chemistry-case-studies/organic-chemistry-colour-dyes.asp [March 2nd, 2018].

[8] Science Clarified, *Advameg, Inc.* **2018**, http://www.scienceclarified.com/Di-El/Dyes-and-Pigments.html [March 2nd, 2018].

[9] D. Jacoby, *Dumbarton Oaks Papers* **2004**, *58*, 197–240.

[10] A. Kraft, *Bull. Hist. Chem.* **2008**, *33*, 61-67.

[11] A. S. Travis, *Technol. Cult.* **1990**, *31*, 51-82.

[12] A. Baeyer, A. Emmerling, *Ber. Dtsch. Chem. Ges.* **1870**, *3*, 514-517.

[13] J. Griffiths, *Chem. Unserer Zeit* **1993**, *27*, 21-31.

[14] V. R. Kanetkar, *Resonance* **2010**, *15*, 794-803.

[15] J. Barber, *Chem. Soc. Rev.* **2009**, *38*, 185-196.

[16] K. Meyer, *Chem. Unserer Zeit* **2002**, *36*, 178-192.

[17] Bertvthul, *Pixabay* **2018** https://pixabay.com/de/blatt-textur-natur-green-frisch-884505/ [March 5th, 2018].

[18] F. P. Schäfer in *Topics in Applied Physics: Dye Lasers*, 3rd enlarged and revised Ed., Springer-Verlag, Berlin **1991**.

[19] R. W. Sabnis, in *Handbook of Fluorescent Dyes and Probes*, John Wiley & Sons, Inc, **2015**.

[20] C. Arcoumanis, J. J. McGuirk, J. M. L. M. Palma, *Exp. Fluids* **1990**, *10*, 177-180.

[21] H. M. Smith in *High Performance Pigments*, 2nd Ed., Wiley-VCH Verlag GmbH & Co. KGaA, Weinheim, **2002**.

[22] R. Scholl, J. Mansfeld, *Ber. Dtsch. Chem. Ges.* **1910**, *43*, 1734-1746.

[23] Z. Yuan, S.-L. Lee, L. Chen, C. Li, K. S. Mali, S. De Feyter, K. Müllen, *Chem. Eur. J.* **2013**, *19*, 11842-11846.

[24] J. Qu, N. G. Pschirer, M. Könemann, K. Müllen, Y. Avlasevic, *BASF SE, Germany; Max-Planck-Gesellschaft zur Förderung der Wissenschaften e.V.* **2008**, *Patent No. WO2008052927A1*, pp. 48.

[25] A. Bohnen, K. H. Koch, W. Lüttke, K. Müllen, *Angew. Chem.* **1990**, *102*, 548-550; *Angew. Chem. Int. Ed. Engl.* **1990**, *29*, 525-527.

[26] Y. Avlasevich, C. Kohl, K. Müllen, *J. Mater. Chem.* **2006**, *16*, 1053-1057.

[27] S. Mais, J. Tittel, T. Basche, C. Bräuchle, W. Göhde, H. Fuchs, G. Müller, K. Müllen, *J. Phys. Chem. A* **1997**, *101*, 8435-8440.

[28] T. Christ, F. Kulzer, T. Weil, K. Müllen, T. Basche, *Chem. Phys. Lett.* **2003**, *372*, 878-885.

[29] A. Herrmann, K. Müllen, *Chem. Lett.* **2006**, *35*, 978-985.

[30] M. Maus, S. Mitra, M. Lor, J. Hofkens, T. Weil, A. Herrmann, K. Müllen, F. C. De Schryver, *J. Phys. Chem. A* **2001**, *105*, 3961-3966.

[31] D. Liu, S. De Feyter, M. Cotlet, A. Stefan, U.-M. Wiesler, A. Herrmann, D. Grebel-Koehler, J. Qu, K. Müllen, F. C. De Schryver, *Macromolecules* **2003**, *36*, 5918-5925.

[32] T. Weil, U. M. Wiesler, A. Herrmann, R. Bauer, J. Hofkens, F. C. De Schryver, K. Müllen, *J. Am. Chem. Soc.* **2001**, *123*, 8101-8108.

[33] A. Herrmann, T. Weil, V. Sinigersky, U.-M. Wiesler, T. Vosch, J. Hofkens, F. C. De Schryver, K. Müllen, *Chem. Eur. J.* **2001**, *7*, 4844-4853.

[34] H. Langhals, *Heterocycles* **1995**, *40*, 477-500.

[35] J. Perlstein, *Chem. Mater.* **1994**, *6*, 319-326.

[36] P. M. Kazmaier, R. Hoffmann, *J. Am. Chem. Soc.* **1994**, *116*, 9684-9691.

[37] K. Y. Law, *Chem. Rev.* **1993**, *93*, 449-486.

[38] M. Kardos, **1913**, *Patent No. DE276358*.

[39] M. Kardos, **1913**, *Patent No. DE276956* (addition to 276, 357; C. A. 278, 3243).

[40] H. G. Löhmannsröben, H. Langhals, *Appl. Phys. B* **1989**, *B48*, 449-452.

[41] R. Reisfeld, G. Seybold, *Chimia* **1990**, *44*, 295-297.

[42] A. J. Breeze, A. Salomon, D. S. Ginley, B. A. Gregg, H. Tillmann, H.-H. Hörhold, *Appl. Phys. Lett.* **2002**, *81*, 3085-3087.

[43] G. Seybold, G. Wagenblast, *Dyes Pigm.* **1989**, *11*, 303-317.

[44] T.-L. Chiu, K.-H. Chuang, C.-F. Lin, Y.-H. Ho, J.-H. Lee, C.-C. Chao, M.-K. Leung, D.-H. Wan, C.-Y. Li, H.-L. Chen, *Thin Solid Films* **2009**, *517*, 3712-3716.

[45] F. Würthner, C. R. Saha-Möller, B. Fimmel, S. Ogi, P. Leowanawat, D. Schmidt, *Chem. Rev.* **2016**, *116*, 962-1052.

[46] C. Huang, S. Barlow, S. R. Marder, *J. Org. Chem.* **2011**, *76*, 2386-2407.

[47] M. Sun, K. Müllen, M. Yin, *Chem. Soc. Rev.* **2016**, *45*, 1513-1528.

[48] S. Demmig, H. Langhals, *Chem. Ber.* **1988**, *121*, 225-230.

[49] H. Langhals, S. Demmig, T. Potrawa, *J. Prakt. Chem.* **1991**, *333*, 733-748.

[50] H. Langhals, S. Demmig, H. Huber, *Spectrochim. Acta, Part A* **1988**, *44A*, 1189-1193.

[51] H. Langhals, J. Karolin, L. B. Å. Johansson, *J. Chem. Soc., Faraday Trans.* **1998**, *94*, 2919-2922.

[52] Z. Chen, V. Stepanenko, V. Dehm, P. Prins, L. D. A. Siebbeles, J. Seibt, P. Marquetand, V. Engel, F. Würthner, *Chem. Eur. J.* **2007**, *13*, 436-449.

[53] A. Rademacher, S. Märkle, H. Langhals, *Chem. Ber.* **1982**, *115*, 2927-2934.

[54] W. E. Ford, P. V. Kamat, *J. Phys. Chem.* **1987**, *91*, 6373-6380.

[55] S. Nakazono, S. Easwaramoorthi, D. Kim, H. Shinokubo, A. Osuka, *Org. Lett.* **2009**, *11*, 5426-5429.

[56] Z. Chen, A. Lohr, C. R. Saha-Möller, F. Würthner, *Chem. Soc. Rev.* **2009**, *38*, 564-584.

[57] F. Pichierri, *J. Mol. Struct.: Theochem* **2004**, *686*, 57-63.

[58] M. Sadrai, L. Hadel, R. R. Sauers, S. Husain, K. Krogh-Jespersen, J. D. Westbrook, G. R. Bird, *J. Phys. Chem.* **1992**, *96*, 7988-7996.

[59] Y. Nagao, *Prog. Org. Coat.* **1997**, *31*, 43-49.

[60] F. Würthner, Z. Chen, V. Dehm, V. Stepanenko, *Chem. Commun.* **2006**, 1188-1190.

[61] F. Würthner, C. Thalacker, S. Diele, C. Tschierske, *Chem. Eur. J.* **2001**, *7*, 2245-2253.

[62] F. Würthner, *Chem. Commun.* **2004**, 1564-1579.

[63] X. Zhang, D. Görl, V. Stepanenko, F. Würthner, *Angew. Chem.* **2014**, *126*, 1294-1298; *Angew. Chem. Int. Ed.* **2014**, *53*, 1270-1274.

[64] V. Dehm, Z. Chen, U. Baumeister, P. Prins, L. D. A. Siebbeles, F. Würthner, *Org. Lett.* **2007**, *9*, 1085-1088.

[65] J. M. Giaimo, A. V. Gusev, M. R. Wasielewski, *J. Am. Chem. Soc.* **2002**, *124*, 8530-8531.

[66] F. Würthner, V. Stepanenko, Z. Chen, C. R. Saha-Möller, N. Kocher, D. Stalke, *J. Org. Chem.* **2004**, *69*, 7933-7939.

[67] F. Würthner, A. Sautter, J. Schilling, *J. Org. Chem.* **2002**, *67*, 3037-3044.

[68] M. Queste, C. Cadiou, B. Pagoaga, L. Giraudet, N. Hoffmann, *New J. Chem.* **2010**, *34*, 2537-2545.

[69] Z. Chen, U. Baumeister, C. Tschierske, F. Würthner, *Chem. Eur. J.* **2007**, *13*, 450-465.

[70] T. Heek, F. Würthner, R. Haag, *Chem. Eur. J.* **2013**, *19*, 10911-10921.

[71] Y. Zhao, M. R. Wasielewski, *Tetrahedron Lett.* **1999**, *40*, 7047-7050.

[72] R. K. Dubey, A. Efimov, H. Lemmetyinen, *Chem. Mater.* **2011**, *23*, 778-788.

[73] A. S. Lukas, Y. Zhao, S. E. Miller, M. R. Wasielewski, *J. Phys. Chem. B* **2002**, *106*, 1299-1306.

[74] V. Sivamurugan, K. Kazlauskas, S. Jursenas, A. Gruodis, J. Simokaitiene, J. V. Grazulevicius, S. Valiyaveettil, *J. Phys. Chem. B* **2010**, *114*, 1782-1789.

[75] N. V. Handa, K. D. Mendoza, L. D. Shirtcliff, *Org. Lett.* **2011**, *13*, 4724-4727.

[76] P. Leowanawat, A. Nowak-Król, F. Würthner, *Org. Chem. Front.* **2016**, *3*, 537-544.

[77] B. A. Jones, A. Facchetti, M. R. Wasielewski, T. J. Marks, *J. Am. Chem. Soc.* **2007**, *129*, 15259-15278.

[78] F. Würthner, *Pure Appl. Chem.* **2006**, *78*, 2341-2349.

[79] R. Schmidt, M. M. Ling, J. H. Oh, M. Winkler, M. Koenemann, Z. Bao, F. Würthner, *Adv. Mater.* **2007**, *19*, 3692-3695.

[80] F. Würthner, P. Osswald, R. Schmidt, T. E. Kaiser, H. Mansikkamaki, M. Konemann, *Org. Lett.* **2006**, *8*, 3765-3768.

[81] M. J. Ahrens, M. J. Fuller, M. R. Wasielewski, *Chem. Mater.* **2003**, *15*, 2684-2686.

[82] M.-J. Lin, A. J. Jimenez, C. Burschka, F. Würthner, *Chem. Commun.* **2012**, *48*, 12050-12052.

[83] P. Rajasingh, R. Cohen, E. Shirman, L. J. W. Shimon, B. Rybtchinski, *J. Org. Chem.* **2007**, *72*, 5973-5979.

[84] V. I. Rogovik, L. F. Gutnik, *Zh. Org. Khim.* **1988**, *24*, 635-639.

[85] B. A. Jones, M. J. Ahrens, M. H. Yoon, A. Facchetti, T. J. Marks, M. R. Wasielewski, *Angew. Chem.* **2004**, *116*, 6523-6526; *Angew. Chem. Int. Ed.* **2004**, *43*, 6363-6366.

[86] Z. An, S. A. Odom, R. F. Kelley, C. Huang, X. Zhang, S. Barlow, L. A. Padilha, J. Fu, S. Webster, D. J. Hagan, E. W. Van Stryland, M. R. Wasielewski, S. R. Marder, *J. Phys. Chem. A* **2009**, *113*, 5585-5593.

[87] U. Rohr, C. Kohl, K. Müllen, A. van de Craats, J. Warman, *J. Mater. Chem.* **2001**, *11*, 1789-1799.

[88] W. Qiu, S. Chen, X. Sun, Y. Liu, D. Zhu, *Org. Lett.* **2006**, *8*, 867-870.

[89] X. Zhan, Z. a. Tan, B. Domercq, Z. An, X. Zhang, S. Barlow, Y. Li, D. Zhu, B. Kippelen, S. R. Marder, *J. Am. Chem. Soc.* **2007**, *129*, 7246-7247.

[90] X. Zhan, Z. a. Tan, E. Zhou, Y. Li, R. Misra, A. Grant, B. Domercq, X.-H. Zhang, Z. An, X. Zhang, S. Barlow, B. Kippelen, S. R. Marder, *J. Mater. Chem.* **2009**, *19*, 5794-5803.

[91] P. Spenst, F. Würthner, *Angew. Chem.* **2015**, *127*, 10303-10306; *Angew. Chem. Int. Ed.* **2015**, *54*, 10165-10168.

[92] M. Son, K. H. Park, C. Shao, F. Würthner, D. Kim, *J. Phys. Chem. Lett.* **2014**, *5*, 3601-3607.

[93] F. Kakiuchi, S. Murai, *Acc. Chem. Res.* **2002**, *35*, 826-834.

[94] F. Kakiuchi, S. Sekine, Y. Tanaka, A. Kamatani, M. Sonoda, N. Chatani, S. Murai, *Bull. Chem. Soc. Jpn.* **1995**, *68*, 62-83.

[95] S. Nakazono, Y. Imazaki, H. Yoo, J. Yang, T. Sasamori, N. Tokitoh, T. Cedric, H. Kageyama, D. Kim, H. Shinokubo, A. Osuka, *Chem. Eur. J.* **2009**, *15*, 7530-7533.

[96] T. Teraoka, S. Hiroto, H. Shinokubo, *Org. Lett.* **2011**, *13*, 2532-2535.

[97] G. Battagliarin, Y. Zhao, C. Li, K. Müllen, *Org. Lett.* **2011**, *13*, 3399-3401.

[98] G. Battagliarin, C. Li, V. Enkelmann, K. Müllen, *Org. Lett.* **2011**, *13*, 3012-3015.

[99] J. Wu, D. He, L. Zhang, Y. Liu, X. Mo, J. Lin, H.-j. Zhang, *Org. Lett.* **2017**, *19*, 5438-5441.

[100] J. R. Lakowicz in *Principles of Fluorescence Spectroscopy*, 3rd Ed., Springer International Publishing AG, **2006**.

[101] J. W. Lichtman, J.-A. Conchello, *Nat. Methods* **2005**, *2*, 910-919.

[102] A. D. McNaught, A. Wilkinson in *IUPAC Gold Book - Compendium of Chemical Terminology*, 2nd Ed., Blackwell Scientific Publications, Oxford **1997**.

[103] B. Herman, J. R. Lakowicz, D. B. Murphy, T. J. Fellers, M. W. Davidson, *Olympus Corporation* **2018**, https://www.olympus-lifescience.com/es/microscope-resource/primer/techniques/confocal/fluoroexciteemit/ [April 16th, 2018].

[104] R. Roy, S. Hohng, T. Ha, *Nat. Methods* **2008**, *5*, 507-516.

[105] B. Prevo, E. J. G. Peterman, *Chem. Soc. Rev.* **2014**, *43*, 1144-1155.

[106] S. Zadran, S. Standley, K. Wong, E. Otiniano, A. Amighi, M. Baudry, *Appl. Microbiol. Biotechnol.* **2012**, *96*, 895-902.

[107] A. Makhal, S. Sarkar, T. Bora, S. Baruah, J. Dutta, A. K. Raychaudhuri, S. K. Pal, *J. Phys. Chem. C* **2010**, *114*, 10390-10395.

[108] Igor Medintz, N. Hildebrandt in *FRET – Förster Resonance Energy Transfer*, Wiley-VCH Verlag GmbH & Co. KGaA, Weinheim, **2013**.

[109] B. Herman, V. E. Centonze Frohlich, J. R. Lakowicz, T. J. Fellers, M. W. Davidson, *Olympus Corporation* **2018**, https://www.olympus-lifescience.com/en/microscope-resource/primer/techniques/fluorescence/fret/fretintro/ [April 13th, 2018].

[110] B. Valeur, M. N. Berberan-Santos, 2nd Ed., Wiley-VCH Verlag GmbH & Co. KGaA, Weinheim, **2012**.

[111] V. Helms in *Principles of Computational Cell Biology: From Protein Complexes to Cellular Networks*, 1st Ed., Wiley-VCH Verlag GmbH & Co. KGaA, Weinheim, **2008**.

[112] D. C. Harris in *Quantitative Chemical Analysis*, 8th Ed., W. H. Freeman and Company, New York, **2010**.

[113] E. Lerner, T. Cordes, A. Ingargiola, Y. Alhadid, S. Chung, X. Michalet, S. Weiss, *Science* **2018**, *359*.

[114] C. Hippius, F. Schlosser, M. O. Vysotsky, V. Böhmer, F. Würthner, *J. Am. Chem. Soc.* **2006**, *128*, 3870-3871.

[115] C. Hippius, I. H. M. van Stokkum, M. Gsänger, M. M. Groeneveld, R. M. Williams, F. Würthner, *J. Phys. Chem. C* **2008**, *112*, 2476-2486.

[116] T.-L. Liu, S. Upadhyayula, D. E. Milkie, V. Singh, K. Wang, I. A. Swinburne, K. R. Mosaliganti, Z. M. Collins, T. W. Hiscock, J. Shea, A. Q. Kohrman, T. N. Medwig, D. Dambournet, R. Forster, B. Cunniff, Y. Ruan, H. Yashiro, S. Scholpp, E. M. Meyerowitz, D. Hockemeyer, D. G. Drubin, B. L. Martin, D. Q. Matus, M. Koyama, S. G. Megason, T. Kirchhausen, E. Betzig, *Science* **2018**, *360*.

[117] A. Ettinger, T. Wittmann, *Methods Cell Biol.* **2014**, *123*, 77-94.

[118] S. Shashkova, M. C. Leake, *Biosci. Rep.* **2017**, *37*, BSR20170031.

[119] E. M. Kudalkar, T. N. Davis, C. L. Asbury, *Cold Spring Harbor protocols* **2016**, 435-438.

[120] A. Diaspro, G. Chirico, M. Collini, *Q. Rev. Biophys.* **2005**, *38*, 97-166.

[121] M. W. Davidson, *Michael W. Davidson and The Florida State University* **2004** https://micro.magnet.fsu.edu/primer/techniques/fluorescence/gallery/cells/bpae/bpaecellsexlarge1.html [April 30th, 2018].

[122] D. Salo, D. Kim, Q. Cao, M. Y. Berezin, *PennWell Corporation* **2014**, https://www.biooptics world.com/articles/print/volume-7/issue-1/features/multispectral-imaging-deep-tissue-imaging-extended-near-infrared-a-new-window-on-in-vivo-bioimaging.html [April 24th, 2018].

[123] E. Wegel, A. Göhler, B. C. Lagerholm, A. Wainman, S. Uphoff, R. Kaufmann, I. M. Dobbie, *Sci. Rep.* **2016**, *6*, 27290.

[124] C.-L. Chiu, K. Patsch, F. Cutrale, A. Soundararajan, D. B. Agus, S. E. Fraser, D. Ruderman, *Sci. Rep.* **2016**, *6*, 22435.

[125] Y. Sako, J. Ichinose, M. Morimatsu, K. Ohta, T. Uyemura, *J. Pharmacol. Sci.* **2003**, *93*, 253-258.

[126] R. N. Day, F. Schaufele, *Mol. Endocrinol.* **2005**, *19*, 1675-1686.

[127] S. Li, P. C. Hu, N. Malmstadt, *Biophys. J.* **2011**, *101*, 700-708.

[128] A. M. Smith, M. C. Mancini, S. Nie, *Nat. Nanotechnol.* **2009**, *4*, 710-711.

[129] M. Chen, M. Yin, *Prog. Polym. Sci.* **2014**, *39*, 365-395.

[130] O. S. Wolfbeis, *Chem. Soc. Rev.* **2015**, *44*, 4743-4768.

[131] Z. Guo, S. Park, J. Yoon, I. Shin, *Chem. Soc. Rev.* **2014**, *43*, 16-29.

[132] S. A. Hilderbrand, F. Shao, C. Salthouse, U. Mahmood, R. Weissleder, *Chem. Commun.* **2009**, 4188-4190.

[133] Z. Liu, X. Li, S. M. Tabakman, K. Jiang, S. Fan, H. Dai, *J. Am. Chem. Soc.* **2008**, *130*, 13540-13541.

[134] J. Maultzsch, R. Pomraenke, S. Reich, E. Chang, D. Prezzi, A. Ruini, E. Molinari, M. S. Strano, C. Thomsen, C. Lienau, *Phys. Rev. B* **2005**, *72*, 241402.

[135] H. Gong, R. Peng, Z. Liu, *Adv. Drug Del. Rev.* **2013**, *65*, 1951-1963.

[136] K. Welsher, S. P. Sherlock, H. Dai, *Proc. Natl. Acad. Sci. U. S. A.* **2011**, *108*, 8943-8948.

[137] A. De La Zerda, C. Zavaleta, S. Keren, S. Vaithilingam, S. Bodapati, Z. Liu, J. Levi, B. R. Smith, T.-J. Ma, O. Oralkan, Z. Cheng, X. Chen, H. Dai, B. T. Khuri-Yakub, S. S. Gambhir, *Nat. Nanotechnol.* **2008**, *3*, 557.

[138] J. Bansal, I. Singh, P. K. Bhatnagar, P. C. Mathur, *J. Biosci. Bioeng.* **2013**, *115*, 438-441.

[139] S. Chae, D. Kim, K.-j. Lee, D. Lee, Y.-O. Kim, Y. C. Jung, S. D. Rhee, K. R. Kim, J.-O. Lee, S. Ahn, B. Koh, *ACS Omega* **2018**, *3*, 5938-5945.

[140] Z. Liu, X. Sun, N. Nakayama-Ratchford, H. Dai, *ACS Nano* **2007**, *1*, 50-56.

[141] E. Heister, V. Neves, C. Tîlmaciu, K. Lipert, V. S. Beltrán, H. M. Coley, S. R. P. Silva, J. McFadden, *Carbon* **2009**, *47*, 2152-2160.

[142] S. Vardharajula, S. Z. Ali, P. M. Tiwari, E. Eroğlu, K. Vig, V. A. Dennis, S. R. Singh, *Int. J. Nanomed.* **2012**, *7*, 5361-5374.

[143] K. Welsher, Z. Liu, S. P. Sherlock, J. T. Robinson, Z. Chen, D. Daranciang, H. Dai, *Nat. Nanotechnol.* **2009**, *4*, 773-780.

[144] Z. Liu, C. Davis, W. Cai, L. He, X. Chen, H. Dai, *Proc. Natl. Acad. Sci. U. S. A.* **2008**, *105*, 1410-1415.

[145] Z. Liu, S. Tabakman, K. Welsher, H. Dai, *Nano Res.* **2009**, *2*, 85-120.

[146] H. Wang, W. Zhou, D. L. Ho, K. I. Winey, J. E. Fischer, C. J. Glinka, E. K. Hobbie, *Nano Lett.* **2004**, *4*, 1789-1793.

[147] M. W. Chik, Z. Hussain, M. Zulkefeli, M. Tripathy, S. Kumar, A. B. A. Majeed, K. Byrappa, *Drug Delivery Transl. Res.* **2018**.

[148] P. Bilalis, D. Katsigiannopoulos, A. Avgeropoulos, G. Sakellariou, *RSC Adv.* **2014**, *4*, 2911-2934.

[149] J. Zhang, M. P. Landry, P. W. Barone, J.-H. Kim, S. Lin, Z. W. Ulissi, D. Lin, B. Mu, A. A. Boghossian, A. J. Hilmer, A. Rwei, A. C. Hinckley, S. Kruss, M. A. Shandell, N. Nair, S. Blake, F. Sen, S. Sen, R. G. Croy, D. Li, K. Yum, J.-H. Ahn, H. Jin, D. A. Heller, J. M. Essigmann, D. Blankschtein, M. S. Strano, *Nat. Nanotechnol.* **2013**, *8*, 959-968.

[150] M. P. Landry, H. Ando, A. Y. Chen, J. Cao, V. I. Kottadiel, L. Chio, D. Yang, J. Dong, T. K. Lu, M. S. Strano, *Nat. Nanotechnol.* **2017**, *12*, 368.

[151] N. B. Saleh, D. Das, J. Plazas-Tuttle, D. Yang, J. T. Del Bonis-O'Donnell, M. P. Landry, *NanoImpact* **2017**, *6*, 90-98.

[152] S. Kruss, A. J. Hilmer, J. Zhang, N. F. Reuel, B. Mu, M. S. Strano, *Adv. Drug Delivery Rev.* **2013**, *65*, 1933-1950.

[153] Y. Bai, H. Xing, G. A. Vincil, J. Lee, E. J. Henderson, Y. Lu, N. G. Lemcoff, S. C. Zimmerman, *Chem. Sci.* **2014**, *5*, 2862-2868.

[154] Q. Zhao, K. Li, S. Chen, A. Qin, D. Ding, S. Zhang, Y. Liu, B. Liu, J. Z. Sun, B. Z. Tang, *J. Mater. Chem.* **2012**, *22*, 15128-15135.

[155] J. R. Taylor, M. M. Fang, S. Nie, *Anal. Chem.* **2000**, *72*, 1979-1986.

[156] A. Reisch, A. S. Klymchenko, *Small* **2016**, *12*, 1968-1992.

[157] K. Werengowska-Ciećwierz, M. Wiśniewski, A. P. Terzyk, S. Furmaniak, *Adv. Condens. Matter Phys.* **2015**, *2015*, 27.

[158] A. Jahn, J. E. Reiner, W. N. Vreeland, D. L. DeVoe, L. E. Locascio, M. Gaitan, *J. Nanopart. Res.* **2008**, *10*, 925-934.

[159] T. Asahi, T. Sugiyama, H. Masuhara, *Acc. Chem. Res.* **2008**, *41*, 1790-1798.

[160] J. B. Beil, S. C. Zimmerman, *Macromolecules* **2004**, *37*, 778-787.

[161] S. C. Zimmerman, J. R. Quinn, E. Burakowska, R. Haag, *Angew. Chem.* **2007**, *119*, 8312-8315; *Angew. Chem. Int. Ed.* **2007**, *46*, 8164-8167.

[162] E. Burakowska, J. R. Quinn, S. C. Zimmerman, R. Haag, *J. Am. Chem. Soc.* **2009**, *131*, 10574-10580.

[163] E. Harth, B. V. Horn, V. Y. Lee, D. S. Germack, C. P. Gonzales, R. D. Miller, C. J. Hawker, *J. Am. Chem. Soc.* **2002**, *124*, 8653-8660.

[164] C. Wu, T. Schneider, M. Zeigler, J. Yu, P. G. Schiro, D. R. Burnham, J. D. McNeill, D. T. Chiu, *J. Am. Chem. Soc.* **2010**, *132*, 15410-15417.

[165] P. S. Weiss, *ACS Nano* **2009**, *3*, 1310-1317.

[166] Y. Li, Y. Bai, N. Zheng, Y. Liu, G. A. Vincil, B. J. Pedretti, J. Cheng, S. C. Zimmerman, *Chem. Commun.* **2016**, *52*, 3781-3784.

[167] J. Pecher, S. Mecking, *Chem. Rev.* **2010**, *110*, 6260-6279.

[168] C. Wu, B. Bull, C. Szymanski, K. Christensen, J. McNeill, *ACS Nano* **2008**, *2*, 2415-2423.

[169] C. Wu, C. Szymanski, Z. Cain, J. McNeill, *J. Am. Chem. Soc.* **2007**, *129*, 12904-12905.

[170] Y. Chen, X. Xiong, *Chem. Commun.* **2010**, *46*, 5049-5060.

[171] K. Li, B. Liu, *Chem. Soc. Rev.* **2014**, *43*, 6570-6597.

[172] H. Kobayashi, M. Ogawa, R. Alford, P. L. Choyke, Y. Urano, *Chem. Rev.* **2010**, *110*, 2620-2640.

[173] J. Qu, C. Kohl, M. Pottek, K. Müllen, *Angew. Chem.* **2004**, *116*, 1554-1557; *Angew. Chem. Int. Ed.* **2004**, *43*, 1528-1531.

[174] E. Hemmer, A. Benayas, F. Legare, F. Vetrone, *Nanoscale Horiz.* **2016**, *1*, 168-184.

[175] S. Kaloyanova, Y. Zagranyarski, S. Ritz, M. Hanulová, K. Koynov, A. Vonderheit, K. Müllen, K. Peneva, *J. Am. Chem. Soc.* **2016**, *138*, 2881-2884.

[176] W. R. Kitley, P. J. Santa Maria, R. A. Cloyd, L. M. Wysocki, *Chem. Commun.* **2015**, *51*, 8520-8523.

[177] J. B. Grimm, L. D. Lavis, *Org. Lett.* **2011**, *13*, 6354-6357.

[178] Q. Zheng, M. F. Juette, S. Jockusch, M. R. Wasserman, Z. Zhou, R. B. Altman, S. C. Blanchard, *Chem. Soc. Rev.* **2014**, *43*, 1044-1056.

[179] L. Song, C. A. G. O. Varma, J. W. Verhoeven, H. J. Tanke, *Biophys. J.* **1996**, *70*, 2959-2968.

[180] T. Christ, F. Kulzer, P. Bordat, T. Basché, *Angew. Chem.* **2001**, *113*, 4323-4326; *Angew. Chem. Int. Ed.* **2001**, *40*, 4192-4195.

[181] N. Kuramoto, T. Kitao, *Dyes Pigm.* **1982**, *3*, 49-58.

[182] R. Bonnett, G. Martinez, *Tetrahedron* **2001**, *57*, 9513-9547.

[183] M. J. Davies, *Photochem. Photobiol. Sci.* **2004**, *3*, 17-25.

[184] H. Sies, C. F. M. Menck, *Mutat. Res., DNAging: Genet. Instab. Aging* **1992**, *275*, 367-375.

[185] M. Platkov, R. Tirosh, M. Kaufman, N. Zurgil, M. Deutsch, *J. Photochem. Photobiol. B: Biol.* **2014**, *140*, 306-314.

[186] R. Mittler, *Trends Plant Sci.* **2017**, *22*, 11-19.

[187] J. Vogelsang, R. Kasper, C. Steinhauer, B. Person, M. Heilemann, M. Sauer, P. Tinnefeld, *Angew. Chem.* **2008**, *120*, 5545-5550; *Angew. Chem. Int. Ed.* **2008**, *47*, 5465-5469.

[188] M. Swoboda, J. Henig, H.-M. Cheng, D. Brugger, D. Haltrich, N. Plumeré, M. Schlierf, *ACS Nano* **2012**, *6*, 6364-6369.

[189] S. J. Lord, N. R. Conley, H. l. D. Lee, S. Y. Nishimura, A. K. Pomerantz, K. A. Willets, Z. Lu, H. Wang, N. Liu, R. Samuel, R. Weber, A. Semyonov, M. He, R. J. Twieg, W. E. Moerner, *ChemPhysChem* **2009**, *10*, 55-65.

[190] N. R. Conley, J. S. Biteen, W. E. Moerner, *J. Phys. Chem. B* **2008**, *112*, 11878-11880.

[191] C. Steinhauer, C. Forthmann, J. Vogelsang, P. Tinnefeld, *J. Am. Chem. Soc.* **2008**, *130*, 16840-16841.

[192] D. Görl, X. Zhang, F. Würthner, *Angew. Chem.* **2012**, *124*, 6434-6455; *Angew. Chem. Int. Ed.* **2012**, *51*, 6328-6348.

[193] H. Langhals, *Fed. Rep. Ger.* **1988***, Patent No. DE3703513A1*, pp. 6.

[194] W. E. Ford, *J. Photochem.* **1987**, *37*, 189-204.

[195] G. Schnurpfeil, J. Stark, D. Woehrle, *Dyes Pigm.* **1995**, *27*, 339-350.

[196] Y. Huang, Y. Yan, B. M. Smarsly, Z. Wei, C. F. J. Faul, *J. Mater. Chem.* **2009**, *19*, 2356-2362.

[197] S. Rehm, V. Stepanenko, X. Zhang, T. H. Rehm, F. Würthner, *Chem. Eur. J.* **2010**, *16*, 3372-3382.

[198] B. Roy, T. Noguchi, D. Yoshihara, Y. Tsuchiya, A. Dawn, S. Shinkai, *Org. Biomol. Chem.* **2014**, *12*, 561-565.

[199] C. Backes, C. D. Schmidt, F. Hauke, C. Böttcher, A. Hirsch, *J. Am. Chem. Soc.* **2009**, *131*, 2172-2184.

[200] Z. Xu, W. Cheng, K. Guo, J. Yu, J. Shen, J. Tang, W. Yang, M. Yin, *ACS Appl. Mater. Interfaces* **2015**, *7*, 9784-9791.

[201] T. Heek, C. Kühne, H. Depner, K. Achazi, J. Dernedde, R. Haag, *Bioconjugate Chem.* **2016**, *27*, 727-736.

[202] J.-H. Ryu, C.-J. Jang, Y.-S. Yoo, S.-G. Lim, M. Lee, *J. Org. Chem.* **2005**, *70*, 8956-8962.

[203] B. Gao, H. Li, H. Liu, L. Zhang, Q. Bai, X. Ba, *Chem. Commun.* **2011**, *47*, 3894-3896.

[204] X. Zhang, Z. Chen, F. Würthner, *J. Am. Chem. Soc.* **2007**, *129*, 4886-4887.

[205] R. Samudrala, X. Zhang, R. M. Wadkins, D. L. Mattern, *Bioorg. Med. Chem.* **2007**, *15*, 186-193.

[206] H. Langhals, W. Jona, F. Einsiedl, S. Wohnlich, *Adv. Mater.* **1998**, *10*, 1022-1024.

[207] Y. Liu, K.-R. Wang, D.-S. Guo, B.-P. Jiang, *Adv. Funct. Mater.* **2009**, *19*, 2230-2235.

[208] N. I. Georgiev, A. R. Sakr, V. B. Bojinov, *Dyes Pigm.* **2011**, *91*, 332-339.

[209] W. Tuntiwechapikul, T. Taka, M. Béthencourt, L. Makonkawkeyoon, T. Randall Lee, *Bioorg. Med. Chem. Lett.* **2006**, *16*, 4120-4126.

[210] K.-R. Wang, H.-W. An, F. Qian, Y.-Q. Wang, J.-C. Zhang, X.-L. Li, *RSC Adv.* **2013**, *3*, 23190-23196.

[211] T. Heek, C. Fasting, C. Rest, X. Zhang, F. Würthner, R. Haag, *Chem. Commun.* **2010**, *46*, 1884-1886.

[212] K. Liu, Z. Xu, M. Yin, *Prog. Polym. Sci.* **2015**, *46*, 25-54.

[213] U. Resch-Genger, M. Grabolle, S. Cavaliere-Jaricot, R. Nitschke, T. Nann, *Nat. Methods* **2008**, *5*, 763.

[214] C. Kohl, T. Weil, J. Qu, K. Müllen, *Chem. Eur. J.* **2004**, *10*, 5297-5310.

[215] A. Margineanu, J. Hofkens, M. Cotlet, S. Habuchi, A. Stefan, J. Qu, C. Kohl, K. Müllen, J. Vercammen, Y. Engelborghs, T. Gensch, F. C. De Schryver, *J. Phys. Chem. B* **2004**, *108*, 12242-12251.

[216] L. Blancafort, M. A. Robb, *J. Phys. Chem. A* **2004**, *108*, 10609-10614.

[217] M. Kasha, *Radiat. Res.* **1963**, *20*, 55-70.

[218] A. S. Davydov in *Theory of Molecular Excitons (translated from Russian by M. Kasha and M. Oppenheimer)*, McGraw-Hill Book Co., **1962**.

[219] E. E. Jelley, *Nature* **1936**, *138*, 1009-1010.

[220] G. Scheibe, *Angew. Chem.* **1937**, *50*, 212-219.

[221] G. Scheibe, L. Kandler, H. Ecker, *Naturwissenschaften* **1937**, *25*, 75.

[222] M. Kasha, H. R. Rawls, M. A. El-Bayoumi, *Pure Appl. Chem.* **1965**, *11*, 371-392.

[223] T. E. Kaiser, H. Wang, V. Stepanenko, F. Würthner, *Angew. Chem.* **2007**, *119*, 5637-5640; *Angew. Chem. Int. Ed.* **2007**, *46*, 5541-5544.

[224] R. F. Fink, J. Seibt, V. Engel, M. Renz, M. Kaupp, S. Lochbrunner, H.-M. Zhao, J. Pfister, F. Würthner, B. Engels, *J. Am. Chem. Soc.* **2008**, *130*, 12858-12859.

[225] F. Würthner, T. E. Kaiser, C. R. Saha-Möller, *Angew. Chem.* **2011**, *123*, 3436-3473; *Angew. Chem. Int. Ed.* **2011**, *50*, 3376-3410.

[226] J. Kang, O. Kaczmarek, J. Liebscher, L. Daehne, *Int. J. Polym. Sci.* **2010**, 7 pages.

[227] J. Lydon, *J. Mater. Chem.* **2010**, *20*, 10071-10099.

[228] H. Tan, H. Liu, Y. Liu, W. Duan, X. Yi, Y. Wu, H. Zhao, L. Bai, *J. Biomater. Sci., Polym. Ed.* **2016**, *27*, 455-471.

[229] B. Muthuraj, S. R. Chowdhury, S. Mukherjee, C. R. Patra, P. K. Iyer, *RSC Adv.* **2015**, *5*, 28211-28218.

[230] J. Zhou, J. Zhang, Y. Lai, Z. Zhou, Y. Zhao, H. Wang, Z. Wang, *New J. Chem.* **2013**, *37*, 2983-2986.

[231] L. Wang, L. Xu, K. G. Neoh, E.-T. Kang, *J. Mater. Chem.* **2011**, *21*, 6502-6505.

[232] F. Liu, J. Mu, X. Wu, S. Bhattacharjya, E. K. L. Yeow, B. Xing, *Chem. Commun.* **2014**, *50*, 6200-6203.

[233] L. Q. Xu, C. Huang, R. Wang, K.-G. Neoh, E.-T. Kang, G. D. Fu, *Polymer* **2011**, *52*, 5764-5771.

[234] E. Maltas, S. Malkondu, P. Uyar, M. Ozmen, *Mater. Sci. Eng. C.* **2015**, *48*, 86-93.

[235] K. Peneva, G. Mihov, F. Nolde, S. Rocha, J. i. Hotta, K. Braeckmans, J. Hofkens, H. Uji-i, A. Herrmann, K. Müllen, *Angew. Chem.* **2008**, *120*, 3420-3423; *Angew. Chem. Int. Ed.* **2008**, *47*, 3372-3375.

[236] T. Cordes, J. Vogelsang, M. Anaya, C. Spagnuolo, A. Gietl, W. Summerer, A. Herrmann, K. Müllen, P. Tinnefeld, *J. Am. Chem. Soc.* **2010**, *132*, 2404-2409.

[237] K. Peneva, G. Mihov, A. Herrmann, N. Zarrabi, M. Börsch, T. M. Duncan, K. Müllen, *J. Am. Chem. Soc.* **2008**, *130*, 5398-5399.

[238] K. Peneva, K. Gundlach, A. Herrmann, H. Paulsen, K. Müllen, *Org. Biomol. Chem.* **2010**, *8*, 4823-4826.

[239] F. J. Cespedes-Guirao, A. B. Ropero, E. Font-Sanchis, A. Nadal, F. Fernandez-Lazaro, A. Sastre-Santos, *Chem. Commun.* **2011**, *47*, 8307-8309.

[240] S. K. Yang, X. Shi, S. Park, S. Doganay, T. Ha, S. C. Zimmerman, *J. Am. Chem. Soc.* **2011**, *133*, 9964-9967.

[241] H. B. Mekelburger, W. Jaworek, F. Vögtle, *Angew. Chem.* **1992**, *104*, 1609-1614; *Angew. Chem. Int. Ed. Engl.* **1992**, *31*, 1571-1576.

[242] J. M. J. Fréchet, *J. Polym. Sci., Part A: Polym. Chem.* **2003**, *41*, 3713-3725.

[243] P. Wu, X. Chen, N. Hu, U. C. Tam, O. Blixt, A. Zettl, C. R. Bertozzi, *Angew. Chem.* **2008**, *120*, 5100-5103; *Angew. Chem. Int. Ed.* **2008**, *47*, 5022-5025.

[244] M. W. P. L. Baars, R. Kleppinger, M. H. J. Koch, S. L. Yeu, E. W. Meijer, *Angew. Chem.* **2000**, *112*, 1341-1342; *Angew. Chem. Int. Ed.* **2000**, *39*, 1285-1288.

[245] S. M. Ryan, G. Mantovani, X. Wang, D. M. Haddleton, D. J. Brayden, *Expert Opin. Drug Delivery* **2008**, *5*, 371-383.

[246] A. E. Beezer, A. S. H. King, I. K. Martin, J. C. Mitchel, L. J. Twyman, C. F. Wain, *Tetrahedron* **2003**, *59*, 3873-3880.

[247] A.-M. Caminade, J.-P. Majoral, *Prog. Polym. Sci.* **2005**, *30*, 491-505.

[248] M. A. Quadir, R. Haag, *J. Control. Release* **2012**, *161*, 484-495.

[249] P. Furuta, J. M. J. Fréchet, *J. Am. Chem. Soc.* **2003**, *125*, 13173-13181.

[250] S. Xiao, N. Fu, K. Peckham, B. D. Smith, *Org. Lett.* **2010**, *12*, 140-143.

[251] T. R. Krishna, M. Parent, M. H. V. Werts, L. Moreaux, S. Gmouh, S. Charpak, A. M. Caminade, J. P. Majoral, M. Blanchard-Desce, *Angew. Chem.* **2006**, *118*, 4761-4764; *Angew. Chem. Int. Ed.* **2006**, *45*, 4645-4648.

[252] B. Zhu, Y. Han, M. Sun, Z. Bo, *Macromolecules* **2007**, *40*, 4494-4500.

[253] I. B. Rietveld, E. Kim, S. A. Vinogradov, *Tetrahedron* **2003**, *59*, 3821-3831.

[254] P. J. Dandliker, F. Diederich, A. Zingg, J. P. Gisselbrecht, M. Gross, A. Louati, E. Sanford, *Helv. Chim. Acta* **1997**, *80*, 1773-1801.

[255] P. J. Dandliker, F. Diederich, J. P. Gisselbrecht, A. Louati, M. Gross, *Angew. Chem.* **1995**, *107*, 2906-2909; *Angew. Chem. Int. Ed. Engl.* **1996**, *34*, 2725-2728.

[256] P. Weyermann, J. P. Gisselbrecht, C. Boudon, F. Diederich, M. Gross, *Angew. Chem.* **1999**, *111*, 3400-3405; *Angew. Chem. Int. Ed.* **1999**, *38*, 3215-3219.

[257] P. J. Dandliker, F. Diederich, M. Gross, C. B. Knobler, A. Louati, E. M. Sanford, *Angew. Chem.* **1994**, *106*, 1821-1824; *Angew. Chem. Int. Ed. Engl.* **1994**, *33*, 1739-1742.

[258] T. Heek, J. Nikolaus, R. Schwarzer, C. Fasting, P. Welker, K. Licha, A. Herrmann, R. Haag, *Bioconjugate Chem.* **2013**, *24*, 153-158.

[259] K. Huth, T. Heek, K. Achazi, C. Kühne, L. H. Urner, K. Pagel, J. Dernedde, R. Haag, *Chem. Eur. J.* **2017**, *23*, 4849-4862.

[260] Y. Li, K. Huth, E. S. Garcia, B. J. Pedretti, Y. Bai, G. A. Vincil, R. Haag, S. C. Zimmerman, *Polym. Chem.* **2018**, *9*, 2040-2047.

[261] K. Huth, M. Glaeske, K. Achazi, G. Gordeev, S. Kumar, R. Arenal, S. K. Sharma, M. Adeli, A. Setaro, S. Reich, R. Haag, *Small* **2018**, *14*, 1800796.

[262] O. Redy-Keisar, K. Huth, U. Vogel, B. Lepenies, P. H. Seeberger, R. Haag, D. Shabat, *Org. Biomol. Chem.* **2015**, *13*, 4727-4732.

[263] Z. Tu, K. Achazi, A. Schulz, R. Mülhaupt, S. Thierbach, E. Rühl, M. Adeli, R. Haag, *Adv. Funct. Mater.* **2017**, *27*, 1701837.

[264] G. M. Fardin, L. Daniel, L. Kai, S. Julian, Z. Benjamin, S. Nikolai, B. Christoph, R. J. P., H. Andreas, A. Mohsen, H. Rainer, *Adv. Funct. Mater.* **2017**, *27*, 1606477.

[265] S. P. Library, *Fine Art America* **2018**, https://fineartamerica.com/featured/human-serum-albumin-molecule-science-photo-library.html [May 26th, 2016].

[266] J. Dernedde, A. Rausch, M. Weinhart, S. Enders, R. Tauber, K. Licha, M. Schirner, U. Zügel, A. Von Bonin, R. Haag, *Proc. Natl. Acad. Sci. U.S.A.* **2010**, *107*, 19679-19684.

[267] T. Weil, T. Vosch, J. Hofkens, K. Peneva, K. Müllen, *Angew. Chem.* **2010**, *122*, 9252-9278; *Angew. Chem. Int. Ed.* **2010**, *49*, 9068-9093.

[268] S. M. Lu, G. D. Fairn, *Crit. Rev. Biochem. Mol. Biol.* **2018**, *53*, 192-207.

Appendix: Supporting Information (SI)

A.1 SI *Chem. Eur. J.* 2017, *23* (20), 4849-4862

A.2 SI *Polym. Chem.* 2018, *9* (15), 2040-2047

A.3 SI *Small* 2018, *14* (28), 1800796

A.4 SI *Org. Biomol. Chem.* 2015, *13* (16), 4727-4732

List of Publications and Conference Contributions

Publications

[1] **K. Huth**,‡ M. Glaeske,‡ K. Achazi, G. Gordeev, S. Kumar, R. Arenal, S. K. Sharma, M. Adeli, A. Setaro, S. Reich, and R. Haag, Fluorescent Polymer–Single-Walled Carbon Nanotube Complexes with Charged and Noncharged Dendronized Perylene Bisimides for Bioimaging Studies, *Small* **2018**, *14*, 1800796.
DOI: 10.1002/smll.201800796

[2] Y. Li,‡ **K. Huth**,‡ E. S. Garcia, B. J. Pedretti, Y. Bai, G. A. Vincil, R. Haag, and Steven C. Zimmerman, Linear Dendronized Polyols as a Multifunctional Platform for a Versatile and Efficient Fluorophore Design, *Polym. Chem.* **2018**, *9*, 2040-2047.
DOI: 10.1039/C8PY00193F

[3] **K. Huth**, T. Heek, K. Achazi, C. Kühne, L. H. Urner, K. Pagel, J. Dernedde, and R. Haag, Noncharged and Charged Monodendronised Perylene Bisimides as Highly Fluorescent Labels and their Bioconjugates, *Chem. Eur. J.* **2017**, *23*, 4849-4862.
DOI: 10.1002/chem.201605847

[4] O. Redy-Keisar, **K. Huth**, U. Vogel, B. Lepenies, P. H. Seeberger, R. Haag, and D. Shabat, Enhancement of Fluorescent Properties of Near-Infrared Dyes using Clickable Oligoglycerol Dendrons, *Org. Biomol. Chem.* **2015**, *13*, 4727-4732.
DOI: 10.1039/C5OB00299K

[5] J. Poppenberg, S. Richter, C. H. H. Traulsen, E. Darlatt, B. Baytekin, T. Heinrich, P. M. Deutinger, **K. Huth**, W. E. S. Unger, and C. A. Schalley, Programmable Multilayers of Nanometer-Sized Macrocycles on Solid Support and Stimuli-Controlled On-Surface Pseudorotaxane Formation, *Chem. Sci.* **2013**, *4*, 3131-3139.
DOI: 10.1039/C3SC50558H

(‡ These authors contributed equally.)

Publication in Preparation

[1] **K. Huth**, M. Glaeske, A. Setaro, A. Faghani, I. S. Donskyi, M. Müller, S. Block, G. Gordeev, R. Arenal, S. Juergensen, K. Ludwig, M. Hilsch, W. Unger, A. Herrmann, M. Adeli, S. Reich, and R. Haag, Covalently Functionalized Single-Walled Carbon Nanotubes with Fluorescent Dendronized Perylene Bisimides for Virus-Sensing Applications.

Poster Presentations

[1] A. Setaro, M. Glaeske, **K. Huth**, M. Adeli, R. Haag, and S. Reich, Perylene-Based Functionalization of Carbon Nanotubes, *International Winter School on Electronic Properties of Novel Materials* **2018**, Kirchberg in Tirol, Austria.

[2] **K. Huth**, M. Glaeske, A. Setaro, M. Adeli, S. Reich, and R. Haag, Nondestructive Functionalization of Single-Walled Carbon Nanotubes Promising Energy Transfer Processes, *Final Symposium SFB 658 on Elementary Processes in Molecular Switches at Surfaces* **2017**, Berlin, Germany.

[3] **K. Huth**, C. Kühne, K. Achazi, J. Dernedde, and R. Haag, Synthesis and Characterization of Sulfated Perylene Bisimides as Fluorescence Labels and their Conjugates with Biomolecules, *11th International Symposium on Polymer Therapeutics: From Laboratory to Clinical Practice* **2016**, Valencia, Spain.

[4] **K. Huth**, M. Glaeske, A. Setaro, M. Adeli, S. Reich, and R. Haag, Nondestructive Functionalization of Single-Walled Carbon Nanotubes Promising Energy Transfer Processes, *7th Innovation Congress Chemistry and Biotechnology on Materials and Processes for the Energy Turnaround-Generation, Storage and Saving* **2016**, Berlin, Germany.

[5] **K. Huth**, M. Glaeske, A. Setaro, M. Adeli, S. Reich, and R. Haag, Nondestructive Functionalization of Single-Walled Carbon Nanotubes Promising Energy Transfer Processes, *International Symposium SFB 658 on Molecular Switches & Functional Surfaces* **2016**, Mittenwalde, Germany.

Oral Presentations

[1] **K. Huth**, R. Haag, Functionalization of Carbon Nanotubes and Investigation of Energy Transfer Processes, *Internal Workshop SFB 658 on Status quo & Future directions* **2015**, Berlin, Germany.

Curriculum Vitae

Due to privacy policy the curriculum vitae is not included in the online version of this thesis.